Master Thesis

Characterization of the electrical properties of injection molded carbon nanocomposites

Jan Philip Jorissen

Technische Universiteit Delft

TU Delft Delft University of Technology

Challenge the future

Master Thesis

Characterization of the electrical properties of injection molded carbon nanocomposites

by

Jan Philip Jorissen

in partial fulfillment of the requirements for the degree of

Master of Science
in Aerospace Structures and Materials

at the Delft University of Technology,
to be defended publicly on Wednesday May 2, 2015 at 13:00 PM.

Supervisor:	Prof. dr. W. A. Groen	
Thesis committee:	Prof. dr. S. van der Zwaag,	TU Delft
	Prof. dr. W. A. Groen,	TU Delft
	Ir. J. Sinke,	TU Delft

TU Delft Delft University of Technology

Preface

This report has been written during the course of a 7 month master thesis research at Novel Aerospace Materials department of the aerospace faculty at the TU Delft. The aim of this report is to describe the experiments and findings of the 7 month research. The focus of this master thesis research is the characterisation of electrical properties of injection molded carbon based nanocompoistes.

At this point I want to use the opportunity to express my gratitude to the people that helped and guided me during my research. First of all I want to thank Prof. Dr. Pim Groen for supervising my thesis and mentoring me during the research process. With his valuable expertise he guided me through my research and helped me to gain a deeper understanding on conductive nanocomposites.
In addition to that I would like to thank Roserio Valente for his supervision and guidance and for providing me with the necessary samples for my experiments. Without his insights during the numerous progress meetings the content of this research would not be the same.
Moreover I would like to thank Frans Oostrum and Dr. Marlies Nijemeisland for their help during the experimental parts of this thesis.
Lastly I would like to thank my parents to provide me with the opportunity to pursue my interests and study at the TU Delft.

Jan Philip Jorissen
Delft, April 2018

Abstract

In this master thesis research the electrical properties of injection molded carbon nanocomposites are characterised. The addition of carbon materials such as carbon nanotubes to an insulating polymer matrix not only enhances the mechanical porperties of the composite but also increases the electrical properties to the composite. This enables the use of carbon nanocomposites in electrical applications such as electromagnetic interference shielding. One further interesting aspect of carbon nanocompistes is that they can be produced via injection molding, which is a widely used production process in the plastics industry as it is a fast and cost efficient method to produce large quantities of plastic components. Due to these interesting potential industrial applications some research already has been conducted with respect to injection molding of carbon nanocomposites and their resulting electrical properties. However some short comings in the current state-of-the-art research have been identified. This master thesis research aims at overcoming the knowledge shortcomings described in literature in order to enable the industrial production and application of carbon nanocomposites.

In order to characterise the electrical properties of injection molded carbon nanocompsites, this master thesis research has been divided into four parts. In the first part of this thesis the effect of the injection molding process on the electrical properties and their in-plane distribution is studied. Followed by that the effect of the polymer matrix material on the resulting electrical properties is investigated. In the third research part the treatment of below melt temperature annealing is investigated in order to enhance the electrical properties of the injection molded composites. Finally in the fourth part the process of dielectrophoresis is described with the aim of improving the electrical properties of the composites.

During this research composites consisting of polypropylene with a filler loading of 5 wt.% carbon nanotubes have been used. Injection molding of these composites resulted in a quasi-DC conductivity in the range of $10^{-7}\ S/cm$ - $10^{-6}\ S/cm$. In addition to that it has been shown that the electrical properties have a non-uniform in-plane distribution, where the electrical property magnitude increases with distance to the injection gate. Looking at the morphology of the composite it has been observed that injection molding leads to the formation of a skin layer with highly oriented carbon nanotubes, which varies in thickness along the injection melt flow. In addition to that it has been indicated that the carbon nanotube concentration in the polymer matrix increases with distance to the injection gate. These two observations are found to be the reason for the non-uniform electrical property-in-plane distribution after injection molding. Looking at the polymer matrix material of the composite it has been shown that a composite with better flow ability properties (high melt flow or low viscosity) leads to overall higher electrical properties. It is expected that a composite with better flow abilities enables the formation of better conductive networks through the sample thickness and leads to the formation of a thinner skin layer. Moreover it has been shown that a below melt temperature annealing treatment at 150 °C can be used to enhance the electrical properties of a composite with good flow ability properties (high melt flow index). An annealing treatment of 0.5 h is sufficient to improve the conductivity up to 3 orders of magnitude into the range of $10^{-5}\ S/cm$ - $10^{-4}\ S/cm$. In addition to that a slight decrease in electrical property non-uniformity has been observed after annealing. However when looking at the composites morphology after annealing it has been shown that the effects of injection molding are not eliminated. The annealing treatment tends to randomise the orientation of the carbon nanotubes which increases the tube-to-tube contacts and thus improves the electrical properties. However the skin layer remains present and the overall filler dispersion due to injection molding is not effected by the annealing treatment. Lastly dielectrophoresis has been preformed by applying an electric field to the composite during annealing treatments below and slightly above the melt temperature of the composite. From the experimental results it has been concluded that the additional application of an electric field during annealing does not further enhance the electrical properties of the composite.

Contents

List of Figures

List of Tables

List of Symbols & Abreviations

ϵ'	Real Permittivity	$[-]$
ϵ''	Imaginary Permittivty	$[-]$
σ'	Conductivity	S/cm
A	Universal Power Law Fitting Parameter	S/cm
a	Linear Regression Coefficient - Slope	
b	Linear Regression Coefficient - Offset	
d	Gate distance	cm
f	Frequency	Hz
s	Universal Power Law Fitting Parameter	S/cm
AC	Alternating Current	
BDS	Broadband Dielectric Spectroscopy	
DC	Direct Current	
DEP	Dielectrophoresis	
DSC	Differential Scanning Calorimetry	
EMI	Electromagnetic Interference	
IM	Injection Molding	
L	Location	
MFI	Melt Flow Index	$g/10min$
PP	Polypropylene	
SEM	Scanning Electron Microscope	

1

Introduction

In this master thesis report the electrical properties of injection molded carbon nanocomposites and the effects of varying processing and material properties on the electrical properties are studied. Carbon materials such as carbon nanotubes posses next to very high mechanical properties, very good electrical properties, which are comparable with the electrical properties of metals [1]. By incorporating carbon nanotubes into an insulating polymer matrix, an increase in the electrical properties of the composite material is seen. This increase in electrical properties enables carbon nanocomposites to be used in a wide range of electronic applications. One potential application of carbon nanocomposites is in electromagnetic interference (EMI) shielding by means of creating housings for electronic devices out of these composite materials [2, 3]. The benefits of using carbon nanocomposites over metals for EMI shielding are the lightweight properties of these composites, no vulnerability to corrosion and easy processing/production [2]. One potential way of producing carbon nanocomposites is by means of injection molding (IM). Injection molding is a cost effective method to produce complex 3D-geometries on a large industrial scale [3, 4]. Hence IM is the most used industrial production process for plastic parts [4].

Based on the good electrical properties and interesting potential applications of carbon nanocomposites there has been extensive research in this area. Aspects such as the effect of composite composition on the electrical properties, the relation between composite morphology and the electrical properties, the impact of the production process on the resulting electrical properties and further treatments to enhance the electrical properties of the composite have been described in literature. In chapter 2 an extensive overview on the state of the art research in the field of carbon nanocomposites is shown. Based on the literature review short comings in the current knowledge on carbon nanocomposites have been identified. These shortcomings have been translated into research questions and research objectives in order to broaden the knowledge on carbon nanocomposites. The research questions and objectives, formulated in chapter 2 serve as a guideline for the research conducted in this master thesis.

The first part of the research is presented in chapter 3, which serves as a baseline for the further thesis research. In this chapter the effect of the injection molding process on the electrical properties and the morphology of the carbon nanocompoiste is studied. In addition to that a repeatability study is presented in order to define the accuracy of the experimental results presented in this thesis. In chapter 4 the impact of the composite materials used on the electrical properties is looked at. Moreover the differences in composite morphology due to varying materials are studied. In the third part of this thesis, shown in chapter 5, the effect of below melt temperature annealing carbon nanocompoistes is explored. With respect to annealing the changes in electrical properties and morphology of the carbon nanocomposites is looked at. This is done with a focus on annealing process parameters: time and cooling rate. Lastly in chapter 6 the process of dielectrophoresis (DEP) with carbon nanocomposites is described. In this chapter it is investigated how varying electric field strengths and processing temperatures effect the electrical properties of the injection molded carbon nanocomposite. The master thesis research is concluded with chapter 7 were the main findings of the thesis research are summarised related to the research questions and research objectives.

2

Literature Review and Research Questions

2.1. Literature Review

In this section the relevant literature for the master thesis work is summarised. In this thesis the mapping of the electrical properties of an injection molded carbon nanocomposite at multiple locations of the composite sample is presented. The carbon material to be used in the composite are carbon nanotubes (CNT) in a polypropylene (PP) polymer matrix. Moreover different injection molding settings are to be used during the production of the samples in order to identify differences in the distribution due to production. In addition to that the effect of using different polymer matrix materials on the resulting electrical properties and their distribution is to be explored. Furthermore treatments such as annealing and dielectrophoresis (DEP), are to be explored in order to enhance the properties of injection molded carbon nanocomposites.
In order to get a better understanding on the topics to be studied in this thesis, some literature and concepts need to be discussed before the discussion of the experimental results. In this section a brief description of the percolation theory and percolation behaviour of carbon nanocomposites is given, followed by a description of the optimal morphology in terms of percolation threshold and optimal electrical properties. In addition to that some literature on the influence of the polymer matrix material on the resulting composite properties is presented. Moreover a short overview on dielectric properties in carbon nanocomposites is given, followed by a review of the effects of injection molding on the electrical properties of the composite. Moreover the state of the art knowledge on annealing and DEP with conductive composites it presented.

Percolation Theory and the Percolation Threshold:

In order to understand the existence of electrical properties in carbon based nanocomposites, the percolation theory needs to be looked at. It is known that most polymers on their own are insulating materials and due to the addition of conductive filler materials a rise in the electrical properties can be seen. In order to better explain the percolation phenomenon a sketch of the conductivity and filler loading is shown in figure 2.1. When looking at figure 2.1 it needs to be noted that this is a schematic representation for the sake of describing the percolation phenomenon.

When looking at figure 2.1 it can be seen that for a very low filler loading the conductivity of the composite remains low. From the sketch of the morphology at a low filler loading it can also be seen that there is no interconnection between the conductive fillers. Thus it can be said that the conductivity is dominated by the electrical properties of the matrix material. Upon further increasing the filler loading, it can be seen that there is a sudden rise in the conductivity at a certain filler volume. The filler volume at which the conductivity strongly increases is called the percolation threshold. When looking at the sketch of the composite morphology it can be seen that the fillers start to form a network and thus the conductivity starts to increase. The percolation threshold is defined as the minimum filler

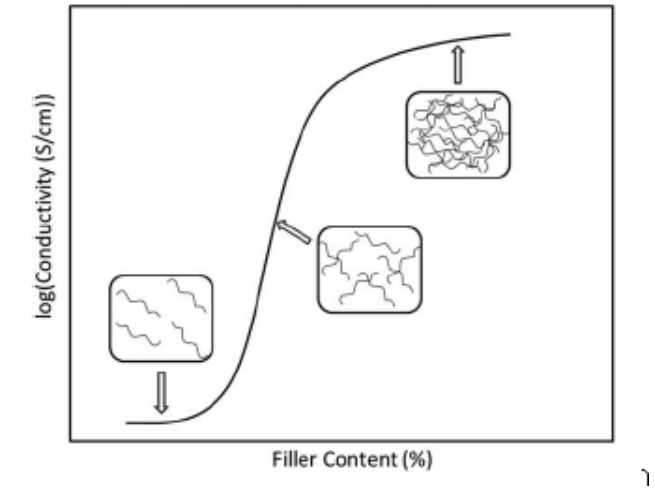

Figure 2.1: Sketch of the change in conductivity due to varying filler loading and the corresponding morphology. [5]

concentration to form a conductive network and thus significantly increases the conductivity [3]. Upon further increasing the filler loading beyond the percolation threshold, a further increase in conductivity can be seen. However at a certain filler volume almost no further increase in conductivity can be measured and thus the conductivity reaches a plateau. This conductivity plateau can be defined as the conductivity of the filler material itself. When looking at the sketch of the morphology it can be seen that at high filler loadings, a tight network of fillers is present and thus is the dominant factor for the conductivity.

When looking at the percolation threshold of CNT fillers in a PP matrix, a range of percolation threshold values can be found in literature. It has been reported by Gulrez et al. [5] that the percolation threshold for CNTs in a PP matrix ranges form 0.5 wt.% to 7 wt.%. However when looking at these threshold values it needs to be recognised that different production processes have been used, which has an impact on the percolation threshold. Moreover geometrical factors of the CNT filler such as the aspect ratio also have an impact on the percolation threshold of the composite. In general it can be said that higher CNT aspect ratios lead to lower percolation thresholds [6, 7]. This however is not further investigated in this report.

Since the production process to be used during the thesis research is injection molding, a plot of the resulting conductivity with varying filler loading of an injection molded sample can be seen in figure 2.2.

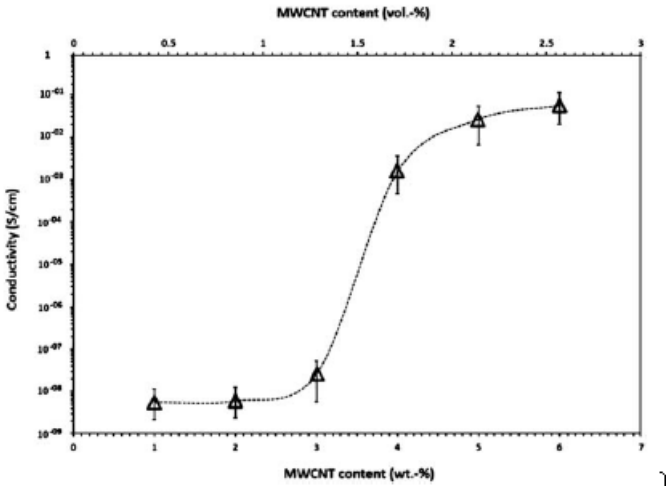

Figure 2.2: Electrical conductivity as a function of CNT filler loading in a CNT/PP composite. [1]

The composite shown in figure 2.2 has been prepared by twin-screw extrusion followed by injection molding [1]. When looking at the graph it can be seen that for a filler loading below 3 wt.% no increase in conductivity can be seen. The conductivity increases by 6 orders of magnitude within the filler range of 3-4 wt.%. Thus it can be said that the percolation threshold for the composite is at 3 wt.% [1]. Similar results also have been found by Ngabonziza et al. [8], where it has been reported that the percolation threshold of an injection molded CNT/PP sample is to be 3.8 wt.%. So it can be concluded that the peroclation threshold for a CNT/PP composite is within the range of 3-4 wt.% of CNT fillers.

Composite morphology:

As a next step some effects of the composite morphology on the resulting electrical properties need to be discussed. This entails a description of the optimal dispersion of the fillers within the matrix and the impact of polymer crystallinity on the percolation threshold. As the master thesis work only deals with CNT fillers, this subsection only will look at the dispersion and the resulting morphology of composites containing CNTs. As already indicated in figure 2.1 the dispersion of the CNTs within the polymer matrix has an impact on the resulting electrical properties. It can be said that in order to achieve good overall electrical properties, the CNT fillers need to form a percolated network.
First of all when working with CNT fillers it needs to be noticed that it is difficult to uniformly disperse them in a polymer matrix due to strong attractive van der Waals forces, which tend to agglomerate the CNT fillers [9]. So high mixing energies are required to break up the CNT agglomerates and ensure a uniform distribution of the fillers. Due to that multiple CNT dispersion states can be found within a polymer matrix, which is shown by the different sketches in figure 2.3.

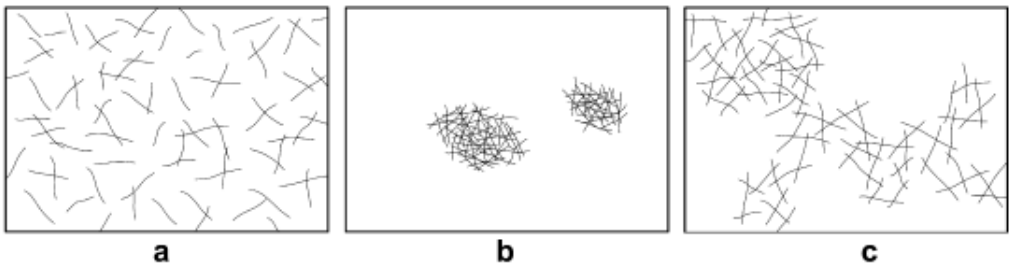

Figure 2.3: Representation of different possible CNT dispersions in a polymer matrix. (a) well dispersed, (b) agglomerated, (c) slight agglomeration. [10]

In figure 2.3 three different dispersion states of the CNT in the polymer matrix are described. In general it can be said that the agglomerated dispersion shown in figure 2.3 (b) is the worst in terms of electrical properties, as there is no interconnected network of fillers present. In terms of achieving the lowest percolation threshold it has been found by researchers that having well dispersed fillers as seen in figure 2.3 (a) is the required type of dispersion, as this leads to the most connections between the fibres [11, 12]. In terms of the highest electrical properties it has been found that a slight degree of agglomeration is beneficial as shown in figure 2.3 (c), as that leads to increased nanotube to nanotube contacts within the composite [10, 13]. In terms of the percolation threshold it is also reported that a slight degree of agglomeration also can have a lowering effect [10, 13]. However when saying that a slight degree of agglomeration is beneficial in terms of lowering the percolation threshold and improving the electrical properties, the impact of the geometrical properties of the CNT filler need to be considered. It has been found that slight agglomeration only is beneficial if the CNT fillers have a large aspect ratios [12, 14].

One further morphology aspect that needs to be discussed when working PP is the crystallinity of the polymer matrix. Some research on the effect of crystallinity on the dispersion of the filler has been conducted and it has been found that polymers with a low degree of crystallinity or even amorphous polymers lead to a more uniform dispersion of CNT fillers [15, 16]. In contrast to that polymers with a high degree of crystallinity tend to have less uniform filler distributions and the fillers have a stronger

tendency to agglomerate [15, 16]. Moreover it has been described in literature that the addition of fillers changes the nucleation of the crystal regions within the polymer matrix. Normally crystal regions nucleate due to homogeneous nucleation during the cooling of the polymer. But due to the addition of fillers to the polymer matrix, the nucleation becomes heterogeneous, which means that the crystal regions start to nucleate at the surface of the filler [17]. So it has been reported that due to the addition of CNTs in a PP matrix, the nucleation of the crystal regions was dominated by heterogeneous nucleation [17]. However it needs to be noted that despite the nucleating effect of the CNTs, the degree of crystallinity is not changed due to the addition of the fillers and even higher filler volumes do not increase the degree of crystallinity [15, 18]. The presence of crystal regions also leads to a form of phase separation. In polymers having crystal regions it has been observed that it is more likely that the fillers disperse into the non-crystalline regions [16].
Since the crystallinity of the polymer matrix has an effect on the dispersion of the filler, it can be said that the percolation threshold and the electrical properties are also impacted by the crystallinity. It has been reported that the percolation threshold of the composite increases with an increasing degree of crystallinity [15]. This is due to the fact that the growing crystal regions tend to break down the filler networks. In addition to that the mobility of the filler to form new networks is also decreased due to the formation of crystal regions. Since the filler networks tend to be broken down, it has been found for the electrical properties that with increasing crystallinity the electrical properties decrease [15, 16].

Dielectric Properties of carbon nanocomposites:

During the master thesis research, the dielectric properties of an injection molded composite are to be studied, the theory of dielectric properties and current knowledge of the dielectric properties of carbon nanocomposites is briefly discussed.
First of all the basic theory of dielectric properties is discussed. The dielectric properties of a material are described by the dielectric constant, which is a dimensionless property. The dielectric constant is a measure for a materials ability to store electrical energy due to the application of an external electric field. In equation 2.1 the composition of the dielectric constant can be seen.

$$\varepsilon = \varepsilon^{'} + i\varepsilon^{''} \tag{2.1}$$

The dielectric constant of a material is made up of two parts. The first part is $\varepsilon^{'}$, which stands for the real permittivity and is a measure for the energy storage capability of the material. The $\varepsilon^{''}$ is the imaginary permittivity of the dielectric constant and is also called the loss factor as it accounts for energy losses due to conductivity and dielectric losses. In general no optimum value for the dielectric constant can be defined as it depends on the desired application. For example for energy storage applications such as batteries, a high real part and a low imaginary part would be required.
On its own a polymer material has relatively low dielectric properties as it is an insulator. But due to the addition of conductive fillers such as CNTs an increase in the dielectric constant can be seen. When reaching the percolation threshold, the composite becomes conductive and thus the dielectric constant increases [19]. Due to the addition of CNTs to a polymer matrix both $\varepsilon^{'}$ and $\varepsilon^{''}$ increase. The real part increases as the CNTs act as micro capacitors and the imaginary part increases due to the conductivity increase which promotes Ohmic losses [20, 21].
When talking about the dielectric properties of a material it needs to be recognised that the dielectric properties change with frequency of the applied electric field. This can be seen in the experimental results shown in figures 2.4 and 2.5, where the real and imaginary perimttivity of a poly(ethylene terephthalate)/CNT composite for a frequency range from 10^{-4} Hz to 3 THz are shown.

When looking at the graphs it can be seen that the real permittivity $\varepsilon^{'}$ remains constant for quite a broad frequency range, until it reaches a frequency of approx. 10^{4} Hz. From that point onwards the real permittivity starts to decrease at an almost constant rate with increasing frequency. Only at a very high frequency of approx. 10^{11} Hz the decline starts to level off, but the permittivity is almost 1 at that point. For the imaginary permittivity $\varepsilon^{''}$ a similar trend can be seen in the low frequency range, however the imaginary permittivity decreases quite strongly from the start of the measurements. The decreasing slope changes to slower decrease at a frequency of about 10^{2} Hz and from this point on-

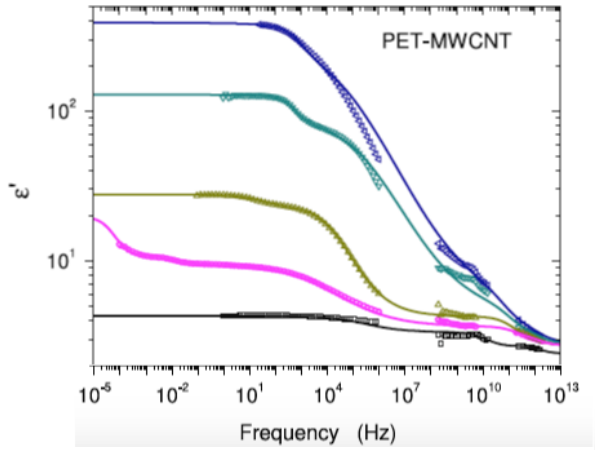

Figure 2.4: Real permittivity of a poly(ethylene terephthalate)/CNT composite from 10^{-4} Hz to 3 THz. [22]

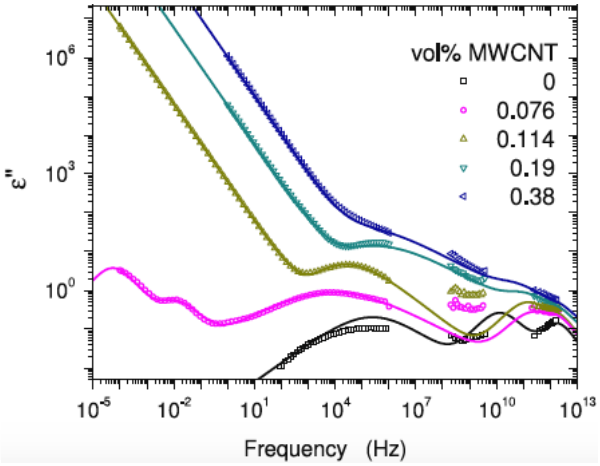

Figure 2.5: Imaginary permittivity of a poly(ethylene terephthalate)/CNT composite from 10^{-4} Hz to 3 THz. [22]

wards some "waviness"can be seen in the decreasing slope.
The changes in dielectric constant can be explained by different relaxation and polarization process that occur within the composite at different frequencies. At high frequencies (10^{14} Hz - 10^{15} Hz) the dielectric loss factor is dominated by electronic and ionic polarization and at low frequencies (10^{2} Hz - 10^{8} Hz) dipole polarization is the biggest factor for the losses [21]. When looking at composites containing CNTs, it has been found that interfacial polarization is a very important factor that needs to be considered for the dielectric properties [21]. This interfacial polarization is dominant at a lower frequency range and contributes to the real permittivity [20]. At higher frequencies the effect of interfacial polarization decreases and CNT polarization becomes the dominant factor influencing the real permittivity [20].

Effect of Injection Molding:

Moreover some literature on the effects of the injection molding process needs to be reviewed. When looking at the injection molding process, two aspects have to be reviewed in literature. First of all the effect of the injection molding settings are studied. This is followed by a review on how the electrical properties of the injection molded composite are distributed within the sample.
Before starting the discussion on the effect of the process parameters, a brief description of the injection molding process itself is given. During injection molding first of all a polymer in granulate form is fed into a hopper, from where it is led into a screw. In the screw the polymer is melted and then the melt is injected via a nozzle into a mold. This process occurs under a certain pressure, temperature and injection velocity. When the mold is filled with material a holding step occurs during which the polymer melt cures under an applied pressure in order to create the finished sample.
There are several processing parameters such as injection velocity, melt temperature, mold temperature, injection pressure and holding pressure that can be changed during the production process and thus influence the resulting properties of the composite. However in literature it can be found that the injection velocity and the melt temperature are the two process parameters with the biggest impact on the resulting properties of the composite [23]. When looking at the effect of the injection velocity, it can be generally said that higher injection velocities lead to a lower composite conductivity and low injection velocities tend to lead to a higher composite conductivity [2, 4, 24]. It has been described that high injection velocities increase the shear forces experienced by the composite melt during processing, which leads to a shortening of the CNT fibres and thus reduces the resulting conductivity [23]. In contrast to that, using lower injection velocities reduces the amount of shear experienced by the melt and it has been found to lead to more uniform electric property distributions [4]. Thus it can be said that in terms of good electrical properties, low injection velocities should be used. When looking at the melt temperature used during injection molding it can be said that higher melt temperatures are favourable in terms of good electrical properties and a uniform distribution of these properties [4]. This can be explained due to the fact that higher melt temperatures give the CNTs more mobility to

disperse in the polymer matrix and form a conductive network.
As already indicated, injection molding can lead to non-uniform distributions of the electrical properties of the composite. Some research has been reported in literature on the resulting distribution of the CNTs and the electrical properties in an injection molded composite. In figure 2.6 the CNT distribution along the injection flow of a CNT/polycarbonate composite can be seen [2] and in figure 2.7 the surface and volume resistivity of an injection molded CNT/polycarbonate composite is mapped [23].

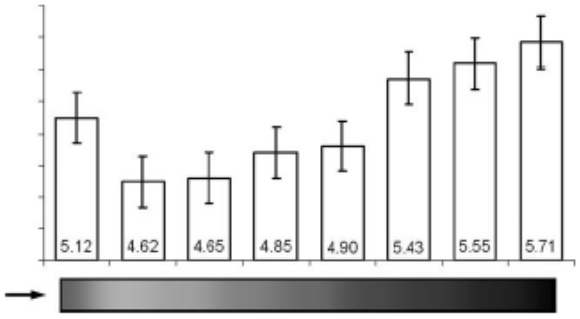

Figure 2.6: CNT distribution along the injection flow. [2]

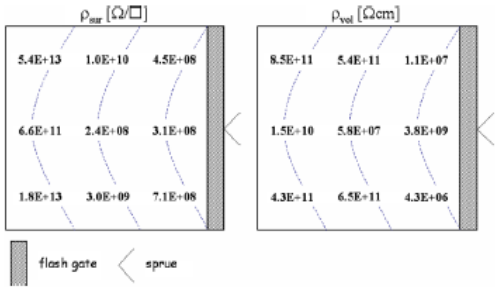

Figure 2.7: Surface and volume resistivity along the injection flow. [23]

When looking at the CNT distribution along the injection flow shown in figure 2.6, it can be seen that the CNTs are not uniformly distributed. From the figure it can be seen that the CNT concentration is higher further away from the injection gate and that closer to the injection gate the CNT concentration tends to be lower. This is due to the fact that the polymer melt and the CNTs have different flow abilities [2]. When looking at the in-plane mapping of both the volume and surface resistivity of the composite it can be seen that both resisitivity value are highest the further away they are from the injection gate and closer to the injection gate lower resistivity values are found. When talking about resistivity it needs to be noted that the conductivity is equal to the inverse of the resistivity ($\sigma = \frac{1}{\rho}$). Thus from the results shown in figure 2.7 it can be derived that the conductivity is higher close to the gate and decreases with distance from the gate.
In contrast to that other research has found by multiple other researches that the conductivity of injection molded composites tends to be lower for locations close to the injection gate and increases with distance to the gate [4, 25, 26]. It is expected that the conductivity close to the gate is lowest since the cooling rate of the melt is highest at the point where the melt touches the mold and thus a thicker skin layer with oriented CNTs is formed close to the gate [25]. However it has also been shown by Ameli et al. [26] that both the skin and core conductivity of the composite are lower close to the gate. Lastly some it has been indicated that the injection molding settings, such as injection speed, do not tend to influence the distribution of the conductivity, if the melt temperature used is sufficiently high [4].
Moreover regions of locally similar resistivity values can be found when looking at figure 2.7, which are indicted in the figure by the semi-circular lines. These regions indicate the flow lines of the polymer melt during the injection of the melt and across these flow line similar electrical properties can be found [23]. The differences in resistivity along the flow are to be explained due to changes in the CNT network resulting from network orientation, network disruption, orientation of separated tube and locally different cluster formations [23]. Moreover it is expected that the differences in CNT distribution and electrical property distribution come from the differences in shear forces experienced by the melt. It has been indicated in literature that by lowering the shear forces exerted on the melt during injection molding, which can be achieved by having lower injection velocities, a more uniform CNT and electrical property distribution can be achieved [4].
One further aspect that already has been indicated in figure 2.7, is the difference between surface and volume resistivity. A more detailed investigation into the differences between surface and volume resistivity has been done by Prak et al. [27]. In their research it is indicated that the electrical properties on the surface are worse than in the core of the composite sample. The resitivity of the composite has shown to have a negative exponential trend towards the core of the sample. This difference again can

be explained with the shear forces experienced during the production process. The surface experiences higher shear forces during production due to direct contact with the mold. Again it has been reported that the differences in electrical properties through the thickness of the composite can be minimised by lowering the shear forces during production by means of using lower injection velocities.

Effect of Annealing:

In addition to that the possibility of annealing a carbon nanocomposite has been reviewed in literature in order to enhance the electrical properties of the composite. When talking about annealing, it needs to be noticed that there are three process parameters that can be influenced. In this section literature on the annealing temperature, annealing time and cooling rate after the treatment are reviewed. It also needs to be noted that all the sources mentioned use isothermal annealing as a heat treatment.
When looking at annealing of composites having a polymer matrix made of polyproylene, it needs to be mentioned that the polypropylene has a melt temperature of approximately 165 °C and the addition of CNTs to the polymer matrix does not change the melt temperature of the composite [28]. When looking at annealing treatments described in literature, it can be seen that there is a distinction between annealing above and below the melt temperature of the composite.
It has been shown that annealing at high temperatures, well above the melt temperature, the biggest improvements in terms of electrical properties are seen. Pan et al. [29], conducted annealing experiments on composites containing PP and 5 wt.% of CNTs and they have found that annealing at 200 °C yields a conductivity improvement of up to 7 orders of magnitude. Whereas annealing at a lower temperature of 165 °C only yields an improvement of up to 2 orders of magnitude. Moreover it has been shown that for higher annealing temperatures, shorter annealing times are needed to reach the maximum conductivity. For annealing at 200 °C a time of 15 minutes is sufficient to reach maximum conductivity, whereas 30 minutes of annealing are needed at 165 °C. It also has been noted that the conductivity reaches a plateau value after a certain time of annealing, which means that further increasing the annealing time does not improve the electrical properties.
Annealing below the melt temperature of a composite containing PP has been described by Kazemi et al. [28]. During their experiments annealing below the melt temperature of 165 °C has been performed for 15 minutes and no significant improvements in conductivity have been found. However it has been noted by their research that annealing at lower temperatures, while applying gas pressure to the composite, is favourable for the dielectric properties as it promotes the formation of lamellar polymer crystals around CNTs and thus insulating the CNTs. When looking at this research it needs to be noticed that a very short annealing time has been used.
It has been indicated by studies conducted on polystyrene, that annealing below the melt temperature ($0.75T_m$) can lead to conductivity improvements of up to 2 orders of magnitude when annealing up to 10 hours [30]. Thus for annealing below the melt temperature, long annealing times are to be used in order to significantly improve the electrical properties of the composite. Moreover it has been indicated that annealing needs to be performed above the glass transition temperature of the composite in order to achieve improvements in the conductivity of the composite [29].
Lastly the impact of the cooling rate after the heat treatment is discussed. In terms of cooling rate, a contrast in findings has been identified in literature. It has been reported that fast cooling is favourable in terms of a low resistivity (high conductivity), as fast cooling leads to a lower degree of crystallinity and thus enhancing the formation of conductive pathways [31]. In contrast to that it has been reported that slow cooling of the composite is beneficial in terms of high electrical properties [32–34]. However the reason why slow cooling is beneficial has not been clearly defined in literature. It has been described that slow cooling leads to a larger volume shrinkage of the composite and thus the distance between neighbouring CNTs is smaller, which enhances the electrical properties [32]. Other sources indicate that slow cooling promotes the formation of order conductive networks due to the formation of crystal structures within the polymer matrix [34]. However it has been indicated that slow cooling and the formation of crystal structures only is beneficial for the electrical properties if filler loadings above the percolation threshold are used [33]. The contrasting views on the effect of different cooling rates and the resulting crystallinity have been summarised in detail by M. Fernández et al. [33].
Lastly it needs to be mentioned that fast cooling can be applied to the composite without decreasing the electrical properties, if the composite has been slowly cooled below the crystallization temperature

[32].
Lastly the impact of the molecular weight of the polymer matrix on the annealing efficiency has been studied by Pan et al. [29]. In their research it has been shown that composites with a lower molecular weight polymer matrix requires longer annealing times to reach the maximum level of conductivity compared to composites with a higher molecular weight matrix.

Effect of polymer matrix properties:

When talking about polymer matrix properties, it needs to be noticed that only literature on the effect of the polymer melt viscosity is reviewed. The viscosity is the measure for a fluids resistance to flow. That means a high viscosity fluid resists motion due to the internal friction forces experienced, whereas a low viscosity fluid flows easily as it experiences less internal friction. [1]
Similarly to that definition it has been described in literature, that the shear stress experienced by a composite melt is directly related to the product of the melt viscosity and the shear rate applied to the melt [3]. That means that a higher melt viscosity leads to an increase in shear stresses experienced by the composite [35, 36]. An increased shear stress experienced by the composite melt can be beneficial and negative for the resulting electrical properties of the composite. During melt mixing a higher shear stress can be beneficial to break down the CNT agglomerates and thus improve the filler dispersion [36]. However when the shear stresses applied to the composite melt are too high, the CNT fibres in the polymer matrix can break and thus the resulting electrical properties of the composite decrease [3, 35]. Similarly during injection molding with a high viscosity composite melt, the shear stresses experienced during processing tend to break down the conductive CNT networks and thus lower electrical properties [36]. In addition to that it has been shown that high viscosity melts during injection molding lead to highly oriented CNTs in the melt flow direction [23]. This orientation in the melt flow direction has been predominantly seen close to the surface of the composite samples and that lead to the formation of an insulating skin layer due to decreased tube-to-tube contacts, which reduced the conductivity of the composite [23]. Lastly it needs to be mentioned that a lower melt viscosity leads to a better wet ability of the CNT agglomerates [3, 35].

Dielectrophoresis of carbon nanocomposites:

Lastly literature on the topic of dielectrophoresis (DEP) of carbon nanocomposites is reviewed. In this section the possibility of annealing the composite in order to enhance the electrical properties already has been reviewed. When looking at annealing it needs to be noted that it leads to a randomisation of the CNT dispersion, as the CNT movement is controlled by Brownian motions. So in addition to heating the composite sample, the DEP process makes use of an electric field in order to control the orientation of the CNTs within the polymer matrix. A schematic representation of the effect of the DEP process on the composite morphology is shown in figure 2.8.

In figure 2.8 it can be seen that before the DEP process a random CNT orientation is found in the composite and upon application of an electric field, the CNTs are oriented along the electric field lines. It has been described that the presence of an electric field leads to the polarisation of the CNTs, which results in an electrostatic force to orient the CNTs along the electric field lines, which enhances the formation of conductive networks [37]. The formation of conductive networks during the DEP process can be described in more detail. When applying an electric field to the composite, the CNTs within the matrix cause inhomogeneities to the electric field which leads to electric field gradients between the CNTs [38, 39]. These inhomogeneities in the electric field between the CNTs cause the CNTs to move towards areas of high electric field strength [38, 39] and thus promotes the formation of conductive networks in the polymer matrix. One further aspect controlling the network formation upon applying an electric field is Coulombic attraction between oppositely charged ends of the CNTs [38]. The dynamic percolation process during DEP has been defined by Osazuwa et al. [39], where the filler loading (ϕ), matrix viscosity (η) and the electric field strength (E) are the major factors influencing percolation time of the DEP process. The corresponding relation can be seen in equation 2.2.

[1] https://www.princeton.edu/~gasdyn/Research/T-C_Research_Folder/Viscosity_def.html

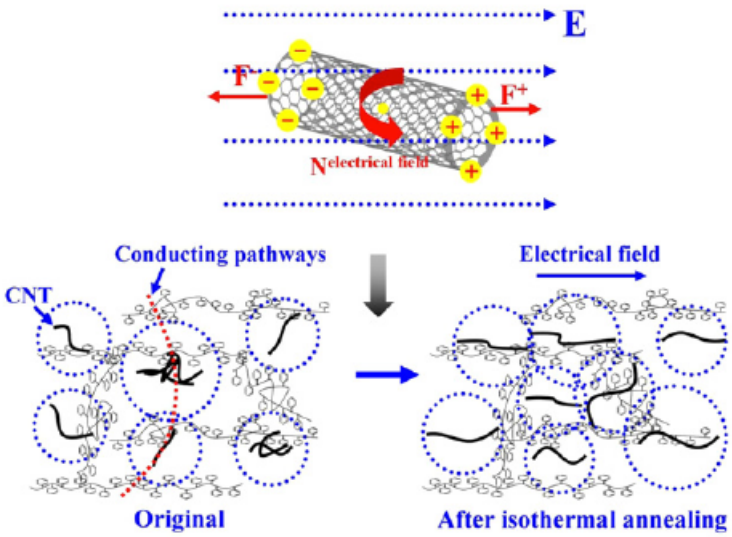

Figure 2.8: Schematic representation of the conductive network before and after annealing under the application of an electric field. [37]

$$t_{m,DEP} \sim \eta E^{-2} \phi^{-1.5} \tag{2.2}$$

In order to achieve a controlled formation of conductive networks along the electric field lines, sufficiently high electric field strengths and/or high filler loadings are required to overcome the control of the Brownian motion on the filler dispersion [39]. Using low electric field strengths and/or filler loadings lead to control of Brownian motion, which leads to random filler orientations [39].
Now that the basic theory behind the DEP process has been explained some experimental results on the electrical properties and morphology of carbon nanocomposites due to DEP presented in literature are discussed. First of all it needs to be noted that presented literature either deals with DEP process where the polymer matrix is a thermoplastic polymer in a molten state [37, 39, 40] or with a thermosetting polymer during curing at elevated temperatures [38, 41]. This indicates that the polymer matrix has a low viscosity during DEP and thus a high mobility for the CNTs to form a conductive network is present. First of all it has been reported that upon applying an electric field to the composite, an improvement of the CNT dispersion is seen. Mainly it has been reported in literature that the application of an electric field during annealing or curing of the composite leads to a reduction of the time needed to form a percolated network [37, 40]. It has been observed that the CNTs tend to orient parallel along the electric field lines, creating conductive networks [39, 41]. This improvement in orientation of the CNTs within a polycarbonate matrix has been reported to improve the resistivity of the composite by 5 orders of magnitude [40]. When talking about applied electric fields, a distinction between DC- and AC-fields needs to be made. It has been reported that the application of DC-fields tends to create a non-uniform filler dispersion as the CNTs start to move towards the anode [38]. Upon application of AC-fields a more uniform dispersion and alignment of the CNTs along the electric field lines through the sample is found, which leads to higher electrical properties [38]. A further aspect that has been described in literature is the electric field strength used during DEP. It has been reported that higher field strengths promote better network formation and thus lead to higher electrical properties [38]. In addition to that higher electric field strengths are required to overcome the Brownian motion and thus fully control the CNT orientation [39]. For example it has been reported when performing DEP with poly-carbonate at 270 °C a field strength of 1 V/cm is not sufficient to control the CNT orientation, whereas a field strength of 500 V/cm is sufficient to align the CNTs along the field lines. Moreover it has been reported that for given electric field strength, the applied temperature (resulting matrix viscosity) is a major factor influencing the network formation [37]. It has been reported that higher temperatures are beneficial for the network formation during DEP [37]. Lastly it needs to be mentioned that higher electric field strengths decrease the time needed to form percolated networks [37, 39, 40].

And it also has been indicated that the application of a strong electric field decreases the percolation threshold of the composite [40].

2.2. Research Questions

In this section the research questions and research objectives of the master thesis research are defined. This is done by reflecting on the state-of-the-art knowledge on the topic of injection molded carbon nanocomposites presented in literature and identifying shortcomings and research opportunities in this research area. Based on that, the research questions and research objectives for further research are formulated. This section is divided into four parts. First of all the research question and objectives studying the effect of the injection molding process on the electrical properties of the carbon nanocomposite are formulated. Followed by that the study of the effect of the polymer matrix material used on the resulting electrical properties of the composite is introduced. The third subsection deals with the introduction of the research questions and objectives studying the impact of an annealing treatment on the electrical properties of the injection molded carbon nanocomposites. Lastly the research question and objectives with respect to the dielectrophoresis treatment are formulated.

Research Questions for Part 1: Study of the electrical properties of Injection Molded nanocomposites

In this section the research questions and objectives related to the first Part are defined. The first Part entails the in-plane mapping of the electrical properties of an injection molded composite. Mappings of composite samples produced at various injection molding settings are to be made. It needs to be noticed that the first Part of this master thesis work serves as the basis/reference for the further experimental work conducted during the thesis. Based on that and the literature review shown in section 2.1, the research questions and research objectives are defined.
From the literature review it can be seen that already some research on the electrical properties of injection molded carbon nanocomposites has been conducted. With respect to the dielectric properties the polarization and relaxation processes at different frequencies have been studied and the dielectric properties of a composite containing CNTs have been measured over a broad frequency range. From literature it can be seen that the dielectric properties of the composite vary with changing frequencies. Moreover the impact of the composite morphology and crystallinity on the resulting electrical properties has been studied as well. In terms of injection molding, intensive research on the effects of the processing conditions has been conducted. And in the literature review some research on the resulting CNT distribution and resistivity distribution has been presented.
As already indicated, the first research part serves as a reference for the further work of the thesis research. Nevertheless some ideas for further new research in Part 1 can be derived from the literature review. From the literature it has been noticed that no in-plane mappings of the dielectric properties of an injection molded sample have been made. From literature it can also be seen that no in-plane mappings of the electric property distributions at various injection molding process settings have been made. Moreover some contradicting results on the resulting distribution of the conductivity in an injection molded sample have been found.
Based on these shortcomings of the state-of-the-art knowledge, the following research questions for Part 1 have been formulated:

Question 1.1: How do the electrical properties vary location wise within the injection molded nanocomposite sample?

Question 1.2: What is the effect of different injection molding settings on the in-plane distribution of the electrical properties within the carbon nanocomposite?

Question 1.3: How do varying injection molding settings impact the magnitude of the electrical properties within a carbon nanocomposite?

Question 1.4: What is the impact of the injection molding process on the resulting composite mor-

phology?

Based on these research questions, some research objectives for Part 1 can be identified. The main objective of the first Part is to make a mapping of the in-plane distribution of the electrical properties within an injection molded composite. Moreover the effect of the injection molding settings on the resulting property distribution and the influence on the property magnitude is to be understood. And lastly the effect of the injection molding process on the resulting composite morphology is to be looked at in order to get a better understanding on the resulting electrical properties. All the objectives presented for Part 1 are to be realised by means of experimentation. Further details on the experiments are presented in chapter 3.

Research Questions for Part 2: Effect of the polymer matrix material on the electrical of injection molded composites

In this section the research questions and objectives for the second part of this mater thesis are defined. This part of the master thesis work deals with the impact of the polymer matrix material used on the resulting electrical properties. Moreover composites containing different polymer matrix materials are to be produced using varying injection molding settings in order to investigate if different matrix materials react differently to changing processing settings. In order to investigate the effect of the materials used and their sensitivity to the processing settings, mappings of the electrical properties within the injection molded samples are to be produced.
From the literature review it can be seen that the effect of varying melt viscosity during the different processing stages have been investigated. It has been established that the melt viscosity is an important parameter to determine the shear forces experienced by the melt during production. Thus some literature on the resulting morphology and electrical properties due to the viscosity during processing can be found. However when looking at the literature presented with respect to the polymer matrix properties, it needs to be noticed that the melt viscosity described in literature has been controlled by the temperature used during the processing steps. Hence further research using polymer matrix materials having different flow abilities at equal processing conditions are to be investigated, as no literature has been found on that topic. Moreover no in-plane mappings of the electrical properties have been produced with respect to composites having different flow abilities during processing. Lastly it has been noticed that effect of varying injection molding settings on the resulting electrical properties has not been studied with respect to different polymer matrix materials used.
Based on these shortcomings the following research questions have been defined for part 2 of this master thesis work:

Question 2.1: What is the effect of the polymer flow ability during injection molding on the resulting electrical property magnitude?

Question 2.2: How is the electrical property in-plane distribution of injection molded composite effected by the flow abilities of the polymer matrix material?

Question 2.3: How do nanocomposites containing different polymer materials respond to varying injection molding settings in terms of electrical property magnitude and their in-plane distribution?

Question 2.4: What are the morphological differences between injection molded nanocomposites containing polymers with different flow abilities?

Based on these research questions, the research objectives of the second part of this master thesis research can be formulated. First of all the differences in resulting electrical property magnitude and the differences in composite morphology due to the use of different polymer matrix materials is to be understood. In addition to that the effect of the polymer matrix flow abilities on the resulting electrical property in-plane distribution after injection molding is to be described. Moreover the impact of the injection molding settings on the resulting electrical properties and their distribution in different composite materials is to be further understood.

Research Questions for Part 3: Annealing of injection molded nanocomposites and the effect on the electrical properties

In this section the research question and objectives with respect to the third part of the master thesis research are defined. The aim of this part is to investigate the effect of an annealing treatment on the electrical properties of a carbon nanocomposite. Therefore different annealing treatments are to be defined and the effect on the electrical property magnitude and their in-plane distribution is to be studied.
From the literature review in section 2.1 it can be seen that there already is extensive research on the topic of annealing carbon nanocomposites and the effect it has on the electrical properties and the resulting morphology of the composite. In literature the effect of annealing parameters such as annealing temperature, annealing time and cooling rate after annealing on the resulting electrical properties has been described in detail. In addition to that the effect of the composite crystallinity on the electrical properties has been studied by some researchers. Looking at the research results described in literature, some opportunities for further research and opposing views which require further can be identified. First of all it can be noticed that the annealing treatments described in literature mainly are for temperatures well above the melting temperature of the composite and almost any research on below melt temperature annealing has been conducted. In addition to that it has been observed that literature only focuses on the electrical property magnitude after annealing. To date no research has been conducted on the effect of annealing on the in-plane distribution of the electrical properties of injection molded composites. In terms of the cooling rate after the annealing treatment some opposing views have been identified. There is research describing that a slow cooling rate is beneficial for high electrical properties and in contrast to that other researchers indicate that fast cooling is better for the electrical properties. Related to the cooling rate after annealing some opposing view on the effect of the composite crystallinity have been found in literature. There are researchers indicating that crystallinity has negative impact on the electrical properties as it tends to break down conductive networks. In contrast to that it also has been described in literature that crystallinity tends to enhance the formation of conductive networks and thus improves the electrical properties.
Based on the short comings and opposing views identified from the state-of-the-art literature, the research questions and research objectives for the third part of this master thesis research can be formulated. In the third part of this thesis the following questions are to be answered:

Question 3.1: What is the impact of below melt temperature annealing on the electrical properties and their in-plane distribution of an injection molded nanocompsite?

Question 3.2: How are the electrical properties of an injection molded composite and their in-plane distribution impacted by the annealing time during below melt temperature annealing?

Question 3.3: How are the electrical properties of an injection molded nanocompsite effected by varying cooling rates after the annealing treatment?

Question 3.4: What impact does the below melt temperature annealing treatment have on the morphology of the injection molded nanocomposite and how does it relate to the electrical properties of the composite?

Based on these questions the main objectives of the third research part can be defined. First of all the effect of below melt temperature annealing on the electrical property magnitude and the property in-plane distribution is to be explored. In addition to that the optimal annealing time to achieve the highest improvements on the electrical properties and their in-plane distribution during below melt temperature annealing is to be found. In addition to that the opposing results on the cooling rate as found literature are to be further investigated. The objective of this research part is to understand how the electrical properties are influenced by the cooling rate used after annealing. And lastly the effect of the annealing treatment and the cooling rate after annelaing on the composite morphology is to be defined. One further objective is to create a better understanding on the effect of the composite crystallinity on the electrical properties.

Research Questions for Part 4: Dielectrophoresis on injection molded carbon nanocomposites and study of the resulting electric properties

In this section the research questions and objectives for the fourth part of the master thesis research are to be defined. The aim of this study is to investigate the effects of different dielectrophoresis treatments on the electrical properties of the carbon nanocomposite.
In literature review of this chapter 2.1 an overview on the current state-of-the-art research with respect to dielectrophoresis of carbon nanocomposites is given. It has been described that an electric field can be used to control the orientation of the CNTs in a polymer matrix and the most important factors controlling the orientation are the matrix viscosity, electric field strength and the filler loading. With respect to these parameters it has been reported that a low matrix viscosity during DEP is favourable and high electric field strengths and high filler loading's are favourable for network formation during DEP. In addition to that DEP experiments on composites have been performed indicating that upon application of a sufficiently strong electric field the CNTs tend to orient parallel to the electric field lines. From that observation it has been shown that this process can be used to improve the morphology of the composites in terms of good electrical properties.
However when looking at the research presented literature on the topic of dielectrophoresis with carbon nanocomposites some shortcomings can be identified. First of all it can be noted that the DEP experiments only have been conducted on thermoset composites during curing reactions or on thermoplastic composites well above their melt temperature. The effect of a DEP treatment on a composite below the melt temperature or slightly above the melt temperature has not been described in literature yet. In addition to that it has been observed that the current literature mainly focuses on the improvement of the percolation time due to DEP. The direct improvement of the electrical properties of the composite due to DEP have not been described yet.
Based on these shortcomings in the current research on DEP with carbon nanocomposites, the research questions and objectives for the fourth part of this thesis research have been defined. The research questions to be answered in the fourth part of this thesis report are:

Question 4.1: What effect does dielectrophoresis have on the electrical properties of a carbon nanocomposite?

Question 4.2: How are the electrical properties of a carbon nanocomposite effected by a dielectrophoresis treatment close to the melt temperature of the composite?

Question 4.3: What is the effect of the electric field strength used during dielectrophoresis on the resulting electrical properties of the carbon nanocomposite?

Based on these research questions the research objectives of the fourth part of this thesis research can be identified. First of all it is to be explored if the DEP treatment can be used to further enhance the electrical properties of the composite. In addition to that the impact of the DEP process parameters on the resulting electrical properties is to be better understood. The objective is to investigate whether a low temperature (close to the melting temperature) DEP treatment can further enhance the electrical properties. In addition to that the electric field strength needed to further enhance the electrical properties of the composite is to be defined.

3

Part 1: Study of the electrical properties of Injection Molded nanocomposites

In this chapter the dielectric and electric properties of carbon based nanocomposites produced via injection molding are to be studied. The aim of this chapter is to answer the research questions and reach the set objectives seen in chapter 2.2 with respect to the first part. In order to answer the research questions, this study entails mappings of the electric properties of the composite in order to better understand how the properties of injection molded composites are distributed. Moreover in-plane mappings of samples produced using varying injection molding settings are to be studied in order to understand the effect of the production process settings on the resulting electric property distribution. Moreover the effect of the injection molding settings on the resulting composite morphology is further investigated.
First of all the experimental procedure used during this study is described in section 3.1. This entails a definition of the composite samples, a description of the preparation of the samples and a description of the measurement set-up used to produce the mappings of the sample. This is followed by section 3.2, where the results of the experiments are presented and discussed. This entails a repeatability study, a symmetry study and a study on the effect of varying injection molding settings. In addition to that this section entails some further investigations on the composite morphology after injection molding. Lastly in section 3.3 the conclusions made from the experimental results are summarised and related to the research questions for this chapter. Moreover some recommendations for further research, based on the findings made, are given.

3.1. Experimental Procedure

In this section the experimental procedure used to study the electrical properties of injection molded nanocomposites is described. As a first step the samples used during the study need to be defined, which entails a description of the materials used and the method used for the sample production. Moreover the preparation step of the samples before being able to measure their electrical properties is described. Lastly the experimental set-up used for the electrical measurements is described.

Sample Definition

Before starting the description of the experimental procedure used during this study, the samples used during the experiments and their production process need to be defined. In terms of the production process it already has been indicated that injection molding is going to be used.
When choosing the materials to be used for the composite, the main requirement is that the polymer needs to be process able via injection molding. For the experiments in this master thesis project the

polymer matrix material is polypropylene (PP), which is a thermoplastic polymer that is widely used for injection molding. PP has been chosen as a matrix material because it is one of the most used plastic materials as it is cheap and has good overall properties. PP has a wide range of applications, ranging from the automotive industry to electrical equipment. [1]. Because of these reasons it is interesting to use PP as a matrix material for a conductive polymer in order to investigate new applications for this already widely used material.
As PP on its own is an insulating material, a conductive filler material needs to be added and thus creating a conductive composite. The filler material used for the studied composites are carbon nanotubes (CNT) as they posses a high electrical conductivity on their own (10^{-6} - 10^{-5} Ωcm^{-1}). In addition to improving the electrical properties, CNTs also lower the percolation threshold due to their large surface area and increase the mechanical properties of the composite. [5]
Now that the materials of the composite have been defined, the composition of the composite needs to be defined. From Literature the percolation threshold of CNT/PP composites made via injection molding is reported to be 3 to 3.8 wt.% of CNT [1, 5, 8]. In order to ensure that a percolated network is formed within the composite and good electrical properties can be measured a slightly higher concentration of 5 wt.% is chosen for this composite. So the final composition of the composite is 95 wt.% of polypropylene and 5 wt.% of carbon nanotubes.
Now that the types of material and the composition of the material are defined, the actual type of materials used in the composite can be identified. The composite has been produced using Plasticyl PP2001, which is a masterbatch containing 80-85 wt.% polypropylene and 15-20 wt.% of short tangled multi walled CNTs. In order to achieve the desired composition of 5 wt.% of CNTs, the masterbatch has been diluted using more polypropylene (PP DOW C705-44 NA HP).
Lastly the size of the test samples needs to be defined. The injection molded samples are rectangular plates with a length and a width of 8 cm. The sample thickness is set to be 2 mm.

Sample Preparation

Now that the material and the composition of the sample are defined, the preparation of the sample itself needs to be described. This entails a description of the production process of the sample and the preparations done in order to be able to map the electrical property distribution of the sample.

As already indicated, the composite has been produced using a masterbatch containing PP and CNTs and it needs to be diluted with more PP in order to reach the desired composition. The dilution of the masterbatch has been done via the masterbatch route. For this a twin screw extruder as been used. The components have been processed at a temperature of 210 °C, using a throughput of 12 kg/h.
After the polymer and the filler have been mixed, the injection molding process can be done in order to produce the samples. As already indicated before the effect of varying injection molding settings is to be studied. Thus samples using different injection molding settings are produced. The settings are defined in the following ways; IM1 is the normal injection molding settings as it would be normally used in industry, IM2 is an intermediate setting and IM3 is the hard setting. The difference of going from IM1 to IM3 is that the process time for production decreases by for example increasing the injection velocity. The temperature of the composite melt used during injection molding, remained the same across all three different settings, with a temperature of 210 °C
After the samples have been produced, the preparation for the electrical measurements starts. In order to make mappings of the in-plane electric property distribution of the sample, measurement locations need to be defined. The mask containing the measurement locations used can be seen in figure 3.1.

In figure 3.1 a total of 16 measurement locations can be seen, which are used for the in-plane mapping of the properties. The sample mask has been made out of printable overhead-sheets and at each measurement location a hole of 9 mm has been punched. In order to be able to make electrical measurements on the surface of the composite, the sample surfaces have been sputtered with gold. Before sputtering, the plastic sample mask has been put on top of the core-side of the composite sample. This has been done to produce the sputtered top electrodes used during the electric measurements. The cavity side of the sample has been sputtered without a mask applied. The sputtering

[1] https://www.creativemechanisms.com/blog/all-about-polypropylene-pp-plastic

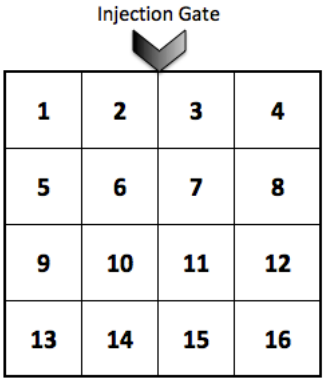

Figure 3.1: Measurement locations used for the in-plane mapping of the electric properties of the composite.

has been done using the sputter coater SCD 040 by Balzers Unions. Each side of the sample has been sputtered for 15 minutes at a current of 15 mA and an applied vacuum of at least 0.1 $mBar$.
After sputtering the sample, the sample has been cut in order to make the sample fit into the measurement set-up. The cutting was done using the boarders for each measurement location as indicated in figure 3.1. After the cutting step a total of 16 individual sub-samples have been created for measurement. An example picture for a cut and sputtered sub-sample can be seen in figure A.6.
In addition to that an additional sample has been prepared in order to further study morphology of the composite sample. In order to study the morphology, the surfaces of the sample has been removed by means of manually grinding the surface of the sample. Before the grinding process, the sample had an overall thickness between 2 mm - 1.96mm and after grinding the overall thickness is between 1.4 mm - 1.7 mm. The skin layer has been removed on both sides of the sample. The grinding has been performed in four steps in order to ensure a smooth sample surface after grinding. First of all rough grinding paper P60 is used, followed by P180, P500 and finally P2000. In between the grinding steps, the thickness of the sample has been measured in order to ensure a uniform thickness removal. After the grinding process is finished, the sample preparation (cutting and sputtering) as explained before is performed in order to prepare the grinded sample for the electrical measurements.

Electric Measurements

The measurement of the electric properties of the composite samples have been done by means of broadband dielectric spectroscopy (BDS) and for this the Novocontrol Alpha-A Analyzer has been used. During the experiments properties the following properties of the sample have been recorded: real permittivity (ϵ'), imaginary permittivity (ϵ''), conductivity (σ') and $Tan(\delta)$. All these properties have been measured over a frequency range from 1 Hz to 10^6 Hz. The measurements have been performed at room temperature (20 $^\circ C$) and no further temperature control during the measurements has been performed. The start and end conditions of the measurement have been set at an AC voltage of 1 $Vrms$.
In order ensure accurate measurement results, each sub-sample is cleaned with ethanol before the measurements. After cleaning the sub-sample, it is mounted into the sample-cell. On top of the sample a small electrode with a diameter of 10 mm has been added to ensure that the electric properties at the sputtered location are measured. An example of the loaded BDS sample cell can be seen in figure A.7. After the sub-sample has been mounted into the sample-cell, the sample-cell has been placed into a cryostat for measuring in order to protect the measurement from temperature changes and environmental noise.

3.2. Experimental Results and Discussion

In this section the experimental results and observations of the repeatability study and the study on the effect of the injection molding process on the resulting electrical properties are described.

The repeatability study has been split up into two parts. As a first step repeatability measurements on one sample have been conducted and analysed. The second part of the repeatability study entails a study of the repeatability experiments using samples from different shots, using the same IM setting. The effect of the injection molding process on the resulting electrical properties entails two main parts as well. First of all the width symmetry of the resulting electrical properties across the injection molded sample is looked at. This is followed by a detailed study on the effect of the injection molding on the electrical properties and their distribution.

3.2.1. Repeatability Study

When studying the electrical properties of injection molded nanocomposites it needs to be noticed that the injection molding process leads to varying electrical properties. The properties are not only non-uniformly distributed throughout the same composite sample but also across different injection shots (using the same IM setting) varying electrical properties at similar locations are to be expected. Thus as a first step in studying the electrical properties of injection molded composites is to make a repeatability study. Using the repeatability study it is to be defined how many measurements per location are required in order to have an accurate representation of the properties and if samples from different shots can be compared in terms of their electrical properties.

As a first step, the repeatability of the BDS measurement itself is to be investigated in order to identify the impact of the experimental procedure on the measurement results. Moreover the impact of the experimental procedure needs to be defined in order to ensure that location wise property variations are due to the variability of the injection molding process and not because of large variations of the BDS measurements. From this first step it is to be determined how many measurements are required to get an accurate representation of the electrical properties per location.
So in order to define the variation of the BDS measurements and check if location wise variations are due to the IM process, locations L1, L2 and L5 as seen in figure 3.1 each have been measured 10 times. For each measurement the same procedure, as described in section 3.1 has been followed. The variations in electrical properties have been studied by looking at the real permittivity ϵ' and σ'. The property variation due to the measurement procedure has been quantified by using the 10 measurements at each location and calculating the mean and standard deviations as seen in equations 3.2.1.

$$\overline{x_n} = \frac{1}{N}\sum_{i=1}^{N} x_i \qquad (3.1)$$

$$\sigma_x = \sqrt{\frac{1}{N-1}\sum_{i=1}^{N}(x_i - \overline{x_n})^2} \qquad (3.2)$$

The mean and standard deviation have been calculated at each frequency for each location and using these values error-bar graphs have been created. In order to check if differences in ϵ' and σ' are due to IM variability, the error-bar plots of neighbouring locations such as L1-L5 and L1-L2 have been compared for overlap. One example of the error-bar plots of both ϵ' and σ' for locations L1-L5 can be seen in figures 3.2 and 3.3.

When looking at the plot for ϵ' in figure 3.2, the difference between the two locations is large, except for the frequencies below 10 Hz. Generally no overlap between the graphs of location 1 and 5 can be seen over the whole frequency range. Looking at the repeatability data of σ' presented in figure 3.3 some overlap in the graphs can be seen. In the range from 1 to 1000 Hz the error bars of the two graphs slightly overlap. But in general it can be seen that σ' of location 1 is slightly larger than for location 5. In contrast to that for the error bar plot of σ' at locations 1 and 2 no overlap in the low frequency range has been seen. For frequency beyond 1000 Hz no more overlap between the measurement results presented in figure 3.3 can be seen.
From these observations it can be said that for further analysis, the measurements of ϵ' below 10 Hz are to be neglected as these measurements are not very accurate. Moreover it can be said that for the rest of the frequency range any or only slight overlapping properties have been found and thus the

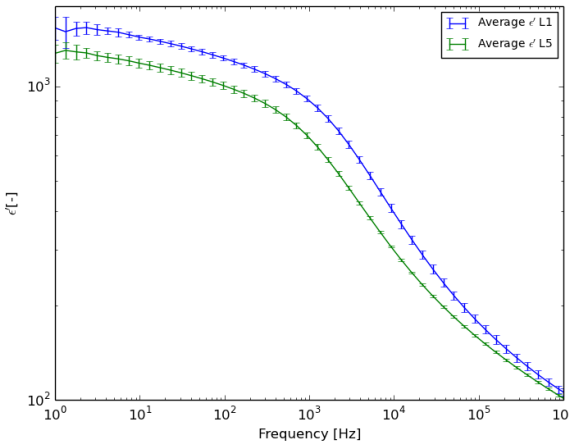

Figure 3.2: Error-bar plots of ϵ' at L1 and L5.

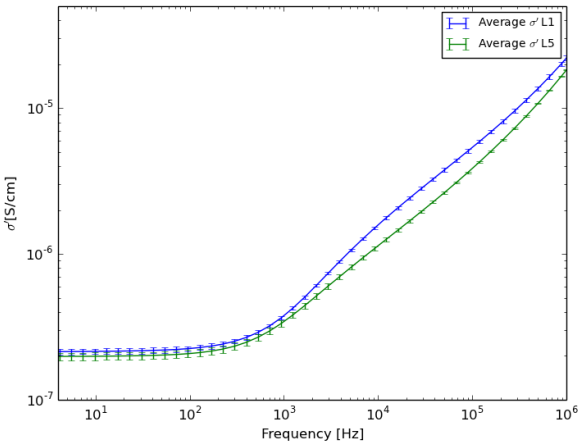

Figure 3.3: Error-bar plots of σ' at L1 and L5.

location wise property variations are due to IM effects and not due to BDS measurement variations. From the mean and standard deviation an average difference in measurement result due to repetition of the measurement has been calculated by expressing the standard deviation as a percentage of the mean. So the variability over the whole frequency range in both ϵ' and σ due to measurement repetition is within a range of $\pm$0.5-4%. From that it can be concluded that one measurement per location is sufficient to study location wise variations over the sample and when comparing the property magnitude the variability due to the measurement procedure should to be kept in mind.

The next aspect that has been looked at is the repeatability across different sample shots that have been produced using setting IM1. By looking at the electrical properties across different shots the consistency in terms of the resulting sample properties of the injection molding process can be checked. So as a first step ϵ' and the conductivity σ' for location 2 across 3 different shots from IM1 have been compared. Again each measurement has been repeated 10 times in order to account for measurement variations and from these 10 measurements the mean and standard deviation as seen in equation 3.2.1 has been determined at each frequency. The resulting error-bar plots for ϵ' and σ' can be seen in figures 3.4 and 3.5.

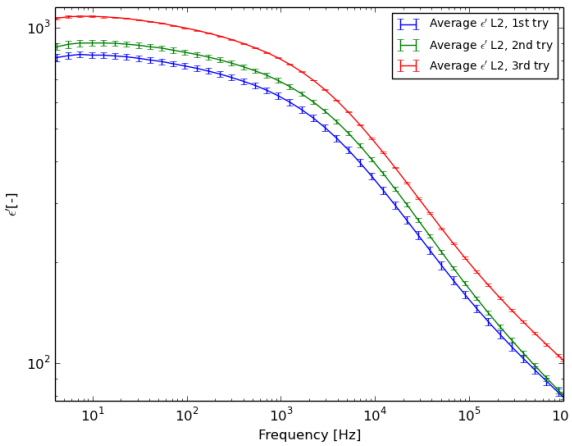

Figure 3.4: Error-bar plots of ϵ' for three different of IM1.

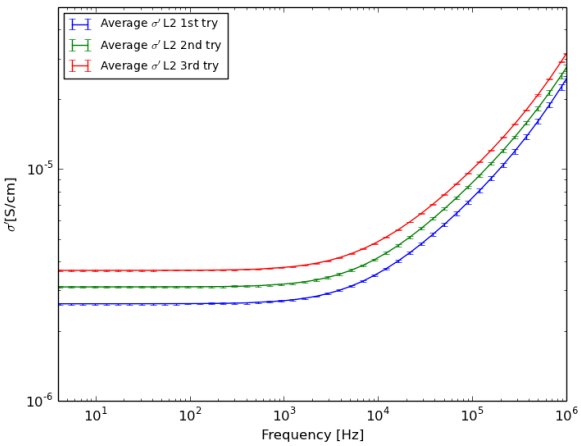

Figure 3.5: Error-bar plots of σ' for three different of IM1.

When looking at the plots shown in figures 3.4 and 3.5 it needs to be noted that the standard deviation of the measurement remains relatively constant throughout the whole frequency range. It

can be seen that for the ϵ' and σ' measurements no overlap across the three shots is found. When calculating a mean and a standard deviation for all the measurements across all three shots it found that the average difference over the whole frequency range for ϵ' and σ' is $\pm$11.5% and $\pm$13% respectively. From these measurements it can be seen that the injection molding process does not lead to uniform electrical properties across different shots. This conclusion also needs to be kept in mind for the further work presented in this thesis. When investigating the effectiveness of a heat treatment, the properties before and after the treatment are to be measured in order to accurately describe the effects of the treatment, as larger differences across sample shots are to be expected.

A further aspect that needs to be looked at is the in-plane distribution of ϵ' and σ' across three different shots produced using setting IM1. This needs to be done in order to be able to compare and distinguish differences in the in-plane property distribution due to varying IM settings and to be able to define general trends on the in-plane distribution of the electrical properties.
In order to observe the difference in the in-plane distribution across different injection shots of setting IM1, the electrical properties of three shots have been mapped according to the sample mask shown in figure 3.1. The different in-plane distributions are to be studied by visual inspection of 3D mappings of ϵ' and σ' at 127 Hz. The mappings of ϵ' at 127 Hz for the three IM1 shots can be found in figures 3.6-3.8.

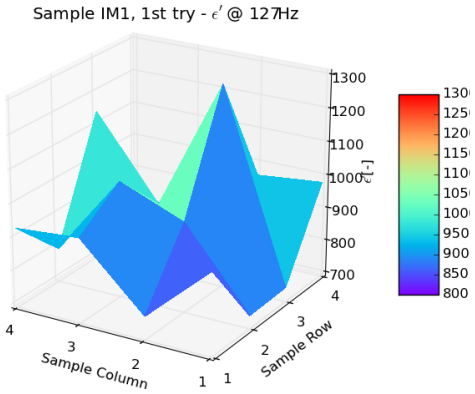

Figure 3.6: Mapping of ϵ' at 127 Hz for sample IM1 shot 1st try.

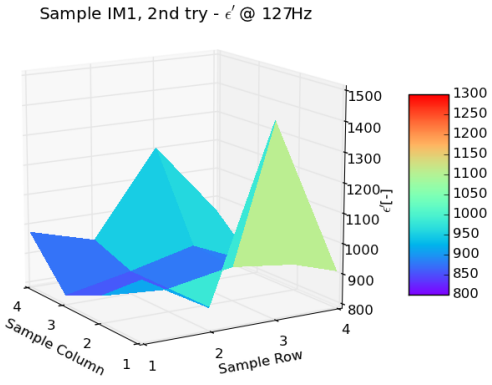

Figure 3.7: Mapping of ϵ' at 127 Hz for sample IM1 shot 2nd try.

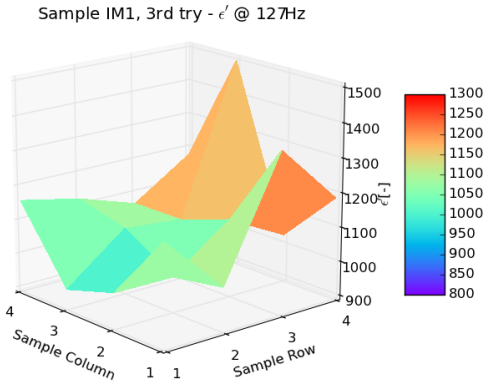

Figure 3.8: Mapping of ϵ' at 127 Hz for sample IM1 shot 3rd try.

Comparing the mappings of ϵ' at 127 Hz in figures 3.6-3.8 some differences in the in-plane distribution across different injection shots can be noticed. First of all it can be noted that the magnitude of ϵ' varies for similar locations as already indicated before in this section. With respect to the in-plane distribution it can be seen that the shots shown in figure 3.7 and 3.8 show a similar trend along the melt flow. Neglecting the location wise peaks of ϵ' it can be seen that for these two shots ϵ' tends increase in magnitude with distance to the injection gate. For the shot shown in figure 3.6 no real trend along the melt flow can be established due to large location wise variations and peaks. But from the other two mappings it can be established that ϵ' has a relatively similar in-plane distribution along the injection melt flow across different injection shots.
Similarly a mapping of the in-plane distribution of σ' at 127 Hz for the three different shots is shown in figures 3.9-3.11.

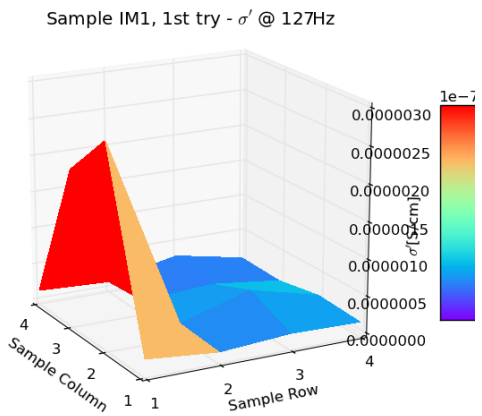

Figure 3.9: Mapping of σ' at 127 Hz for sample IM1 shot 1st try.

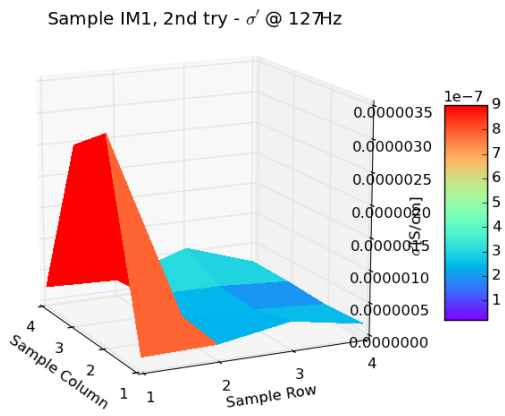

Figure 3.10: Mapping of σ' at 127 Hz for sample IM1 shot 2nd try.

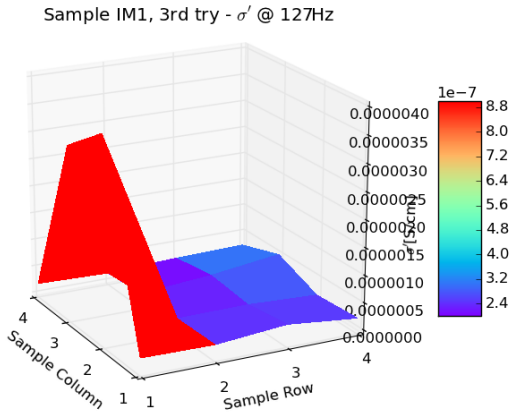

Figure 3.11: Mapping of σ' at 127 Hz for sample IM1 shot 3rd try.

Comparing the in-plane distribution of σ' at 127 Hz in figures 3.9-3.11, it can be seen that the distribution of σ' is relatively similar across the three shots. For all three shots a comparatively high magnitude of σ' is found in locations 2 and 3. Further along the melt flow it can be seen the σ' slightly increases in magnitude with increasing distance to the gate. It thus can be concluded that the in-plane

distribution of σ' across the different shots has found to be very similar.
From the observations made on the in-plane distribution of the electrical properties across different sample shots it can be concluded that the in-plane distribution across shots is not exactly the same but for samples made with equal IM settings a general trend that holds true across shots can be found. So for further studies in this thesis it can be assumed that samples produced with equal IM settings have similar in-plane distributions of their electrical properties.

All in all some conclusions on the in-plane distribution of the electrical properties of an injection molded composite can made from the findings of this repeatability study. When looking at neighbouring locations on the same sample, it can be said that the differences in electrical properties are larger than the variation in measurement result due to the experimental procedure. The measurement variability has been determined to be $\pm$0.5-4%. Thus it can be concluded that the location wise property variations are due to processing effects and only one BDS measurement is sufficient to quantify the electrical property magnitude and their in-plane distribution. Moreover the property magnitude at equal locations across different sample shots have been compared. From that it has been concluded that a large variation in property magnitude across different shots is to be expected and thus the electrical property magnitude should not be studied across samples as they are not directly comparable. Lastly the in-plane distribution of the electrical properties across sample shots have been looked at. It has been concluded that the exact in-plane property distribution varies across different shots but the general trend of the in-plane distribution is similar across different sample shots. Thus it can be be assumed for further work that samples produced with equal IM settings have similar overall electrical property distributions along the melt flow.

3.2.2. Effect of Injection Molding on the electrical properties and their distribution

In this subsection the effect of the injection molding process on the resulting electrical properties and their in-plane distribution is studied. First of all the width symmetry of an injection molded sample is investigated. Followed by a study on the effect of the injection molding settings on the resulting magnitude of the electrical properties and their in-plane distribution along the melt flow.
Before starting the discussion on the impact of the injection molding process on the resulting electrical properties and their in-plane distribution, the magnitude of the real permittivity ϵ' and conductivity σ' is looked. Looking at ϵ' and σ' is done in order to get a deeper understanding on the resulting magnitude of electrical properties and how these properties vary over the measured frequency range from 1 Hz to 10^6 Hz. In figure 3.12 and 3.13 the measured values of ϵ' and σ' for locations 7&11 in sample IM1 can be found.

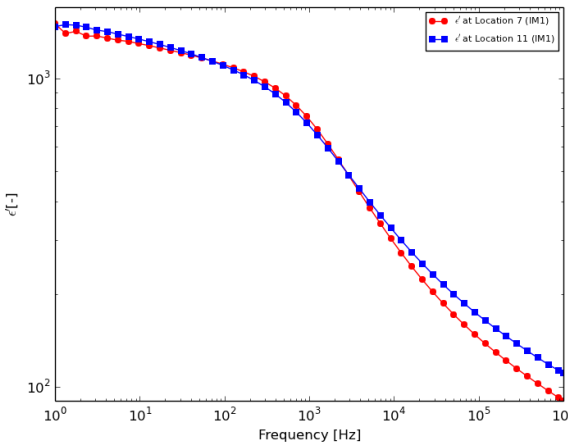

Figure 3.12: Measurement results of ϵ' at locations 7&11 of sample IM1.

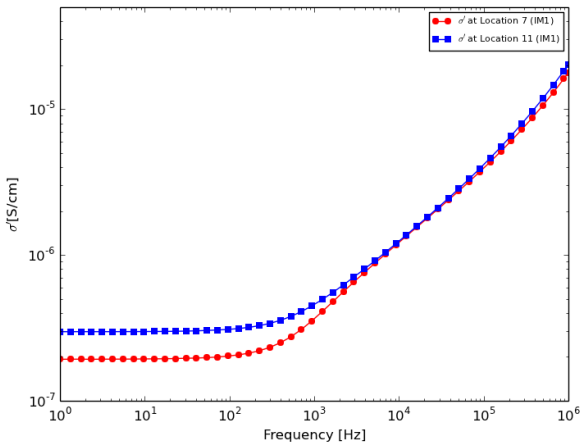

Figure 3.13: Measurement results of σ' at locations 7&11 of sample IM1.

First of all it needs to be noted that the measurement results presented in figures 3.12 and 3.13 are representative for all the samples described in this chapter. Looking at the real permittivity it can be seen that in the low frequency range from 1 Hz to 10^3 Hz, only a slight decrease in magnitude of ϵ' is seen. The magnitude at 127 Hz is 1081 and 1064 for locations 7 and 11 respectively. In this low frequency range the magnitude of ϵ' is dominated by interfacial polarisation between the CNTs [42], which represents the accumulation of charges in the interface region of the CNTs and the polymer matrix. Thus the CNTs within the polymer matrix can be regarded as microcapacitors, which enable the storage of electrical charges [42]. Beyond 10^3 Hz a stronger decrease in ϵ' is found and the lowest magnitude is recorded at 10^6 Hz with 90 and 110 for locations 7 and 11 respectively. With increasing frequencies of external AC electric field, it has been described in literature that the polarisation processes responsible for the charge storage can not follow the change in electric field and thus relaxation processes occur, which lead to a decrease in ϵ' [42].
Looking at the measurement results for the conductivity σ' it can be noticed that the conductivity remains relatively constant for the frequency range from 1 Hz to 500 Hz with a magnitude of 2.065*10^{-7} S/cm at location 7 and 3.129*10^{-7} S/cm at location 11. This is described as the (quasi-) DC-conductivity of the composite, which is not dependent on the frequency of the applied electric field [42]. In this frequency range, the DC-conductivity is mainly dependent on the resistance of the composite material and no charges flow through the insulating dielectric layer of the composite [42]. Beyond 500 Hz it can be seen that the conductivity σ' linearly increases with frequency. This increase results in a maximum conductivity of 1.784*10^{-7} S/cm and 2.026*10^{-7} S/cm at 10^6 Hz. Beyond 500 Hz the conductivity of the composite is dominated by the AC-conductivity, which is dependent on the frequency of the applied electric field [43]. The increase in conductivity with increasing conductivity is attributed to the process of space charge polarisation removal [43]. So similarly as described for the real permittivity ϵ', interfacial polarisation is the responsible process for the increase in σ'. The process of interfacial polarisation leads to the accumulation of charges in the CNT-polymer interface region and these accumulated charges move due to the changing AC-field [42]. These charge movements thus lead to an increase in σ' due to increasing frequency.
Now that the basic electric behaviour over the measured frequency range is described, the impact of the injection molding settings on the resulting electrical properties and their in-plane distribution can be studied.

Symmetry Study

As already mentioned in the literature review section for this chapter found in chapter 2.1, it has been shown by multiple researchers that the electrical properties of an injection molded sample are non-uniformly distributed along the melt flow [4, 23, 25, 26]. However it also has been indicated that there are semi-circular regions across the sample width of equal resisitivity, which would correspond to the flow lines during the injection process [23]. From this finding it has been indicated that the electrical properties in an injection molded composite sample have some form of symmetry across the width of the sample. So in order to gain a better understanding on how the electric properties are distributed within an injection molded sample, the width symmetry of the electric properties is to be studied.
As already indicated in literature, no symmetry along the melt flow direction of the injection molded sample is to be expected. Thus the symmetry study is only conducted over the width of the composite sample. For the study only one sample containing 5 wt.% CNTs produced using setting IM1 used and the symmetry over the width of the real permittivity ϵ' and the conductivity σ' is studied. Both these properties are to be studied at a frequency of 127 Hz.
Over the width of the sample there are 2 pairs of symmetric points that need to be compared. When looking at figure 3.1, it can be seen that there are outside-symmetric points such as L1-L4 and L5-L8 and there are middle-symmetric point such as L2-L3 and L6-L7. In order to study the symmetry of the electrical properties, the difference of the property magnitude of the symmetric locations is calculated as illustrated in equation 3.3.

$$Difference[\%] = \left| 100 - \frac{x_{left-side}}{x_{right-side}} * 100 \right| \tag{3.3}$$

Using equation 3.3, a small difference in property magnitude would indicate a symmetric distribution

of the electrical properties over the sample width, whereas a large difference indicates no symmetry. The differences for the outside- and middle-symmetric points for the complete composite sample can be seen in table 3.1.

Table 3.1: Differences in ϵ' and σ' at 127 Hz for symmetric locations across an IM1 sample.

Outside-Sym. Loc.	**Difference ϵ'**	**Difference σ'**
L1 - L4	2.9%	39.3%
L5 - L8	9.2%	58.6%
L9 - L12	27.8%	75.5%
L13 - L16	0.8%	8.7%

Middle-Sym. Loc.	**Difference ϵ'**	**Difference σ'**
L2 - L3	4.9%	18.6%
L6 - L7	8.3%	1.5%
L10 - L11	4.7%	29.1%
L14 - L15	31.5%	66.3%

First of all it can be noted from the mappings of ϵ' and σ' produced via setting IM1 shown in figures 3.14 and 3.17, that the electrical properties in the same row are within 1 order of magnitude. So generally no large variations in property magnitude across equal rows can be found. Based on that observation it is indicated that the electrical properties are similar in magnitude across the width of the composite sample. Moreover it is indicated in the mappings that the electrical properties are symmetrical across the width of the sample. In order to further investigate the symmetry of the electrical properties, the differences presented in table 3.1 are studied.
When looking at the differences presented in table 3.1, some observations on the width symmetry of the injection molded sample can be made. Firstly it can be noticed that the differences of the outside- and middle-symmetric locations for ϵ' are relatively small with differences of 1%-9% (except for two outliers at L9 - L12 and L14 - L15). From that it can be seen that there is some form of width symmetry for ϵ'. However when looking at the differences for σ' it can be seen that for both outside- and middle-symmetric locations, the differences are larger compared to the ϵ' differences. So the conductivity σ' is not very symmetrically distributed over the width of the composite sample, as the differences for both outside- and middle-symmetric locations mainly range from 18% to 75%. However it can be noticed that the values of σ' are somewhat similar over the width of the sample, as for the middle-symmetric locations relatively small differences of 1.5%, 18.6% and 29.1% can be seen and for the outside-symmetric locations 8.7% of difference has been measured. These relatively small differences in σ' again suggest that the conductivity is similar in magnitude over the width of the sample.
Looking at the results of the study of the width-symmetry it can be said that the real permittivity ϵ' has been found to be relatively symmetric over the width of the sample, which would be in line with the finding of regions with equal electrical properties over the width of a sample as reported by Villmow et. al. [23]. However it needs to be noticed that there have been some outlier results for ϵ', which indicated that there is no direct symmetry over the width of the sample. Moreover for the conductivity σ' larger differences over the sample width and thus no direct symmetry has been found. But some form of similarity over the width of the sample of σ' has been indicated by the measurement results. Thus it is concluded that generally the distribution of the electrical properties over the width of the sample is not directly symmetric. But the measurement results indicate that the electrical properties in the same row are similar in magnitude and thus confirms the finding of regions of equal electrical properties as described in literature [23].

Effect of Injection Molding settings

In the literature of chapter 2.1 it has been mentioned that the settings of the injection molding process have a direct influence on the resulting electrical properties of the composite. It has been indicated in literature that the injection velocity and the temperature of the composite melt are the two biggest factors influencing the resulting electrical properties [23]. In terms of the injection velocity it has been shown that higher injection speeds result in a lowering of the electrical properties [2, 4, 24] and for the the melt temperature it is said that a higher temperature is favourable good electrical properties with a uniform distribution [4]. In order to investigate the effect of the injection molding settings on the resulting electrical properties, different composite samples have been produced using varying injection molding settings (IM1, IM2, IM3), as mentioned in section 3.1. The studied conducted on these samples can be divided into two parts. At first the effect of the processing settings on the resulting

in-plane distribution of the electrical properties along the injection melt flow is studied. This is followed by a study of the location wise electrical property magnitude due to varying injection molding settings.

As a first step in studying the impact of varying IM settings on the resulting electrical properties of the composite, the impact on the in-plane property distribution along the melt flow is investigated. In the literature review of chapter 2 it already has been indicated by multiple researchers that the injection molding process results in a non-uniform distribution of the electrical properties along the injection melt flow. Moreover different findings on the in-plane property distribution have been found as some researchers found that the conductivity is higher for locations close to the gate and decreases along the melt flow [23]. Whereas other researchers found that for locations close to the injection gate a lower conductivity is found and with increasing distance the conductivity increases [4, 25, 26]. Thus in this section the resulting in-plane distribution of the real permittivity ϵ' and the conductivity σ' of an injection molded sample is to be studied in order to get a better understanding on the resulting property distribution. Moreover the effect of varying injection molding settings on the resulting property distribution is looked at.

The impact of the IM settings on the resulting in-plane distribution of the electrical properties is to be studied by means of studying the experimental data in form of 3D mappings. In order to produce the 3D mappings of the electrical properties specific frequency points have been chosen. The in-plane distribution of both ϵ' and σ' are further investigated at a low frequency point of 127 Hz because from the graphs presented in the repeatability study 3.2.1, it can be seen that in the low frequency range ϵ' displays very high values which remain relatively constant and σ' displays quasi-DC behaviour in this low frequency range. Moreover mappings of σ' in the high frequency range of 1MHz are investigated. For the high frequency range only the conductivity is studied as for high frequencies highly conductive behaviour can be seen.
First of all the mappings of the real permittivity ϵ' at 127 Hz is to be studied. The mappings of ϵ' for all three IM settings can be found in figures 3.14 - 3.16. The x- and y-axis of the 3D mappings correspond to the measurement locations described in figure 3.1. For example in the mapping the coordinated (1,1) correspond to location 1 of the sample mask.

When looking at the presented mappings of ϵ' at 127 Hz shown in figures 3.14 - 3.16, the a clear trend for the in-plane distribution from can be seen in all three mappings. The mappings show that for all three IM settings the magnitude of $\acute{\epsilon}$ tends to be smaller for locations close to the gate and an increase in magnitude is seen along the melt flow with increasing distance to the injection gate. Moreover when looking at the mappings it can be noted that the increasingly hard IM settings tend to lead to larger property non-uniformity across the rows. Looking at the first 3 rows of samples IM1 and IM2, shown in figures 3.14 and 3.15, it can be seen that the difference in property magnitude across these rows is relatively small. However when looking at figure 3.16 increasing non-uniformity across the first 3 rows of sample IM3 can be seen. Moreover it can be seen that for harder IM settings such as IM2 and IM3, that row 4 has significantly larger property magnitude compared to the first 2 rows.
In order to better quantify the increasing differences across the sample rows and in order to establish a trend on how the IM settings impact the resulting in-plane distribution of the electrical properties, the difference across the rows has been calculated. For each row the average magnitude of ϵ' at 127 Hz has been determined and the difference across rows has been calculated using equation 3.4.

$$Difference[\%] = 100 - \frac{\varepsilon_{R1/2} - \varepsilon_{R4}}{\varepsilon_{R4}} * 100 \tag{3.4}$$

When looking at equation 3.4 it needs to be noted that in order to quantify the effect of the IM settings on the in-plane distribution only the difference between Row 1&2 and Row 4 has been determined. This has been done as it has been indicated by the in-plane mappings that the difference in magnitude increases most between the rows closest and furthest away from the injection gate. Moreover it needs to be noted that a negative difference indicates that the average magnitude of ϵ' is larger in row 4 and a positive difference indicates that row 4 has a smaller property magnitude compared to the rows close to the gate. The resulting differences of ϵ' at 127 Hz across the rows due to the three IM settings used can be seen in table 3.2.

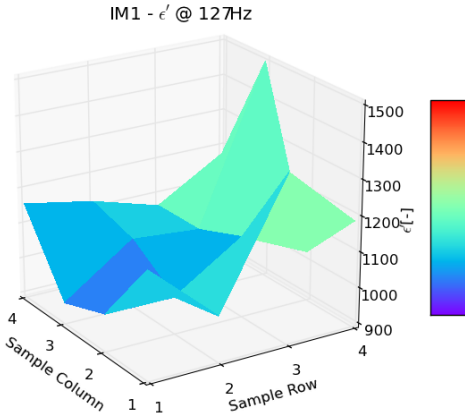

Figure 3.14: In-plane mapping of ϵ' at 127 Hz for sample IM1.

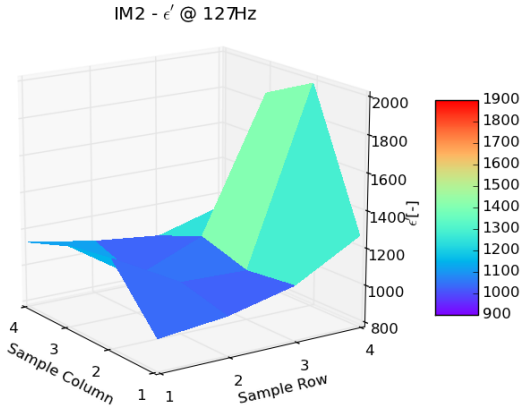

Figure 3.15: In-plane mapping of ϵ' at 127 Hz for sample IM2.

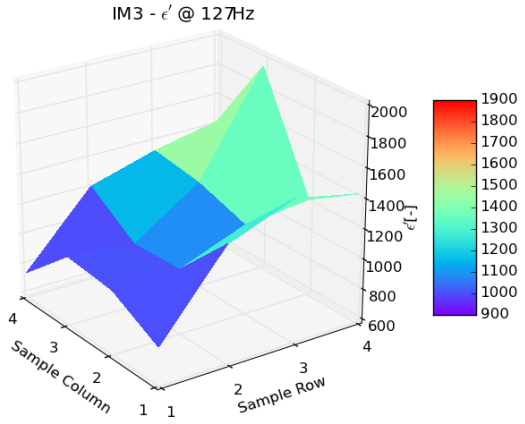

Figure 3.16: In-plane mapping of ϵ' at 127 Hz for sample IM3.

Table 3.2: Differences of ϵ'-row-averages at 127 Hz across row 1&2 and row 4 due to varying IM settings.

ϵ' **at 127** Hz	**Difference R1-R4**	**Difference R2-R4**
IM1	-13.2%	-13.8%
IM2	-27.01%	-34.6%
IM3	-40.1%	-24.4%

Looking at the differences presented in table 3.2 a clear trend on the effect of the IM settings on the in-plane distribution of ϵ' can be established. First of all it can be noted that that all the differences are negative, which indicates that $\acute{\epsilon}$ increases with distance to the injection gate. Moreover it has been determined that for the normal setting IM1 the difference across the first rows and the last row is -13.2 % and -13.8%, which indicates a relatively small property non-uniformity along the melt flow. When looking at the resulting differences for the harder IM settings it can be seen that the differences across the rows tend to increase. Moreover the largest difference of -40.1% has been found across row 1 and row 4 for sample IM3. Thus from these results it can be concluded that with respect to the in-plane

distribution of ϵ', the processing settings used have an impact on the resulting distribution. From the observations made it can be concluded that increasingly harder IM settings result in larger differences in property magnitude and thus increase the non-uniformity of the in-plane property distribution along the melt flow.
As a next step the effect of varying IM settings on the magnitude of σ' at 127 Hz and 1 MHz is investigated. The in-plane mappings of σ' at 127 Hz can be seen in figures 3.17 - 3.19 and the mappings of σ' at 1 MHz can be found in Appendix A.

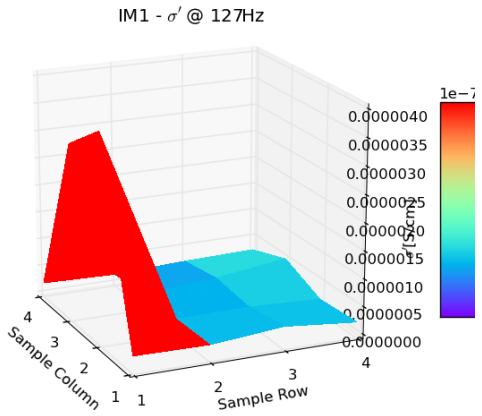

Figure 3.17: In-plane mapping of σ' at 127 Hz for sample IM1.

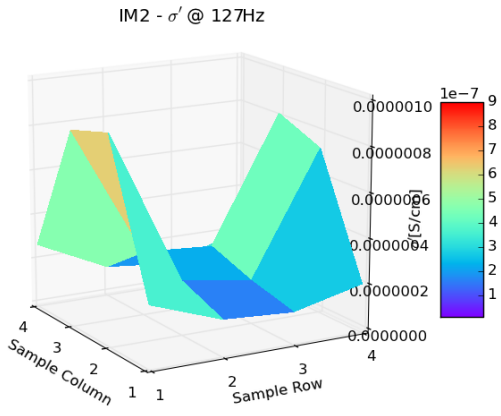

Figure 3.18: In-plane mapping of σ' at 127 Hz for sample IM2.

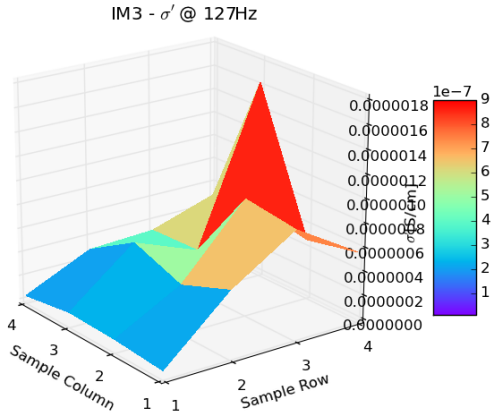

Figure 3.19: In-plane mapping of σ' at 127 Hz for sample IM3.

Looking at the mappings of sample IM1 and IM2 in figures 3.17 and 3.18 it can be seen that in row 1 very high conductivity values can be seen. For sample IM1 locations 2 and 3 have a σ' magnitude which is one order of magnitude larger than the rest of the sample. For sample IM2 again locations 2 and 3 have σ' magnitudes which are 3 to 4 times larger than for their neighbouring locations. These locally very high conductivity values can be explained due to the random nature of the injection molding process, which can lead to very well networked CNT structures. Also looking at figure 2.6 it has been indicated by researchers that for locations directly behind the injection gate a higher CNT loading can be found [2]. This increased CNT loading close to the gate can be used to explain the high conductivity at locations 2 and 3. However looking at the overall conductivity values at 127 Hz for locations close

to the gate it should be assumed that these high conductivity values of sample IM1 and IM2 in row 1 are outliers. Keeping that in mind it again can be seen that for all three mapping a non-uniform in-plane distribution of σ' is found. Similarly to the findings presented before, it can be seen that the conductivity σ' tends to be smaller for locations close to the gate and increases in magnitude along the melt flow. Moreover it can be seen from the mappings at 127 Hz, that the non-uniformity across the rows tends to increase with harder IM settings used.
Moreover when looking at the mappings of σ' at 1 MHz, shown in figures A.1-A.3 in Appendix A similar trends can be seen as in the low frequency domain. That entails that the conductivity σ' generally tends to be lower close to the gate and increases with distance to the gate and that increasing non-uniformity can be observed due to increasingly harder IM settings. When looking at the mappings at 1 MHz, it can also be seen that the conductivity in the first row of samples IM1 and IM2 is not significantly higher compared to the surrounding locations and thus should not be treated as outliers.
In order to establish a trend on how the in-plane distribution of σ' at a low and high frequency is influenced by the processing settings used, the differences across the sample rows are determined. This is done using the same procedure as explained for the premittivity ϵ' and equation 3.4. The calculated differences of σ' at 127 Hz and 1 MHz across the rows can be found in table 3.3.

Table 3.3: Difference across row 1&2 and row 4 for σ'-row-average at 127 Hz and 1 MHz.

$\acute{\sigma}$ **at 127** Hz	**Difference R1-R4**	**Difference R2-R4**
IM1	-21.2%	-26.9%
IM2	-45.4%	-61.1%
IM3	-92.2%	-45%

σ' **at 1** MHz	**Difference R1-R4**	**Difference R2-R4**
IM1	-18.6%	-42.2%
IM2	-56.4%	-63.6%
IM3	-64.5%	-58.7%

Looking at the differences presented in table 3.3, it again needs to be noted that the calculated differences at 127 Hz between row 1 and row 4 for IM1 and IM2 do not include the outlier measurements at locations 2 and 3. By omitting these outlier locations from the study, clear trends along the melt flow can be observed. For setting IM1 it can be observed that the difference at 127 Hz along the melt flow is relatively small with differences of -21.2% and -26.9%. But with increasingly harder IM settings again an increase in σ' magnitude difference along the melt flow can be observed. This again indicates that harder IM settings increase the non-uniformity of the electrical property in-plane distribution. Looking at the differences of σ' at 1 MHz across the rows again an increase in non-uniformity with harder IM settings can be observed.

Based on the observations made for ϵ' and σ' with respect to their in-plane distribution, some conclusions can be made. All in all has been established that both these properties tend to be smaller in magnitude close to the injection gate and increase in magnitude with increasing distance to the gate. This trend can be established irrespective of the IM setting used. In addition to that it can be concluded that increasingly harder IM settings lead to an increase in the non-uniformity of both ϵ' and σ' along the injection melt flow.
When looking at literature, similar results with respect to the in-plane distribution of the electrical properties can be found. In literature it also has been described that electrical properties close to the injection gate tend to be smaller and increase with distance to the gate [4, 25, 26]. The resulting electrical properties, such as the conductivity, of the composite are determined by the shear experienced by the composite melt during the injection moulding process. The CNTs in the polymer melt tend to orient parallel to the melt flow direction, if the composite melt is exposed to high shear forces and this orientation tends to decrease the conductivity [3]. During the injection molding process the highest shear forces are experienced by the melt are at the injection gate [3]. The distribution of the electrical properties can thus be explained due to the fact that cooling rate of the composite melt is highest close to the gate, when first touching the mold. This fast cooling rate results in a thick solid skin layer in which the CNT fibres are oriented in the melt flow direction, which reduces the electrical properties of the composite [25]. Moreover it has been shown that if any shear forces are applied to the melt, the CNTs tend to re-orientate and form percolated networks, hence enhancing the electrical properties [3]. Using this finding it can be explained that for locations further away from the injection gate higher electrical properties are found, as the shear forces experienced are lower.

Moreover it has been noticed in literature that varying injection molding settings (injection velocity) have an influence on the electrical property magnitude along the melt flow and thus increase the property non-uniformity along the melt flow, but the in-plane distribution trend of the properties remains the same for varying injection molding settings [4]. The increase in property non-uniformity due to increasingly hard injection settings (eg. higher injection velocities) can be explained by the shear forces experienced by the melt. The shear rate during injection molding is related to the injection velocity and higher velocities increase the shear rate [3]. Thus the increase in shear results in a higher degree of orientation of the CNTs and thus further reduces the electrical properties. This finding also is in line with the experimental results presented in this chapter.

Now that the effect of the IM settings on the resulting in-plane distribution of the electrical properties has been described, the impact of the IM settings on the location wise property magnitude is to be studied. In order to study the effect of the injection molding settings on the location wise magnitude, ϵ' and σ' at 127 Hz are looked at. For each location of the sample the percentage-wise difference in magnitude due to the varying IM settings is calculated in order to clearly quantify the effect of the IM settings on the property magnitude. The equation used to quantify the differences across the different samples can be seen in equation 3.5. When looking at the equation used to calculate the difference, it needs to be noted that the difference has been calculated using the property magnitude of sample IM1 as a reference value.

$$Difference[\%] = 100 - \frac{x}{x_{IM1}} * 100 \tag{3.5}$$

When determining differences using equation 3.5 it needs to be noticed that a negative difference indicates that the property magnitude of sample IM1 is smaller and a positive difference indicates that the IM1 sample has a higher property magnitude. As a first step the differences between the locations of the three IM samples of ϵ' at 127 Hz have been determined and studied. The magnitude of ϵ' at 127 Hz at each location and the resulting differences across the samples are presented in table 3.4.

Table 3.4: Measurement values of ϵ' and location wise differences between the IM settings at 127 Hz.

	L1	**L2**	**L3**	**L4**	**L5**	**L6**	**L7**	**L8**
ϵ' **- IM1**	1189.63	993.7	947.71	1156.21	1017.32	992.03	1081.46	1119.96
ϵ' **- IM2**	949.52	1252.63	1214.52	1130.99	986.88	1052.65	973.78	1065.7
ϵ' **- IM3**	827.46	1002.15	1035.7	741.41	1353.28	1004.26	987.27	1204.21
Difference IM2	20.18%	-26.06%	-28.15%	2.18%	2.99%	-6.11%	9.96%	4.84%
Difference IM3	30.44%	-0.85%	-9.28%	35.88%	-33.02%	-1.23%	8.71%	-7.52%

	L9	**L10**	**L11**	**L12**	**L13**	**L14**	**L15**	**L16**
ϵ' **- IM1**	1359.81	1114.89	1064.53	1064.2	1184.76	1026.95	1499.96	1175.49
ϵ' **- IM2**	1071.37	1042.01	1123.19	1026.25	1266.46	1987.43	1854.3	1127.68
ϵ' **- IM3**	1519.13	1171.19	1279.59	1332	1428.77	1220.04	1946.18	1422.94
Difference IM2	21.21%	6.54%	-5.51%	3.57%	-6.90%	-93.53%	-23.62%	4.07%
Difference IM3	-11.72%	-5.05%	-20.20%	-25.16%	-20.60%	-18.80%	-29.75%	-21.05%

Looking at the ϵ' magnitudes presented in table 3.4, it needs to be noted that these values are also used for the mappings presented in figures 3.14-3.16. Thus again looking at those values it can be seen that irrespective of the IM settings used, the resulting property magnitude is within one order of magnitude. When looking at the calculated differences it can be seen that the location wise differences are relatively spread over a wide range of differences, with values ranging from -93.53% to 30.44%. In addition to that it can be observed that differences are both positive and negative. When looking at the differences between sample IM3 and IM1 it can be observed that the differences are mainly negative, ranging between -0.85% and -33.02%. This result would indicate that harder IM settings result in overall higher ϵ' magnitudes. However this trend is not confirmed when looking at the differences between IM2 and IM1, these differences are more diverse. Thus based on the calculated differences it can be said that for the location wise magnitude of ϵ' no conclusive trend on the impact of the IM settings can be established.

The same procedure as explained for ϵ', has been performed using the measurements of σ' at 127 Hz. The measurement values of σ' and the corresponding differences can be seen in table 3.5. It again should ne noted that the σ' values presented in this table can also be seen in the mappings presented in figures 3.17-3.19.

Table 3.5: Measurement values of σ' and location wise differences between the IM settings at 127 Hz.

	L1	**L2**	**L3**	**L4**	**L5**	**L6**	**L7**	**L8**
σ' **[S/cm] - IM1**	2.5E-07	3.7E-06	3.1E-06	1.8E-07	2.3E-07	2.1E-07	2.1E-07	1.4E-07
σ' **[S/cm] - IM2**	2.6E-07	9.0-07	8.5E-07	2.6E-07	1.5E-07	2.2E-07	2.7E-07	1.1E-07
σ' **[S/cm] - IM3**	4.4E-08	7.9E-08	9.3E-08	3.0E-08	5.4E-07	3.8E-07	5.3E-07	2.8E-07
Difference IM2	-4.92%	75.71%	73.0%	-48.76%	36.17%	-5.93%	-28.33%	20.89%
Difference IM3	82.33%	97.89%	97.1%	82.97%	-136.52%	-78.67%	-157.31%	-97.98%

	L9	**L10**	**L11**	**L12**	**L13**	**L14**	**L15**	**L16**
σ' **[S/cm] - IM1**	3.4E-07	2.2E-07	3.1E-07	1.9E-07	2.1E-07	1.6E-07	4.8E-07	2.3E-07
σ' **[S/cm] - IM2**	1.2E-07	1.7E-07	2.4E-07	8.1E-08	2.0E-07	7.2E-07	8.1E-07	1.9E-07
σ' **[S/cm] - IM3**	8.8E-07	9.5E-07	3.2E-07	3.1E-07	5.6E-07	4.7E-07	1.6E-06	4.9E-07
Difference IM2	63.58%	22.12%	22.26%	58.05%	4.74%	-344.97%	-68.78%	17.43%
Difference IM3	-158.97%	-325.82%	-3.48%	-59.74%	-168.04%	-189.41%	-238.33%	-114.59%

When looking at the values presented in table 3.5, again a wide range of differences from -344.97% to 97.89% can be seen across the locations of the different samples. When trying to establish a trend of the IM settings on the resulting property magnitude, it can be recognised that there is a large variability in the magnitude of the difference. Looking at the differences between IM2 and IM1 it can be seen that the difference is mainly positive indicating that a milder process results in higher conductivity values. In contrast to that the differences between IM3 and IM1 are mainly negative indicating that harder IM settings result in higher conductivity magnitudes. Based on these results again no conclusive trend on the effect of the IM settings on the resulting magnitude of σ' can be made.
Due to the investigations made on the impact of the injection molding settings on the resulting magnitude of ϵ' and σ', it can be said that no direct influence of the injection molding settings on the resulting electrical property magnitude can be seen. This result is contrary to the findings indicated in literature, since it has been reported that extreme processing settings such as high injection speeds or low melt temperatures lead to a reduction of the electrical properties [2, 4, 24]. However it needs to be noticed that the effect of higher injection speeds on the resulting electrical properties is relatively small if filler loading's well above the percolation threshold are used [23, 24]. Since all the tested samples had a filler loading of 5 wt.% CNTs, which is well above the percolation threshold, and a high melt temperature of 210 °C has been used, only a small impact of more extreme injection molding conditions is to be expected. When looking at composites with lower filler loading's it has been shown that varying injection speeds result in larger differences in property magnitude [4]. Based on these findings described in literature, the experimental results with respect to the location wise electrical property tend to be in-line with the results described in literature.

Impact of the injection molding process on the composite morphology

In the previous part of this section it has been concluded that the non-uniform in-plane property distribution along the injection melt flow is due to formation of an insulating skin layer. It has been reported in literature that the CNT fillers in the skin layer are oriented in the melt flow direction, due to the shear forces experienced during molding [23, 25]. This inhibits the formation of conductive networks through the thickness of the sample and thus reduces the conductivity. Moreover it has been noted that the shear forces experienced by the melt become negligible towards the core of the sample [3]. Thus towards the core of the composite sample more conductive networks through the sample thickness are found [25].
In order to further prove the conclusion made on the source of the non-uniformity of the in-plane distribution of the electrical properties, the skin layer of the sample has been removed by grinding as described in the sample preparation part of section 3.1. In literature it has been described that an injection molded a low viscosity polycarbonate/CNT has a skin layer thickness close to the injection

gate of 10 μm - 17 μm [23] and in a foamed PP/CNT composite skin layer thickness of 400 μm close to the gate has been reported [25]. Based on that information a layer of 150 μm - 200 μm has been removed on each side of the sample in order to ensure the removal of insulating skin layer.
In order to study the effect of the insulating skin layer, the effect on the conductivity σ' due to the skin layer removal is looked at. In figure 3.20 the conductivity σ' of an IM2 sample at L10 before and after the skin layer removal is shown.

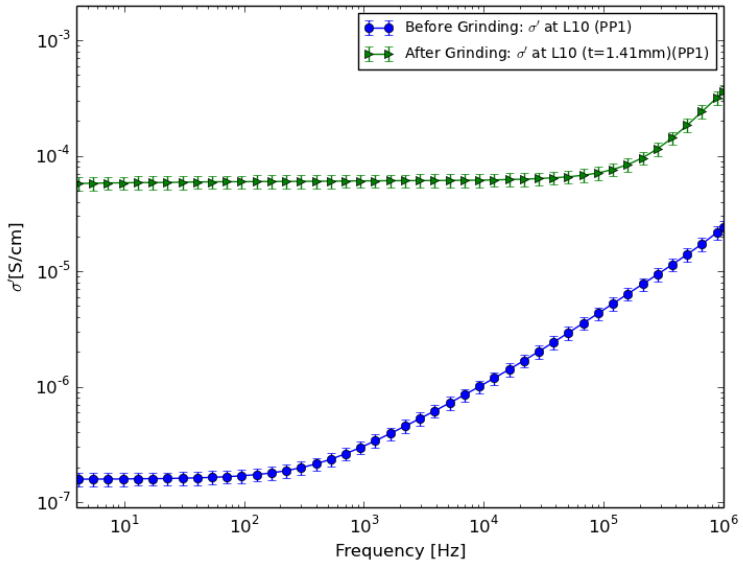

Figure 3.20: Comparison of σ' of sample IM2 at L10 before and after skin layer removal.

Looking at figure 3.20 it can be noticed that the conductivity overall improved due to the removal of the skin layer. At this location the sample after grinding had a remaining thickness of 1.41 mm, which is equal to the removal of ~300 μm at each side of the sample and thus ensures the removal of the insulating skin layer. Looking at the improvement in the low frequency range from 1 Hz to 10^3 Hz it can be seen that σ' improved by 2 orders of magnitude due to the skin layer removal. Moreover it can be seen that that the frequency range of quasi-DC-conductivity behaviour improved. Before grinding the transition to the AC-regime is at a frequency of ~400 Hz, whereas after grinding the transition starts at ~10^5 Hz. Similarly to the improvements in σ' at L10, the same change in σ' after grinding has been seen at all the other locations of sample IM2. These increases and improvements in conductivity due to the removal of the sample skin layer can be used prove for the existence of an insulating skin layer. The large overall increases in σ' indicate that towards the core of the sample more conductive networks through the thickness are formed, as indicated in literature [23, 25].
Since the conductivity improvement due to the skin layer removal proves the presence of the skin layer, the skin layer itself is to be studied in more detail. This is done by grinding one sample side to a remaining thickness of ~ 300 μm. This remaining thickness corresponds to the skin layer thickness that has been removed from each sample side when studying the electrical properties of the composite core. The resulting conductivity of the skin layer conductivity at locations 1 and 5 can be seen in figures 3.21 and 3.22.

In figures 3.21 and 3.22 the conductivity σ' of the composite skin layer is compared with the conductivity of the as injection molded sample. First of all it can be noted that the conductivity of the skin layer and the as injection molded sample are within the same order of magnitude and behave similarly with increasing frequency. However it is indicated that the difference in conductivity between the skin layer and as injection molded sample tends to increase with increasing frequency. From both figures it can be seen that the overall σ' magnitude of the skin layer is smaller than the σ' of the as injection molded sample. Compared to the σ' of the sample core, the skin layer conductivity is about 2 orders

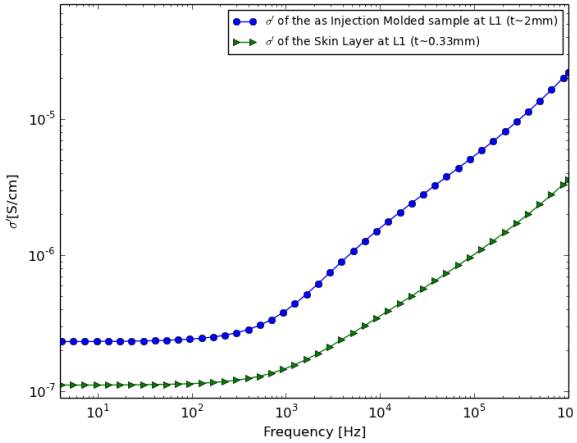

Figure 3.21: Comparison of σ' of the skin layer with the as injection molded sample at L1.

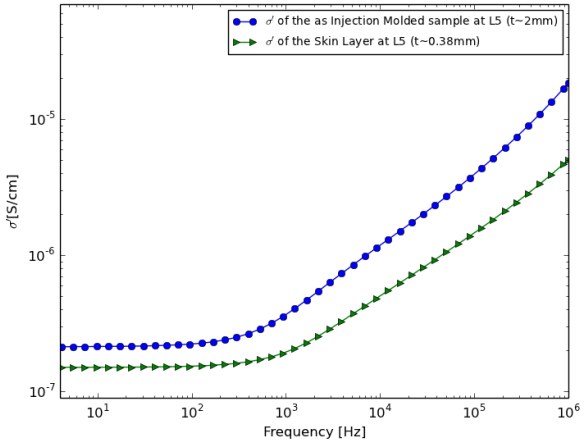

Figure 3.22: Comparison of σ' of the skin layer with the as injection molded sample at L5.

of magnitude lower. These observations again indicate the presence of a skin layer with overall lower electrical properties due to oriented CNTs in the melt flow direction. It also can be noted that the skin layer conductivity is similar to the conductivity of the as injection molded sample. It thus is expected that the BDS measurements of the conductivity are mainly dominated by the skin layer of the composite. However it also needs to be noted that the remaining thickness of $\sim 300\ \mu$m of the skin layer is still quite thick. Thus a further explanation for the similar σ' magnitude of the skin layer and the as injection molded sample might be that the sample core has not been removed entirely. Nevertheless from the observations made on the surface removal experiments it can be said that injection molding leads to the formation of a skin layer, which lowers the electrical properties, and that the core is less effected by the shear forces of the production process as higher electrical properties are found, which indicates a networked CNT morphology.
Moreover it needs to be mentioned that it has been described that the insulating skin layer tends to be thicker for locations close to the injection gate [25]. These differences in skin layer thickness are also a reason for the electrical property non-uniformity along the injection melt flow. Differences in skin layer thickness along the melt flow and thus differences in σ' are also indicated in the measurement results shown in table 3.6. In table 3.6 two locations close and far away from the gate with similar thickness after grinding are compared with respect to the resulting σ' at 127 Hz.

Table 3.6: Comparison of the skin layer thickness for Locations close and far from the injection gate.

	Location 2	**Location 14**	**Location 4**	**Location 13**
Thickness	1,57 mm	1.57 mm	1.66 mm	1.64 mm
σ' **at 127** Hz	2.47*10^{-6} S/cm	1.34*10^{-4} S/cm	1.67*10^{-5} S/cm	1.03*10^{-4} S/cm

The conductivity values at 127 Hz shown in table 3.6 indicate that skin layer thickness varies with respect to the distance to the injection gate. Comparing L2 and L14 is can be seen that the same amount of skin layer removal result in 2 orders of magnitude difference in conductivity. Similarly between L4 and L13 a difference of 1 order of magnitude in σ' can be seen. It can be observed that similar amounts of skin layer removal further away from the gate result in higher conductivity values. Moreover when looking at the σ' graphs at these locations shown in figures A.4 and A.5 it can be seen that the transition from quasi-DC behaviour to AC behaviour is different for the locations close and far from the gate. For the locations close to the gate it can be seen that the transition frequency is lower. The differences in σ' magnitude and the earlier transition to AC behaviour indicate that for locations close to the gate there are less conductive networks through the thickness of the sample. This can be explained with differences in skin layer thickness along the melt flow, as described in literature [25], where close to the gate a thicker skin layer is formed and the skin layer thickness decreases with

distance to the gate.
In order to further investigate the morphology of the injection molded composites and the effect of the skin layer on the electrical properties, the conductive behaviour is further studied. This is done by using the universal power law proposed by Jaschner [44], which describes the frequency dependent conductivity behaviour of the composite. The conductivity power law equation can be seen in equation 3.6.

$$\sigma'(f) = \sigma_{DC} + A * (2\pi f)^s \tag{3.6}$$

According to the power law relation in equation 3.6, the frequency dependent conductivity σ' is dependent on the quasi-DC conductivity σ_{DC} and on the empirical coefficients A and s [45]. It has been established that the exponent s is a measure for the degree of interaction of mobile charges with the environment [46]. It has been described by Mauritz [47] that a value of $s = 0.5$ would suggest a would suggest an imperfect microstructure, containing bad interconnection and imperfections in the conductive network. A high exponent of $s = 1$ however would suggest a microsturucture, where the conductive pathways span the whole sample dimension. For samples containing disorganised conductive pathways, such as the composites used in this discussion, exponents below 1 are generally found [46, 47]. The coefficient A has been described to reflect the local chemical-structural environment experienced by the migrating ions [47]. However it needs to be noted that the full physical meaning of the coefficients A and s has not been established yet [45].
Using the measurement data of σ', the coefficients A and s have been determined by a power law fitting. The coefficients have been determined for all the sample locations for all the three injection molding settings. The resulting exponent s from the power law fitting has been related to the distance of the measurement location to the injection gate. The resulting plots of the exponent s against the distance to the gate d can be seen in figures 3.23 - 3.25. When looking at the presented gate distances, it needs to be noted that only the melt flow distance per row has been considered (eg.: Row 1 (L1 - L4), d1 = 1.83cm).

Looking at the data points for s against the gate distance d, a linear trend is indicated and thus a linear regression is performed in order to further study the trends. From the regression analysis it can be seen that all three samples experience an increase in s with increasing gate distance. This trend is similar to the established trend for the in-plane distribution of both σ' and ϵ'. Furthermore when looking at the slopes and offsets of the linear regression curves, it can be noted that the slopes remain similar for all three IM settings. This indicates again that the IM settings do not have a direct influence on the resulting in-plane distribution of the electrical properties. The increase in s with increasing gate distance indicates that the morphology of the composite and the conductivity behaviour changes along the melt flow. Comparing the findings of Mauritz [47] with the magnitude of the exponent s found in the presented experiments, it can be said that for locations further away from the gate more conductive networks through the thickness of the sample are to be expected compared to locations close to the gate. This fact can be related to the insulating skin layer due to the injection molding process. Moreover the linear increase in s can also be used to support the finding that the insulating skin layer decreases in thickness with distance to the gate. In other words, based on the analysis of s it is expected that a lower magnitude of s represents a location with a bad conductive filler network through the sample thickness, due to a thick insulating skin layer. These locations are primarily found close to the injection gate. Whereas a high magnitude of s represents a location with a well connected conductive network through the sample thickness due to the presence of a thin skin layer, which are mainly found further away from the injection gate. In addition to the insulating skin layer, the CNT distribution along the injection melt flow as described by Wegrzyn et al. [2] needs to be considered when describing the differences in morphology along the melt flow. It has been reported that the CNT concentration tends to increase with distance to the injection gate. This increase in CNT concentration along the melt flow can also be used to explain the increasing magnitude of s with increasing gate distance, as higher CNT concentrations increase the network formation. Hence it is expected that the non-uniform electrical property distribution and the linear increase of s with distance to the gate is due to varying skin layer thicknesses and varying CNT concentrations along the melt flow. The CNT concentration along the injection melt flow is further investigated in the morphology discussion of chapter 5.2.

A further aspect that can be noticed when studying the plots in figures 3.23 to 3.25 is the change

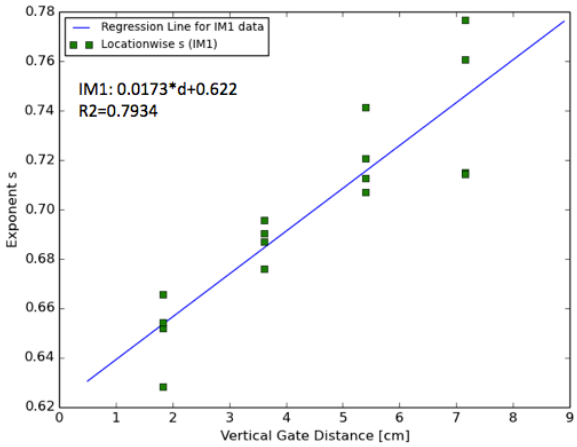

Figure 3.23: Linear Regression of exponent s against the gate distance for sample IM1.

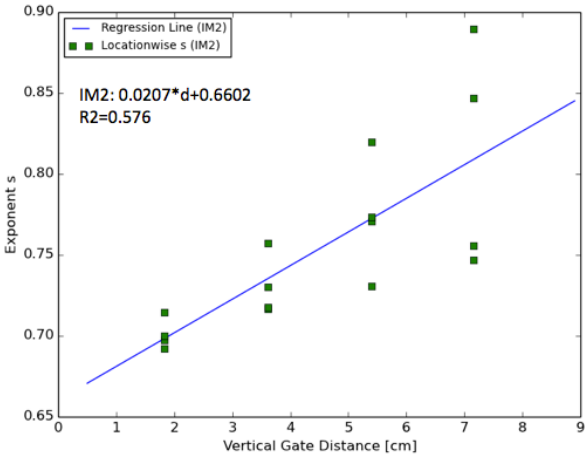

Figure 3.24: Linear Regression of exponent s against the gate distance for sample IM2.

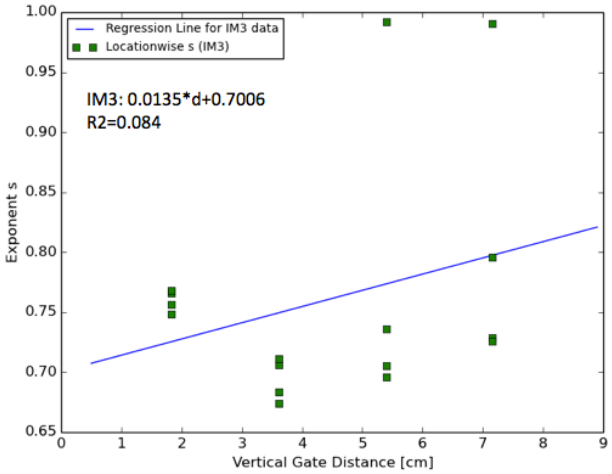

Figure 3.25: Linear Regression of exponent s against the gate distance for sample IM3.

in scatter of the exponent s due to the varying IM settings. For the normal setting IM1 a slight scattering of the exponent s over the whole sample is found and thus a relatively good regression fit with an R^2 value of 0.793 is achieved. In contrast to that the hard setting IM3 resulted in more scatted exponents s across the sample, which reflected in the R^2 value of 0.084 for the linear regression. The increase in scatter indicates that increasingly harder IM settings result in larger anisotropy in the morphology across the sample. This observation again can be used to explain the increase in non-uniformity of the electrical properties along the melt flow due to increasingly harder IM settings.
Looking at the location wise plotted exponent s in figures 3.23 - 3.25, some further observations can be made. Looking at the plotted points, some symmetry for exponents at the same gate distance (row) is indicated. In order to further investigate this observation a linear regression analysis using the exponent s per column along the injection melt flow is performed. For example column 1 corresponds to the locations 1, 5, 9 and 13 as shown in figure 3.1. The regression analysis has been performed for 4 columns across the three different injection molded samples. In table 3.7 the results of the linear regression for all three samples are summarised. The table entails the regression coefficient a, which represents the slope of the linear regression curve, the coefficient b, which is the offset of the curve and the R^2 value, which represents the goodness of the fit.

Comparing the summarised regression parameters in table 3.7 some further observations on the effect of the varying injection molding settings on the morphology can be made. First of all it needs to be noted that columns 1 and 4 and columns 2 and 3 are symmetric over the sample width. So when

Table 3.7: Regression parameters of the column wise linear regression for the three injection molded samples.

		Coefficient - a	Coefficient - b	R^2
IM1	Column 1	0.023	0.5946	0.94
	Column 2	0.0135	0.6387	0.66
	Column 3	0.0107	0.6459	0.8
	Column 4	0.0221	0.6083	0.95
IM2	Column 1	0.0312	0.6319	0.96
	Column 2	0.0062	0.6992	0.92
	Column 3	0.0128	0.6779	0.76
	Column 4	0.0328	0.6322	0.9
IM3	Column 1	0.0552	0.6096	0.65
	Column 2	-0.053	0.7455	0.2
	Column 3	-0.0074	0.7608	0.36
	Column 4	0.0115	0.6866	0.27

comparing the coefficients a and b of these symmetric columns, regions of similar morphology are indicated. For example it can be seen that the coefficients a and b of columns 1 and 4 and columns 2 and 3 for sample are similar in magnitude. Similar observations can be made for the regression coefficients of sample IM2. This observation confirms the finding of regions of similar electrical property magnitude over the width of the sample, as described in the symmetry study of section 3.2.2. Thus the regions of similar electrical properties are due to similar a morphology for locations with an equal distance form the injection gate.
However when comparing the coefficients of the hard setting IM3, larger differences in the coefficient magnitude can be seen. This again indicates that harder injection molding settings lead to larger anisotropy of the sample morphology. Thus for the hard IM setting the morphology over the sample width is not similar and no regions of similar electrical property magnitude are expected to be found. The overall increase in anisotropy of the morphology also can be observed when looking at the R^2 values of the columns wise linear regression. For settings IM1 and IM2 high R^2 values are achieved, indicating a relatively isotropic morphology across the sample. However for setting IM3 low R^2 values are found, indicating a less uniform morphology across the sample. So again it can be said that harder injection molding settings lead to anisotropy of the sample morphology. This observation again can be used to explain the increase in non-uniformity of the in-plane distribution of the electrical properties, as described earlier in this section.
All in all from the observations made on the resulting conductivity due to the removal of the skin layer and from the analysis of the exponent s, it can be said that the injection molded samples have an insulating skin layer, which varies in thickness along the melt flow. Moreover it is expected that the CNT concentration varies along the injection melt flow, which also is a reason for the non-uniform electrical property distribution. Based on that it can be concluded that the non-uniformity in electrical properties along the melt flow arises due to the insulating skin layer and varying CNT concentrations along the melt flow. Moreover it has been shown that sample morphology tends to become more anisotropic due to harder injection modling settings. Thus it is concluded that the increased electrical property non-uniformity along the injection melt flow is due to the increase anisotropy of the morphology.

3.3. Summary and Recommendations

In this section the findings on the electric properties of an injection molded composite presented in this chapter are summarised and reflected on the research questions presented in chapter 2.2. In addition to that some recommendations for further research in this area based on the results of this study are given.
With respect to research question 1.1 on the topic of how the electrical properties vary location wise within an injection molding composite sample, some conclusions have been made in this chapter. The in-plane distribution of the real perimittivity ϵ' and the conductivity σ' have been studied over the width of an injection molded sample and along the melt flow direction. When looking at the width distribution of the electrical properties within an injection molded sample, it has been shown that both

ϵ' and σ' have a similar magnitude for locations within the same row. However it needs to be noted that within a row there are some differences in property magnitude and the electrical properties are not symmetrically distributed over the sample width. For the property distribution along the melt flow it has been seen that both ϵ' and σ' tend to be smaller in magnitude for locations close to the injection gate and with increasing distance to the gate both these properties tend to increase in magnitude. So from the investigations made, it can be seen that the electrical properties within an injection molded sample are not uniformly distributed over both the width and the length of the composite sample.
The second research question, question 1.2, deals with the effect of varying injection on the resulting in-plane distribution of the electrical properties. From the experimental results presented in this chapter, it has been indicated that the injection molding settings used had no impact on the resulting in-plane distribution of the electrical properties. For all three injection molding settings used it has been seen that both ϵ' and σ' are lower close to the injection gate and larger with increasing distance to the gate. However it has been concluded that the non-uniformity of the electrical properties along the injection melt flow increases due to harder IM settings used during production.
The third research question for this chapter, question 1.3, is about the effect of varying injection molding settings on the resulting magnitude of the electrical properties. The experimental results presented in this chapter do not indicate a clear trend on the electrical property magnitude with respect to varying injection molding settings. Further research will be required in order to fully answer this research question.
Lastly the fourth research question deals with the influence of the injection molding process on the resulting composite morphology. In this chapter it has been established that during injection molding an insulating skin layer is formed on the surface of the composite sample and towards the core of the sample more conductive networks through the thickness of the sample are found. In addition to that it has been observed that the insulating skin layer varies in thickness along the injection melt flow. It has been shown that the skin layer is thicker close to the injection gate and decreases in thickness with distance to the gate. The presence of this insulating skin layer can be used to explain the non-uniform in-plane distribution of the electrical properties. A further reason for the non-uniform in-plane distribution is said to be a non-uniform CNT concentration, where the CNT concentration increases with gate distance. In addition to that it has been observed that the processing settings used have an effect on the sample morphology. It has been shown that increasingly harder injection molding settings increase the anisotropy of the samples morphology.

When looking at the conclusions made with respect to the effect of varying injection molding settings on the resulting in-plane distribution and magnitude of the electrical properties, it needs to be noted that all the samples contained a high filler loading of 5 wt.% CNTs and a high melt temperature of 210°C has been used during processing. In literature it has been indicated that more non-uniformity of the electrical properties can be seen for composites made with low temperatures [26] and it also has been indicated that injection molding parameters, such as injection velocity, only have an impact on the resulting composite properties for filler loading's close to the percolation threshold. So in order to better study the effect of varying injection molding settings on the resulting electrical property magnitude and their in-plane distribution, it is recommended for further research to use composites containing lower filler loading's or reduce the melt temperature used during the production process.
Moreover some recommendations on the mapping of the electrical properties within an injection molded sample can be given, as this research only gave an approximate trend on the in-plane property distribution. In order to get a more detailed mapping of the electrical properties the use of a finer mesh grid is recommended. Furthermore it has been indicated in literature that the electrical properties form regions of semi-circular shape, which correspond to the injection flow lines, with equal electrical properties [23]. So for further research it is recommended to use a different mesh type, such as a mesh based on polar coordinates, in order to account for these semi-circular regions. Lastly it is recommended to further investigate the resulting morphology of the injection molded sample. It has been indicated that the insulating skin layer varies in thickness along the melt flow. For further research it is interesting to measure the skin layer thickness along the injection melt flow in order to gain a deeper understanding on the in-plane distribution of the electrical properties. Moreover the conductivity has been measured on samples with a remaining thickness of ~ 300 μm. For further research it recommended to further reduce the sample thickness to ~ 200 μm to accurately determine the conductivity of the composite skin layer.

4

Part 2: Effect of the polymer matrix material on the electrical of injection molded composites

In this chapter the impact of using different polymer matrix materials on the resulting electrical properties and their in-plane distribution is studied. The aim of this chapter is to answer the research questions presented in section 2.2. In order to understand the impact of the polymer matrix material used, samples containing polymers with a different melt flow index have been produced via injection molding. Moreover these composite samples have been produced using varying injection molding settings in order to investigate if different polymer matrices are differently impacted by changing processing settings. In order to quantify the effect of the polymer matrix material used and the injection molding settings used, the location wise magnitude and the in-plane distribution of the electrical properties has been studied.
In section 4.1 a short description of the materials used, processing conditions and the experimental procedure used to study the electrical properties. This is followed by section 4.2, where the experimental results are analysed and discussed. Lastly this chapter is concluded with section 4.3 where the experimental findings are summarised and recommendations for further research are given.

4.1. Experimental Procedure

The experimental procedure used during the experiments presented in this section are the same as described in section 3.1. That means that sample preparation and the procedure used to measure the electrical properties also applies for this chapter.
In terms of the sample definition however there is a difference. In this chapter again a carbon based nanocomposite is produced via injection molding. Again the composites are made up of polypropylene and a filler loading of 5 wt.% CNTs is used. In order to study the effect of varying polymer matrix properties on the resulting electrical properties, composites containing polypropylene with different melt flow indices are used. The first composite contains polypropylene with a very high melt flow index (MFI) of 44 $g/10min$ and composites containing this polymer are referred to as PP1. Moreover it needs to be noticed that the experiments described in chapter 3 are conducted using this very high MFI polymer matrix material.
The second type composite that has been produced contains polypropylene with a low MFI of 4 $g/10min$. Composites containing the low MFI polymer are referred to as composite PP2 in this chapter.

4.2. Experimental Results and Discussion

In this section the experimental results with respect to the influence of varying polymer matrix materials on the resulting electrical properties of the composite are presented. The presentation of the results has been divided into 2 parts. As a first step a direct comparison of the electrical properties between composites containing polymers with a different MFI is done. This comparison entails a study on how the electrical property magnitude of the composite is affected by the matrix material used. The second part of this section investigates how polymer composites with a different MFI are impacted by varying injection molding settings. The impact of the injection molding settings again is studied by looking at the resulting electrical property magnitude and the in-plane distribution of the electrical properties.

Effect of the Polymer Matrix Material

First of all a look at the literature presented in section 2 with respect to the effect of the polymer matrix material used for the composite has to be made. The literature shown only described the effect of the melt viscosity during the production of the composite and in this section the effect of a varying melt flow index is studied. It needs to be noted that the melt flow index is inversely related to the melt viscosity of the polymer. That means a high MFI indicates a low viscosity and a low MFI indicates a high viscosity. Moreover it is indicated that that the MFI of the polymer is related to the molecular weight of the polymer, where a low molecular weight results in a high MFI. [1]

Having clarified the definition of the melt flow index, the effect of varying MFIs on the resulting electrical property magnitude of the composite can be studied. For this the magnitude of the real permittivity ϵ' and the conductivity σ' of composites containing PP1 and PP2 are being looked at. In order to have comparable results both the composites studied have been produced using the normal injection modling setting IM1 and both composites contain a filler loading of 5wt.% CNTs.

The effect on the magnitude of ϵ' and σ' over a frequency range from 1 Hz to 10 ^{6} Hz has been studied by comparing equal locations across the two composite samples. In figures 4.1 and 4.2 the measurement results of ϵ' at locations 2 and 14 can be seen. Moreover in figures 4.3 and 4.4 the resulting σ' magnitudes at location 2 and 14 are presented. These locations have been chosen in order to represent the impact on the property magnitude for locations close to the gate and locations far away from the gate.

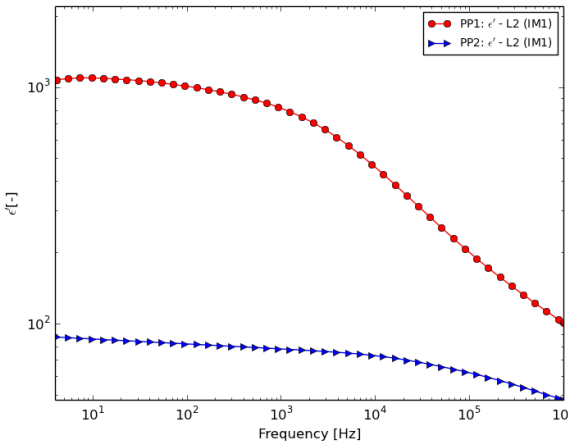

Figure 4.1: ϵ' at L2 for the PP1 and PP2 composites.

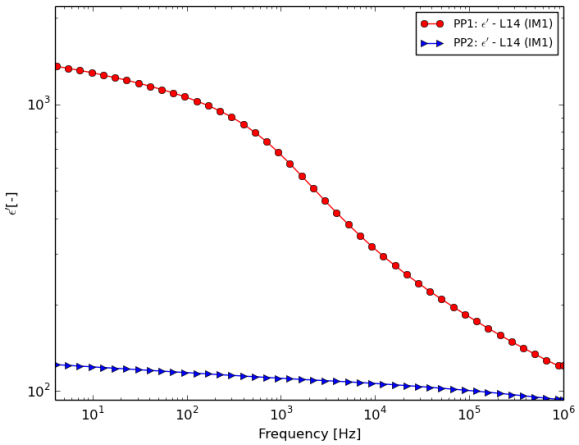

Figure 4.2: ϵ' at L14 for the PP1 and PP2 composites.

Firstly looking the measurement results of the real permittivity ϵ' shown in figures 4.1 and 4.2 some differences between the two polymer matrix materials can be seen. Over the whole measured frequency range it has been found that the high MFI polymer PP1 has higher ϵ' values compared to

[1] https://en.wikipedia.org/wiki/Melt_flow_index

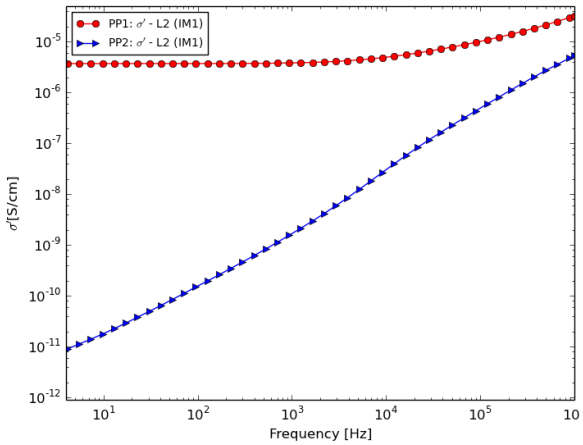

Figure 4.3: σ' at L2 for the PP1 and PP2 composites.

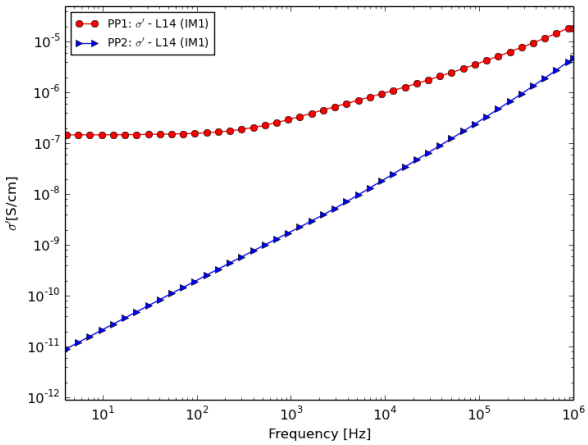

Figure 4.4: σ' at L14 for the PP1 and PP2 composites.

the PP2 composite. The difference in the low frequency domain, at 127 Hz is higher compared to the difference in magnitude in the high frequency domain at 1 MHz. For frequencies around 127 Hz for both locations shown, the PP1 composite has a ϵ' which is one order of magnitude larger than the ϵ' of the PP2 composite. At 1 MHz this difference is smaller and it has been found that the PP1 composite has a ϵ' magnitude which is 111% and 31% larger than the magnitude of the PP2 composite at locations 2 and 14.

Similarly when looking at figures 4.3 and 4.4, some differences in σ' of the PP1 and PP2 composite can be noticed. First of all it can be seen that the conductivity of the PP2 composite does not show quasi-DC behaviour in the low frequency range. The measurement data shows that the PP2 composite exhibits dielectric behaviour over the whole frequency range. Moreover it can be seen that in the low frequency range very high differences in the magnitude of σ' can be found. At a frequency of 127 Hz, the PP1 composite exhibits quasi-DC behaviour and the magnitude of σ' is 4 to 5 orders of magnitude larger compared to the PP2 composite. Towards higher frequencies this difference tends to decrease as the PP1 composite also starts to show dielectric behaviour. At a frequency of 1 MHz, the magnitude of σ' only is 1 order of magnitude larger compared to the PP2 composite.

When comparing the differences in electrical property magnitude at the two locations shown, it can be said that the lower MFI polymer resulted in smaller electrical properties irrespective of the distance to the gate. However the effect of injection molding using a low MFI polymer is further explored in the second part of this section.

Based on the observations made with respect to the measurement data shown before, some conclusions on the effect of the polymer matrix material on the resulting electrical properties can be made. From the measurements it has been shown that a higher melt flow index polymer is beneficial in terms of high overall electrical properties. This indicates that using a high MFI polymer leads to a more favourable microstrucutre in terms of high electrical properties. When talking about injection molding it needs to be noticed that shear flow is the dominant mode of flow during processing [3]. Moreover it needs to be mentioned that the shear stress experienced by the composite melt is related to the product of the viscosity and the shear rate [3]. Thus a higher viscosity/lower MFI leads to an increase in the shear stress experienced during production of the composite. This increase in shear rate has a direct effect on the resulting composite morphology. It has been reported that higher shear stresses during injection molding lead to an orientation of the CNT fillers in the melt flow direction, which leads to a reduction of the electrical properties [3, 23]. This reduction in electrical properties due to the orientation of the CNTs can be explained due to the fact that less conductive networks are formed. In addition to the orientation of the CNTs, the viscosity/MFI of the composite also has an impact on the dispersion of the CNTs. Increased shear rates lead to higher dispersion of the CNTs within the composite sample and in addition to that higher shear stresses tend to lead to fibre breakage [3]. In the literature review of chapter 2, it already has been indicated that highly dispersed CNTs are not favourable in terms of high electrical properties as it leads to larger distances between the CNTs and

thus less conductive networks are formed. Breakage of the CNT fibres further enhances the reduction of conductive network formation.
Based on that it can be said that the findings in literature support the conclusion that a high MFI polymer leads to overall better electrical properties. Based on the knowledge presented in literature, it is expected that the CNT fibres in the low MFI composite are highly oriented along the injection melt flow and well dispersed and thus less conductive networks are formed, which leads to the reduction electrical properties. However further investigations into the resulting morphology of the low MFI composite are to be made in order to make a conclusion on the resulting composite microstructure and its effect on the electrical properties. The morphology of the low MFI composite is further investigated at the end of this section.

Effect of varying injection moldig settings

When looking at the presented effects of varying injection molding settings on the resulting electrical properties of the composite, it needs to be noted that in this chapter only experimental results of composites containing the low MFI polymer PP2 are shown. The experimental results studying the effect of varying injection molding settings on composites containing the high MFI polymer PP1 are shown in section 3.2.
From the experimental results presented before it already has been indicated that a lower MFI composite leads to overall lower electrical properties and that higher shear stresses are experienced by the composite melt during processing. Hence it has been further investigated how the electrical properties and their in-plane distribution are impacted due to varying injection molding settings.
The first aspect that is being investigated is the resulting in-plane distribution of ϵ' and σ' of the low MFI composite and how the in-plane distribution is impacted by the injection molding settings. In chapter 3 it already has been established that when using a high MFI polymer matrix material, the electrical properties are non-uniformly distributed along the melt flow. Where locations close to the gate generally have smaller property magnitudes compared to locations further away from the gate. Moreover it has been shown that increasingly harder IM settings result in larger property non-uniformity along the injection melt flow.
In order to study the electrical property in-plane distribution, 3D-mappings of the measurements of ϵ' and σ' are to be looked at. The mappings have been produced on the basis of the sample mask shown in figure 3.1. The in-plane distribution of ϵ' is studied at a frequency of 127 Hz and the resulting mappings can be seen in figures 4.5 - 4.7.

The mappings of ϵ' presented in figures 4.5 - 4.7 show a similar in-plane distribution for all three IM settings. For all three IM settings it is indicated that ϵ' is smaller close to the injection gate and increases in magnitude with increasing distance to the gate. Upon closer inspection of the ϵ' mappings it can be noticed that the magnitude of the permittivity in row 4 increases with increasingly harder IM settings. For settings IM1 shown in figure 4.5, the magnitude of ϵ in row 4 is within the range of 115-147. Whereas for setting IM3 shown in figure 4.7, the magnitude of ϵ' in row 4 is in the range of 170-218. This thus indicates that changing IM settings result different in-plane distributions for ϵ'. Moreover it needs to be mentioned that similar observations on the in-plane distribution of ϵ' at 127 Hz have been made for the samples containing the high MFI polymer PP1. This thus indicates that the polymer matrix material does not influence the resulting in-plane property distribution of ϵ'.
In order to further investigate the effect of the IM settings on the in-plane distribution, the differences across locations close to the gate and far away from the gate have been determined. This has been done using equation 3.4, which calculates the difference between the row averages of ϵ' at 127 Hz in row 1/2 and row 4. The resulting differences can be found in table 4.1. When looking at the presented differences, it needs to be noted that negative differences indicate that the average magnitude of ϵ' in row 4 is larger compared to the average magnitude in row 1/2.

Comparing the differences in ϵ' across the rows close to the gate and far away from the gate in table 4.1, it can be seen that harder injection moldig settings result in larger differences across the rows. For IM1 a difference in the range of -38% between row 1/2 and row 4 is found, whereas for IM3 the difference is in the range of -50%. These results indicate that harder IM settings result in a larger non-uniformity in ϵ' along the injection melt flow. These results are also very similar to the

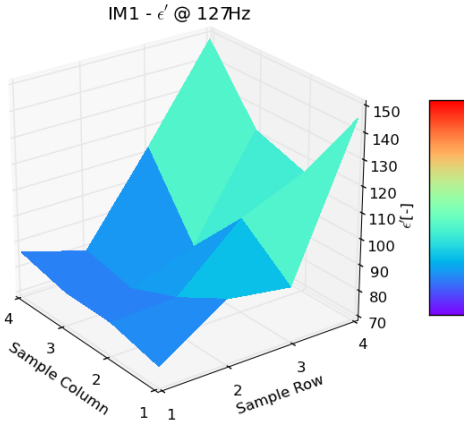

Figure 4.5: Mapping of ϵ' at 127 Hz for sample IM1 containing PP2.

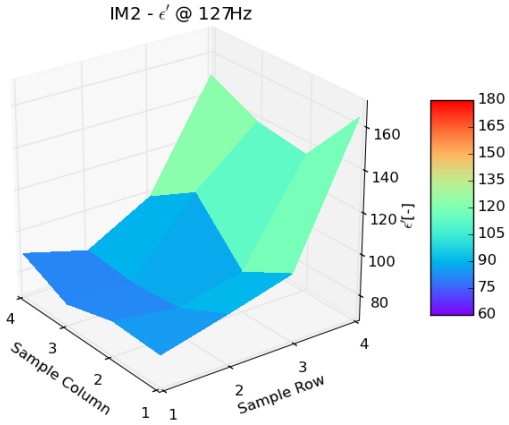

Figure 4.6: Mapping of ϵ' at 127 Hz for sample IM2 containing PP2.

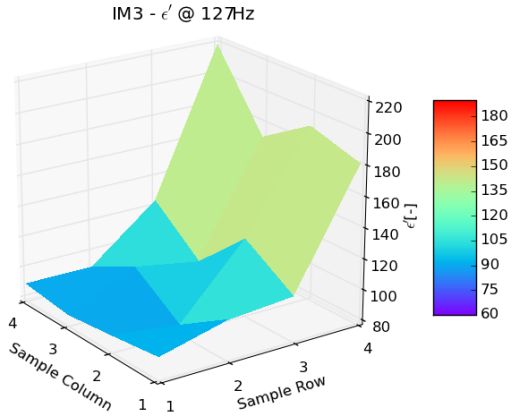

Figure 4.7: Mapping of ϵ' at 127 Hz for sample IM3 containing PP2.

Table 4.1: Differences of ϵ'-row-averages of the PP2 samples at 127 Hz across row 1&2 and row 4 due to varying IM settings.

ϵ' **at 127** Hz	**Difference R1-R4**	**Difference R2-R4**
IM1	-38.4%	-37.8%
IM2	-42.6%	-43.5%
IM3	-53.3%	-50.0%

differences of between the rows of the PP1 composite, shown in table 3.2. Both the differences of the PP1 and PP2 composite show similar trends with increasingly harder IM settings are within a similar range of magnitude. From that it can be concluded that the impact of the IM settings on the in-plane distribution of ϵ' is not influenced by the MFI/viscosity of the polymer used during injection molding. In addition to the permittivity ϵ', the in-plane distribution of the conductivity σ' is looked at. Mappings of σ' at 127 Hz can be seen in figures 4.8 - 4.10 and in addition to that mappings of σ' at 1 MHz are shown in figures B.1 - B.3 in Appendix B.

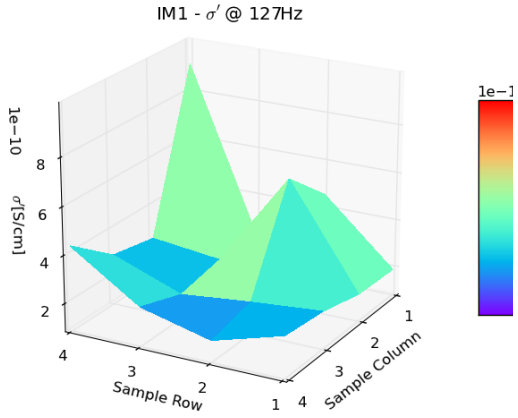

Figure 4.8: Mapping of σ' at 127 Hz for sample IM1 containing PP2.

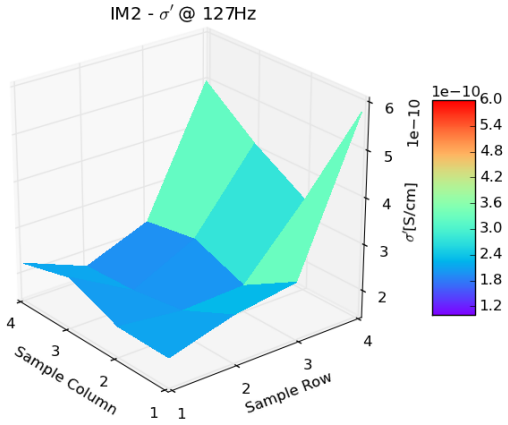

Figure 4.9: Mapping of σ' at 127 Hz for sample IM2 containing PP2.

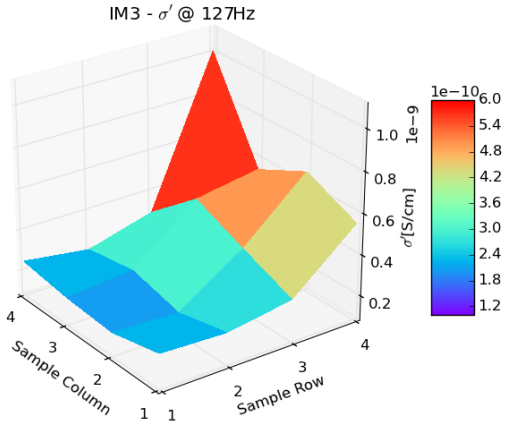

Figure 4.10: Mapping of σ' at 127 Hz for sample IM3 containing PP2.

Looking at the in-plane mappings of σ' at 127 Hz some observations can be made. The in-plane distribution of sample IM1 shown in figure 4.8 indicates only a slight non-uniformity along the injection melt flow. The mapping indicates that σ' tends to be slightly smaller in magnitude close to the injection gate and a bit larger far away from the gate. In contrast to that the samples IM2 and IM3 shown in figures 4.9 and 4.10 larger non-uniformity is found. For both these samples it can be clearly seen that the conductivity increases with distance to the gate. Similar observations can be made when investigating the mappings of σ' at 1 MHz shown in Appendix B. Comparing the in-plane mappings of σ' of the samples containing PP1 and PP2 it can be said that similar in-plane distributions of σ' are found for both polymer matrix materials.
Based on the observations made on the in-plane mappings of σ', the effect of the IM settings on the resulting in-plane distribution is further studied. Similarly as for ϵ', the differences in magnitude of σ' row averages for rows 1/2 and row 4 have been determined using equation 3.4. The resulting differences across the rows for frequencies 127 Hz and 1 MHz can be found in table 4.2.

Looking at the differences in σ' between the rows close to the gate and far away from the gate it again can be seen that harder IM settings result in larger differences across the rows. Looking at the

Table 4.2: Difference across row 1&2 and row 4 for σ'-row-average at 127 Hz and 1 MHz.

$\acute{\sigma}$ **at 127** Hz	**Difference R1-R4**	**Difference R2-R4**
IM1	-53.3%	-22.7%
IM2	-51.3%	-57.2%
IM3	-66.9%	-68.6%

σ' **at 1** MHz	**Difference R1-R4**	**Difference R2-R4**
IM1	-8.9%	-17.3%
IM2	-22.0%	-41.3%
IM3	-34.9%	-51.1%

differences between row 2 and row 4 for σ' at 127 Hz it can be seen that for IM1, row 4 is 22.7% larger than row 2. But this difference increases to 68.6% for setting IM3. Similar trends can be observed when looking at the row differences for σ' at 1 MHz shown in table 4.2. Based on these results it can again be concluded that for the conductivity σ' of the samples containing a low MFI polymer, harder IM settings result in a larger non-uniformity of the in-plane distribution along the injection melt flow. Moreover the differences across rows due to varying IM settings of the PP2 composite can be compared to the differences of the PP1 composite shown in table 3.3. Comparing these differences it can be seen that for both composite samples similar effects on σ' due to the IM settings can be seen. Moreover it can be noticed that for both composite samples the increase in non-uniformity due to harder IM settings is within the same range of magnitude. Thus it can be said that irrespective of the polymer matrix material used, the impact of the IM settings on the resulting in-plane distribution of σ' remains the same.
All in all it can be concluded that for the composite samples containing a low MFI polymer a non-uniform in-plane distribution of both ϵ' and σ'. For both these properties it has been observed that the magnitude tends to be smaller for locations close to the gate and an increase in magnitude is found along the melt flow. Similarly to the conclusion made on the in-plane distribution of the high MFI samples in chapter 3, it is expected that non-uniform property in-plane distribution is due to the formation of an insulating skin layer for locations close to the gate [25]. During injection molding shear forces are experienced by the melt, which tend to orient the fibres in the melt flow direction and thus reduce the electrical properties [3]. And it has been pointed out that locations close to the injection gate experience higher shear forces during the production process [3]. So when first touching the mold, the melt experiences a fast cooling rate [25], which freezes the oriented fibres and thus the insulating skin layer is formed.
Moreover it has been shown that the in-plane distribution of both these properties is effected by the IM settings used. It has been shown that harder IM settings result in larger property non-uniformity along the melt flow. Lastly it has been shown that the resulting in-plane distribution of the electrical properties and the effect of the IM settings on this distribution is the same for composites containing low and high MFI polymers. It thus can be concluded that the MFI of the composite has no impact on the resulting in-plane distribution of the electrical properties of an injection molded composite.

In addition to the in-plane distribution, the effect of the injection molding settings on the location wise electrical property magnitude of the low MFI composites is studied. In literature review section 2.1 it already has been pointed out that harder IM settings in terms of higher injection velocities lead to an overall lowering of the electrical properties. So similarly to the study on the location wise electrical property magnitude due to varying IM settings shown in chapter 3.2, the location wise magnitude of ϵ' and σ' of the low MFI composites is to be studied. During this study, both these properties are studied at a frequency of 127 Hz. In order to quantify the differences in magnitude due to varying IM settings equation 3.5 is used. The equation is used to calculate the difference between the electrical properties, using the magnitude of the IM1 sample as a reference value. Again when studying these differences it needs to be mentioned that a negative difference indicates that the property magnitude of IM1 is smaller and a positive magnitude shows that the IM1 property magnitude is larger. So as a first step the impact of the IM settings on the location wise magnitude of ϵ' at 127 Hz is studied. The corresponding magnitudes of ϵ' for samples IM1 - IM3 and the differences can be seen in table 4.3.

When looking at the presented differences for ϵ' across the three different samples, presented in table 4.3, a wide range of differences is found. The difference between IM2 and IM1 ranges between -36.16% and 16.4% and the differences between IM3 and IM1 range from -65.8% to -0.64%. The first thing that can be noticed is that the calculated differences are mainly negative, indicating that

Table 4.3: Measurement values of ϵ' and location wise differences between the IM settings at 127 Hz for the low MFI composites.

	L1	**L2**	**L3**	**L4**	**L5**	**L6**	**L7**	**L8**
ϵ' **- IM1**	76.83	81.45	81.76	86.19	93.5	82.55	74.7	78.62
ϵ' **- IM2**	84.0	85.12	78.73	89.57	92.1	80.5	78.5	80.91
ϵ' **- IM3**	92.61	88.55	85.0	89.0	103.61	83.1	104.77	88.931
Difference IM2	-9.33%	-4.5%	3.72%	-3.93%	1.48%	2.47%	5.1%	-2.91%
Difference IM3	-20.54%	-8.7%	-3.96%	-3.28%	-10.86%	-0.64%	-40.29%	-13.11%

	L9	**L10**	**L11**	**L12**	**L13**	**L14**	**L15**	**L16**
ϵ' **- IM1**	89.61	104.84	83.11	112.25	145.1	115.1	121.6	147.82
ϵ' **- IM2**	100.84	87.64	113.16	98.3	164.34	134.84	138.5	149.95
ϵ' **- IM3**	107.1	127.9	97.2	123.2	180.76	190.82	170.2	218.24
Difference IM2	-12.53%	16.4%	-36.16%	12.44%	-13.28%	-17.17%	-13.9%	-1.44%
Difference IM3	-19.5%	-22.0%	-16.95%	-9.74%	-24.6%	-65.8%	-40.0%	-47.64%

harder IM settings lead to higher ϵ' magnitudes. Moreover it has been noticed that the hard setting IM3 leads to generally higher ϵ' magnitudes for all sample locations. Based on these observations it can be said that for the low MFI composites, increasingly harder IM settings lead to higher ϵ' values. Next to the location wise magnitude of the real permittivity ϵ', the conductivity σ' at 127 Hz has been studied. The corresponding magnitudes and differences across the samples can be found in table 4.4.

Table 4.4: Measurement values of σ' and location wise differences between the IM settings at 127 Hz for the low MFi composite.

	L1	**L2**	**L3**	**L4**	**L5**	**L6**	**L7**	**L8**
σ' **[**S/cm**] - IM1**	1.9E-10	1.96E-10	2.4E-10	2.6E-10	4.6E-10	6.2E-10	2.1E-10	1.7E-10
σ' **[**S/cm**] - IM2**	2.0E-10	2.0E-10	2.5E-10	2.2E-10	2.4E-10	1.9E-10	1.7E-10	1.7E-10
σ' **[**S/cm**] - IM3**	2.5E-10	2.0E-10	2.1E-10	2.5E-10	2.4E-10	1.8E-10	2.4E-10	2.0E-10
Difference IM2	-7.71%	-5.67%	-5.41%	-13.29%	46.36%	69.14%	18.52%	2.17%
Difference IM3	-33.23%	-0.53%	10.28%	3.28%	47.49%	70.65%	-13.18%	-18.02%

	L9	**L10**	**L11**	**L12**	**L13**	**L14**	**L15**	**L16**
σ' **[**S/cm**] - IM1**	2.2E-10	2.2E-10	1.8E-10	2.4E-10	9.1E-10	2.5E-10	2.9E-10	4.3E-10
σ' **[**S/cm**] - IM2**	2.6E-10	1.9E-10	2.4E-10	2.2E-10	5.7E-10	3.4E-10	4.1E-10	5.0E-10
σ' **[**S/cm**] - IM3**	2.9E-10	3.9E-10	4.5E-10	2.9E-10	5.5E-10	6.6E-10	5.4E-10	1.0E-10
Difference IM2	-19.35%	10.71%	-31.58%	9.0%	36.65%	-33.15%	-40.7%	-13.62%
Difference IM3	-29.83%	-75.6%	-169.11%	-18.61%	-39.47%	-160.0%	-87.4%	-130.17%

Again when looking at the differences in σ' shown in table 4.4, a wide range of differences can be seen. It also can be noted that all the presented σ' values are within one order of magnitude. The differences between the IM2 and IM1 location ranges from -40.7% to 69.14%. But the location wise difference between these samples mainly is negative, which indicates that the harder setting IM2 leads to higher magnitudes of σ'. Similarly for the differences between IM3 and IM1 a range from -169.11% to 70.65% can be seen. But again it needs to be said that the difference across these two sample mainly is negative, indicating that the hard setting IM3 leads to higher conductivity magnitudes. When looking at the presented magnitudes of σ' it is indicated that increasingly harder IM settings lead to higher values for σ'.
So based on the observations made for ϵ' and σ' it can be said that increasingly harder injection molding settings lead to higher property magnitudes, irrespective of the measurement location. This finding stands in contrast with the findings presented in literature, as it has been reported that harder IM settings tend to decrease the electrical properties [2, 4, 24], since harder IM settings lead to higher shear forces experienced by the melt [23]. Comparing these results with the effect of IM settings on the location wise electrical property magnitude of the high MFI composite, shown in chapter 3.2, some similarities can be found. For the high MFI samples it also has been indicated that harder settings lead to higher property magnitudes. But this trend has not been directly confirmed due to larger diversity in the differences. Based on that it is expected that the location wise magnitude of ϵ' and σ' for both the high and low MFI responds similar to varying IM settings. For both these composites it has been

indicated that harder IM settings tend to increase the electrical property magnitude across the whole sample.

Impact of the injection molding process on the composite morphology

In the previous section it has been concluded that the non-uniform in-plane distribution of the electrical properties of the low MFI composite is due to the formation of an insulating skin layer and a non-uniform CNT concentration along the melt flow. In literature it has been reported that the responsible shear forces for the formation of the insulating skin layer diminish towards the core of the sample [3] and thus more conductive networks are found in the core of the composite sample [25]. This finding has been confirmed by the grinding experiments presented in chapter 3, as due to the removal of the skin layer increases of up to 2 orders of magnitude in σ' of the high MFI composite have been reported.
So in order to study the effect of the insulating skin layer on the electrical properties of the low MFI composite, this layer has been removed by manually grinding the surface of the sample. The grinding procedure used for the skin layer removal is the same as described in the experimental section 3.1. Before grinding the samples had a thickness in the range of 2 mm - 1.96 mm and after grinding the thickness ranges from 1.7 mm - 1.4 mm. So on each side of the sample a thickness between 150 μm - 300 μm has been removed, which should be sufficient to remove the insulating skin layer based on the observations made in literature [23, 25] and in chapter 3.2.
So in order to further study the effect of the skin layer of the PP2 composites, the location wise conductivity σ' has been studied. In figure 4.11 the conductivity of an IM2 sample at location 10 before and after the grinding process is shown.

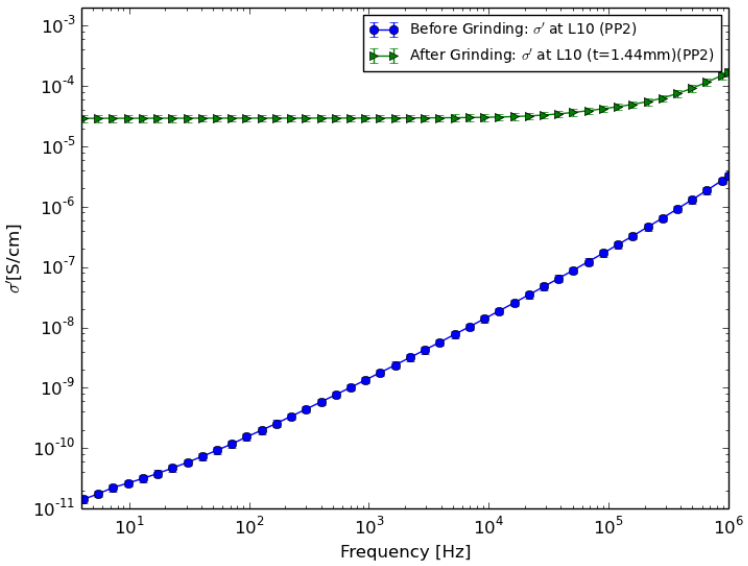

Figure 4.11: Comparison of σ' of sample IM2 with PP2 at L10 before and after skin layer removal.

Comparing the resulting σ' measurement results before and after surface removal of 280 μm on each side of the sample large differences in magnitude can be seen. In the low frequency range improvements of 6 orders of magnitude can be seen. Moreover it can be noticed that due to the removal of the surface layer the conductive behaviour switched from frequency dependent AC-conductivity behaviour to quasi-DC behaviour for a frequency range of 1 Hz to 4*10^4 Hz. These changes in the magnitude of σ' and difference in conductive behaviour over the whole frequency range show that due to the injection molding process an insulting skin layer is formed, which for the low MFI composite leads to a significant reduction in electrical properties. The large improvement in σ' after the skin layer removal also indicates that the low MFI polymer is less affected by shear towards the core of the sample, as conductive networks in the core of the sample.
Moreover differences in skin layer thickness along the injection melt flow are indicated when comparing

the conductivity of locations close and far away from the gate with similar thicknesses after grinding. In figures 4.12 and 4.13 the resulting magnitude of σ' for locations close and far away from the gate with similar thicknesses after grinding are shown.

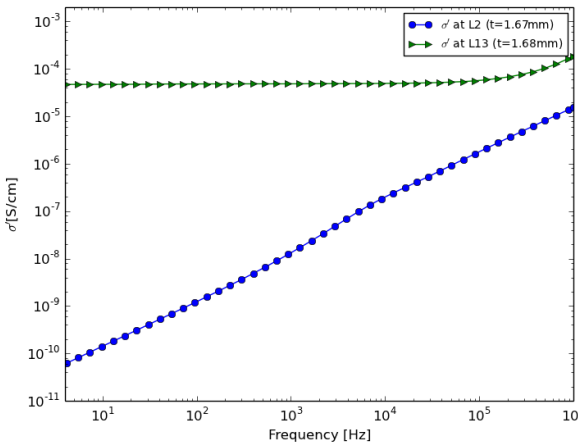

Figure 4.12: Comparison of σ' after grinding at locations 2 and 13.

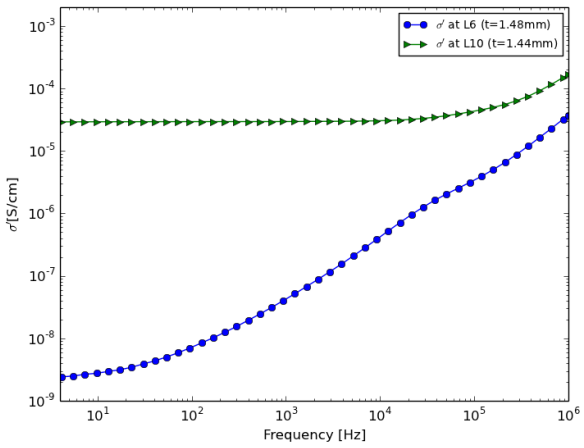

Figure 4.13: Comparison of σ' after grinding at locations 6 and 10.

First of all the σ' data of locations 2 and 13, shown in figure 4.12, is looked at. Comparing the two graphs it first of all needs to be noticed that after grinding both locations had a thickness in the range of 1.67 mm - 1.68 mm. For location 2, which is located close to the gate, σ' shows frequency dependent AC-conductivity behaviour over the whole frequency range. Whereas the location further away from the gate (location 13), shows quasi-DC behaviour over a broad frequency range. In the low frequency domain a difference in σ' of 6 orders of magnitude between the two locations is indicated. Looking at figure 4.13 similar observations can be made. But it needs to be noted that these locations a thinner, with thicknesses of 1.44 mm - 1.48 mm. In the low frequency domain a difference in σ' of up to 4 order of magnitude between the locations is found. However for the location close to the gate (location 6) the formation of quasi-DC behaviour is indicated in the frequency range of 1 Hz to 400 Hz. Based on the observations made on the thickness of the removed surface layer, some conclusions surface layer thickness along the melt flow can be made. The experimental results show that the skin layer closer to the gate is thicker compared to locations further away from the gate. This observation would be in line with the findings reported in literature, that the skin layer tends to be thicker close to the gate [25]. These difference in skin layer thickness along the melt flow also can be used to explain the fact that the electrical properties tend to be smaller close to the gate and increase with distance to the gate.

Looking at the observations of the grinding experiments for the low MFI composite, it can be said that the injection molding process results in an insulating skin layer and that towards the core more conductive networks through the sample thickness are found. Moreover it has been observed that the skin layer thickness reduces with increasing distance to the gate. Similar observations with respect to the skin layer have been made for the high MFI composite, shown in chapter 3.2. However when directly comparing the results of the grinding experiments for the high and low MFI composite, some differences in the resulting morphology can be observed. For both composites the experimental results indicate that the core of the samples have conductive networks through the thickness. However when comparing locations across samples with similar thicknesses it can be observed that the high MFI composite generally has higher magnitudes of σ'. Examples for this can be seen when comparing the plots of σ' at locations 10 and 12 for the high MFI composite in figures B.4 and B.5. Both these locations have a similar thickness, but the high MFI composite has a higher magnitude in σ'. This trend is also indicated at several other locations across the two samples and thus indicates that the core of the high MFI composite is better connected with conductive networks through the sample thickness. In addition to that when comparing the improvements in σ' due to the amount of skin layer removal for different locations, some further differences across the two composites can be observed. Looking

at the data of the PP2 composites, it is indicated that for locations close to the gate an overall thickness removal of ~0.6 mm is required in order to achieve large improvements in σ' (eg. see location 6 in figure 4.13). However for the high MFI composite it can be seen for locations close to the gate that the overall surface removal of ~0.3 mm already is sufficient to improve the conductivity of the sample (eg. see location 4 in figure A.5). In addition to that it should be noted that similar observations on the skin layer thickness across the samples can be made for locations further away from the injection gate. These differences indicate that the low MFI composite has a thicker insulating skin layer compared to the high MFI composite.
Using these observations on the morphology differences across the two composites, the differences in electrical properties shown in figures 4.1 - 4.4 can be explained. Based on the observations of the grinding experiments it expected that the low MFI composite exhibits overall worse electrical properties due to the formation of a thicker insulating skin layer and due to the fact that less conductive networks are formed through the core of the composite sample compared to the high MFI composite.

4.3. Summary and Recommendations

In this section the main findings of this chapter on the effect of the polymer matrix material on the resulting electrical properties and how different matrix materials respond to changing injection molding settings are summarised. This is done by reflecting the main findings to the research questions for this chapter, presented in section 2.2.
The first research question that is to be answered deals with the effect of the polymer flow ability on the resulting electrical properties of an injection molded composite. When directly comparing the electrical properties of composites containing a high MFI polymer and a low MFI polymer, it can be seen that the high MFI polymer leads to overall higher and better electrical properties. In terms of the conductivity σ' it has been shown that the low MFI composite is 4 to 5 orders of magnitude smaller in the low frequency range. In addition to that the low MFI composite exhibits AC-conductivity behaviour over the whole frequency range. Similarly for the real permittivity ϵ' a difference of 1 order of magnitude has been found in the low frequency range. It is expected that the low MFI composites has lower electrical properties as a lower MFI increases the shear forces experienced by the melt during the IM process, which leads to an orientation of the CNTs in the melt flow direction and thus lowers the electrical properties.
The next question that needs to be answered compares the resulting electrical property in-plane distribution of composites containing polymers with a different flow ability. When comparing the in-plane distribution of ϵ' and σ' after injection molding of a high and low MFI composite, no differences in the distribution are found. Both polymer matrix materials result in a non-uniform distribution, where the electrical properties tend to be smaller for locations close to the injection gate and an increase in magnitude is seen with increasing distance to the gate.
The third question that is answered deals with the effect of varying injection molding settings on the electrical property in-plane distribution and magnitude for composites containing different polymer matrix materials. As already mentioned before, both the high and low MFI composites result in a non-uniform electrical property distribution after injection molding. Moreover it has been found that for both composites the non-uniformity along the melt flow tends to increase using harder IM settings. It has been indicated that harder IM settings increase the difference in magnitude between locations close and far away from the injection gate. With respect to the location wise property magnitude it has been indicated that harder IM settings tend to increase the magnitude of both ϵ' and σ'. This trend has been indicate for both composites containing the high and low MFI polymer.
Lastly the fourth question deals with the morphological differences between injection molded samples containing polymers with different flow ability properties. For both the high and low MFI composites it has been found that during the injection molding process a skin layer with oriented CNTs is formed and that towards the core of the sample more conductive networks through the thickness are formed. However there are some differences in morphology between the high and low MFI composites. It has been indicated that the core of the high MFI composite contains better conductive networks through the sample thickness. Moreover it has been seen that the insulating skin layer of the low MFI composite overall tends to be thicker. Thus the thicker skin layer and the worse conductive networks in the sample core of the low MFI composite can be used to explain the overall worse electrical properties.

Based on the observations and conclusions made in this chapter, some recommendations for further research can be given. Similarly to the recommendations of chapter 3.3, it again is recommended for further research to produce in-plane mappings of the high and low MFI samples using a a finer mesh or a mesh based on polar coordinates in order to get a more accurate representation of the electrical property distribution. This will also help to further distinguish differences in the in-plane distribution of composites containing different polymer matrix materials. Moreover further research on the resulting morphology of the low and high MFI composite is needed. It has been indicated that different MFI polymers result in different skin layer thicknesses. For further research it is interesting to exactly quantify the skin layer thickness along the injection melt flow of samples containing different polymer matrix materials.

5

Part 3: Annealing of injection molded nano-composites and the effect on the electrical properties

In this chapter the effect of varying annealing treatments on the resulting electrical properties of the carbon nanocomposites is presented. In the previous chapters it has been pointed out that injection molding of carbon nanocomposites results in lower and non-uniformly distributed electrical properties within the composite. Thus the effect of an annealing treatment on the electric property magnitude and their in-plane distribution is studied. The effect of different annealing times and varying cooling rates are studied in further detail in this chapter. Moreover some further investigations on the impact of annealing on the composite morphology are presented in this chapter.
As a first step the experimental procedures used for the study presented in this chapter are given in section 5.1. This section entails a description of the samples used, a definition of the annealing treatment and a short description electrical measurements. This is followed by section 5.2 where the results of the annealing experiments are presented. This entails the description on how varying annealing times and cooling rates influence the electrical properties and their in-plane distribution. In addition to that some further details on the resulting composite morphology are described in this section. Finally this chapter is concluded with section 5.3, where the finding of the annealing experiments are summarised and related to the research questions of chapter 2.

5.1. Experimental Procedure

In this section the experimental procedure used to study the effect of the annealing treatment on the resulting electrical properties of the composites is described. It needs to be noticed that the sample definition, the sample preparation and the electrical measurements used for the study in this chapter are similar as described in the experimental procedure section 3.1.
However some further remarks on the samples used during the annealing experiments need to be made. Similarly to the chapters before, annealing has been performed using composite samples containing polypropylene and 5 wt.% of CNTs. The annealing experiments have been performed using both the high melt flow index polymer PP1 and the low melt flow index polymer PP2 in order to observe differences in annealing efficiency due to varying matrix properties. In addition to that it needs to be mentioned that all the composite samples used during the annealing experiments have been produced using the hardest injection molding setting IM3. Setting IM3 has been chosen as it leads to the highest non-uniformity in electrical in-plane distribution for both PP1 and PP2 and thus larger improvements in electrical properties due to annealing are to be expected.
In addition to that some further remarks on the electrical measurement procedure used to quantify the effect of the annealing treatments need to be given. In the repeatability study of section 3.2.1 it has been defined that the electrical properties and their in-plane distribution are not comparable

across different shots of the same injection molding settings. Hence the electrical properties of the composite samples have to be measured before and after the annealing treatment in order to precisely quantify the effect of the annealing treatment on the electrical properties. Thus the sample preparation (cutting and sputtering) of the composite, as described in section 3.1, has been performed before the annealing treatment in order to perform BDS. And after annealing has been performed and the BDS measurements have been repeated to quantiy the effect of the annealing treatment.

Determination of melt temperatures and definition of annealing treatment

A further aspect that needs to be described are the annealing experiments itself. As a first step in the definition of the annealing treatments, the melt temperatures of the composites used have to be determined. This has been done by means of differential scanning calorimetry (DSC), using the PerkinElmer DSC8000. In order to determine the melting temperature of the composites containing PP and CNTs, DSC has been performed on a temperature range from 25 °C to 250 °C with a heating and cooling rate of 10 °C/min. This heating and cooling cycle has been repeated twice in order to get a more accurate presentation of the melt temperatures. The results of the DSC measurements of the composites containing PP1 and PP2 can be seen in figures 5.1 and 5.2.

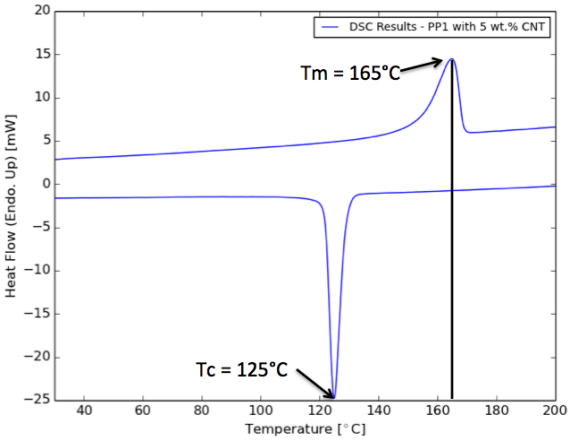

Figure 5.1: DSC results of the PP1/CNT composite.

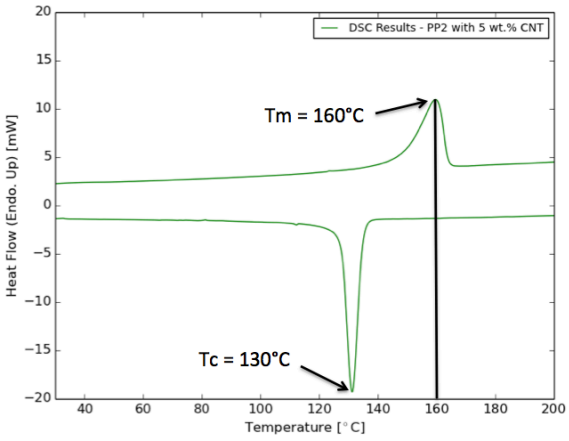

Figure 5.2: DSC results of the PP2/CNT composite.

Looking at figure 5.1, the melt and crystallization temperature of the PP1 composite can be seen. The upward facing peak represents the melting of the composite material and the peak is located at 165 °C and the onset of this melt peak starts at a temperature of 155 °C. The downward facing peak represents the crystallization of the composite material during cooling down. Crysatllization of the material occurs at a temperature of 125 °C. Looking at the DSC results of the PP2 composite in figure 5.2, again the two peaks for the melting and crystallization of the composite can be seen. For the PP2 composite, the maximum of the melting peak is at a temperature of 160 °C and the onset of the melting peak is at 149 °C. The maximum of the crystallization peak is found at a temperature of 130 °C.

Based on the finding of the DSC experiments, the temperatures used during annealing are defined. First of all it needs to be noted that only isothermal annealing is to be performed in this study. Moreover it has been defined that annealing is to be performed below the melt temperature of the composite in order to ensure geometrical stability of the sample. For the annealing experiments the Heraeus WU6100 oven has been used and the samples are placed the middle oven rail. For the PP1 composite, the melting onset is found to be at 155 °C. Thus annealing of the PP1 composites is to be performed at 150 °C, in order to account for temperature inaccuracies of the DSC and the annealing oven used. Similarly for the PP2 composites, the melt onset is determined to be at 149 °C and thus the annealing of the PP2 samples is to be performed at a temperature of 145 °C.

As a next step the annealing times used need to be defined. From the literature review presented in chapter 2 it is known that annealing below the melt temperature requires long annealing times in order to achieve large improvements of the electrical properties. Based on that annealing times of 0.5 h, 1

h and 3 h have been defined for the annealing experiments. During the study of the annealing time on the resulting electrical properties, the samples have been atmospherically cooled down after the annealing treatment.
The other annealing parameter to be studied is the cooling rate after annealing. For this the samples are to be annealed at 150/145 °C for 0.5 h and after the treatment different cooling rates are used. A slow cooling rate has been defined as letting the samples atmospherically cool down to room temperature. And a fast cooling rate has been defined as quenching the samples in tap cold water after the annealing treatment.

5.2. Experimental Results and Discussion

In this section the results of the annealing experiments are described. The discussion of the experimental results has been split up into three parts. First of all the effect of different annealing times on the electrical properties of the composite is shown. This contains a discussion on the electrical property magnitude and their in-plane distribution. Moreover the effect of annealing on composites with different flow abilities is compared. Followed by that the effect of the cooling rate after the annealing treatment on the resulting electrical property magnitude is discussed. And lastly the effect of annealing on the composite morphology is evaluated and related to the resulting electrical properties.

Effect of Annealing Time

In this subsection the effect of varying annealing times on the electrical properties of the composite is studied. The effect of annealing time has been studied with respect to the location wise property magnitude and the resulting in-plane distribution. This has been done using both the high MFI composite PP1 and the low MFI composite PP2. As already indicated in section 5.1, isothermal annealing 0.5 h, 1 h and 3 h has been performed and the temperatures used were 150 °C and 145 °C for the PP1 and PP2 composites respectively.
As a first step the effect of the annealing treatments on the magnitude of the real permittivity ϵ' and the conductivity σ' of the high MFI composite PP1 is studied. In figures 5.3 - 5.6 the graphs of ϵ' and σ' at location 2 and 14 over a frequency range from 1 Hz to 10^6 Hz before and after annealing is shown. Again the locations of the measurement shown correspond to the sample mask shown in figure 3.1.

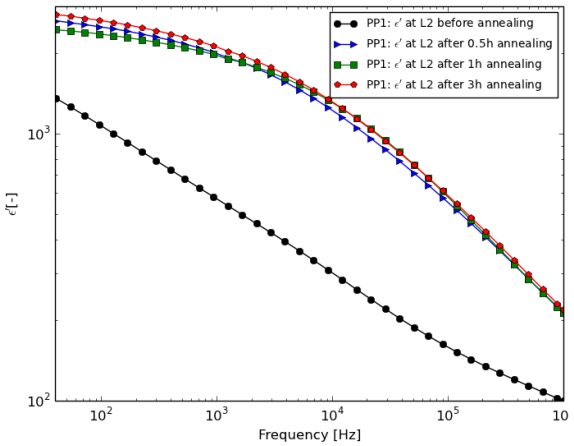

Figure 5.3: Measurements of ϵ' at L2 before and after isothermal annealing of the PP1 samples.

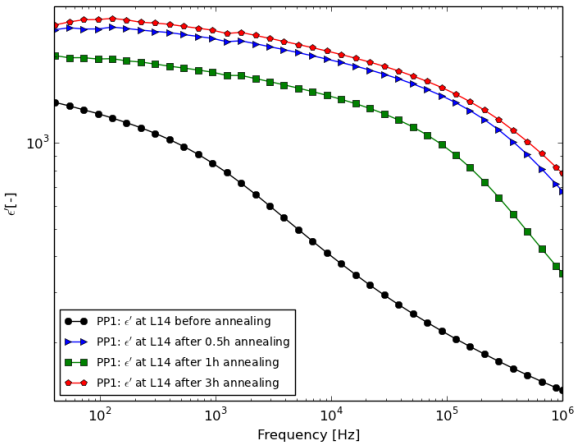

Figure 5.4: Measurements of ϵ' at L14 before and after isothermal annealing of the PP1 samples.

Looking at the effect of the different annealing treatments on the magnitude of ϵ', shown in figures 5.3 and 5.4, it can be seen that ϵ' increased in magnitude after annealing, but it stayed within one order of magnitude. Before annealing ϵ' at 127 Hz was found to be 1000 and 1200 at locations 2 and 14 and after 3 h of annealing an increase to 2600 and 2700 at these locations has been seen. This

would correspond to an improvement in magnitude of 160% and 125% respectively. In addition to that it can be noticed that due to the annealing treatment the shape of the graphs over the whole frequency range changed. Before annealing it can be seen that ϵ' steadily decreases with increasing frequency. But after annealing the magnitude of ϵ' shows only small changes in magnitude up to a frequency of 10^4 Hz - 10^5 Hz. So the highest improvements in magnitude can be seen in the range of 10^4 Hz - 10^5 Hz, with improvements of 300% to 350%. So it can be seen that annealing improved the real permittivity of the composite over the whole frequency range. In terms of the effect of varying annealing times on the ϵ' some further observations can be made. From the shown graphs it can be seen that all three annealing times lead to a similar magnitude. In addition to that it can be seen that a longer annealing time does not necessarily lead to higher magnitudes of ϵ'. These observations thus indicate that annealing the high MFI composite for 0.5 h is sufficient to fully enhance the magnitude of ϵ'.
Similarly when looking at the graphs of σ' at locations 2 and 14 before and after the annealing treatment, shown in figures 5.5 and 5.6, some changes in magnitude over the whole frequency range can be observed.

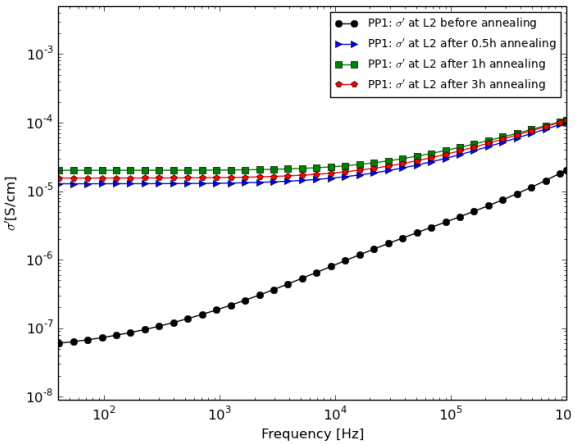

Figure 5.5: Measurements of σ' at L2 before and after isothermal annealing of the PP1 samples.

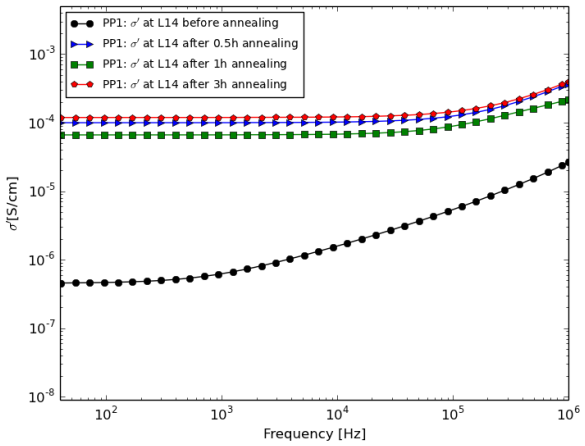

Figure 5.6: Measurements of σ' at L14 before and after isothermal annealing of the PP1 samples.

Comparing the the magnitude of σ' before and after annealing, it can be seen that in the low frequency range improvements of up to 3 orders of magnitude can be seen. Before annealing at 127 Hz a σ' magnitude of 7.9*10^{-8} S/cm at location 2 and 4.7*10^{-7} S/cm at location 14 has been measured. After annealing the conductivity improved to 1.5*10^{-5} S/cm at location 2 and 1.2*10^{-4} S/cm at location 14. In addition to that it can be seen that frequency range of quasi-DC conductivity behaviour increased. Before annealing the transition to AC behaviour occurs in a frequency range of 500 Hz to 1000 Hz and after annealing the transition occurs in the frequency range of 10^4 Hz to 10^5 Hz. Looking at the magnitude of σ' at high frequencies, it can be seen that all the annealing treatments increased σ' about one order of magnitude. In order to further study the effect of the annealing time on the conductivity σ' at 127 Hz and 100 kHz are plotted against the annealing time as shown in figures 5.7 and 5.8. It has to be noticed that error bars of $\pm$13% have been incorporated into the plot in order to account for differences in magnitude across different shots, as explained in section 3.2.1.

Looking at figure 5.7 again the increase in magnitude of up to 3 orders of magnitude can be observed. However it can be noted that this improvement already is reached after annealing for 0.5 h. Beyond 0.5 h the conductivity reaches a plateau, where the magnitude of σ' does not further increase with increasing annealing time. Similarly when looking at the conductivity at 100 kHz shown in figure 5.8 it can be seen that the maximum conductivity improvement of about 1 order of magnitude is reached after 0.5 h of annealing. After 0.5 h the conductivity magnitude reaches a plateau and no further improvement is achieved. Based on these observations it can be concluded that annealing at 150 °C for 0.5 h is sufficient to fully improve the conductivity of the high MFI composite

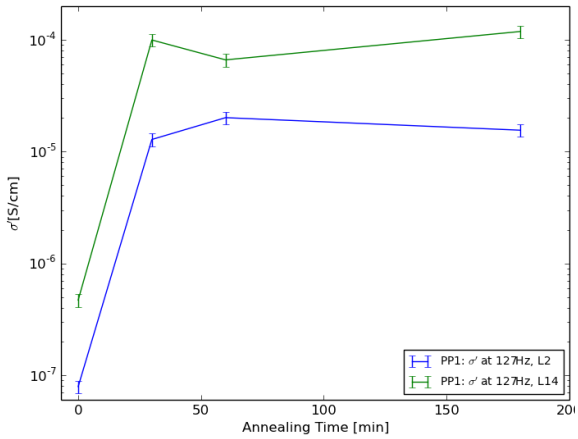

Figure 5.7: Conductivity σ' at 127 Hz as a function of annealing time.

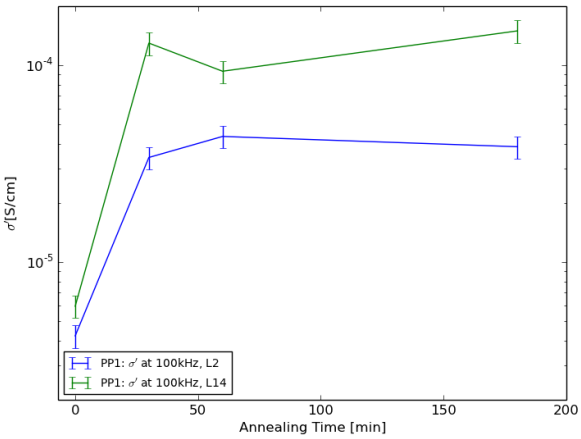

Figure 5.8: Conductivity σ' at 100 kHz as a function of annealing time.

The observations made on the resulting electrical property magnitude with respect to different annealing times can be compared to similar research presented in literature. It has been shown that annealing of PP with 5 wt.% of CNTs at 165 °C lead to an improvement of 3 orders of magnitude after 0.5 h and no further enhancement has been seen for longer annealing times [29]. Annealing times of 15 min at 160 °C to 175 °C for a similar composite have been reported not to be effective in terms of conductivity improvement [48]. When comparing the results shown in this section with the results found by Fei et al. [30], it again has been seen that annealing below the melt temperature of the composite can yield up to 2 orders of magnitude improvement of the conductivity. However very long annealing times of up to 10 h are required to achieve this improvement. So the based on the findings shown in literature, the improvements in electrical properties found in this section are similar to the improvements reported in literature. However in contrast to the findings reported in literature, it has been shown that relatively short annealing times can be used to achieve this improvement, despite annealing below the melt temperature of the composite.
In addition to that annealing has been performed using the low MFI composite PP2 in order to study the effect of varying annealing times on the magnitude of ϵ' and σ'. It should be noticed that annealing has been performed at 145 °C for the PP2 composites. The resulting magnitude of ϵ' at location 2 and 14 before and after 0.5 h, 1 h and 3 h annealing are shown in figures 5.9 and 5.10.

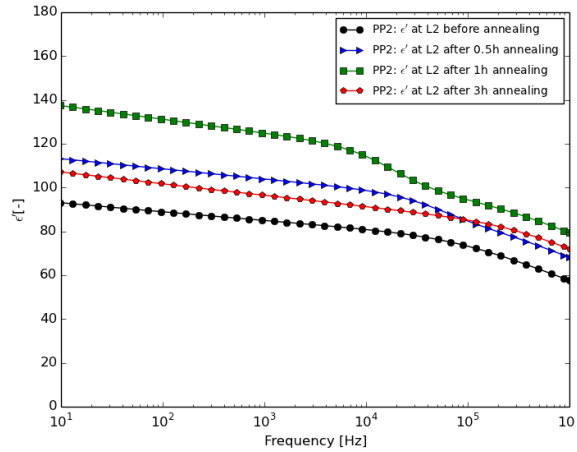

Figure 5.9: Measurements of ϵ' at L2 of the PP2 composite before and after annealing.

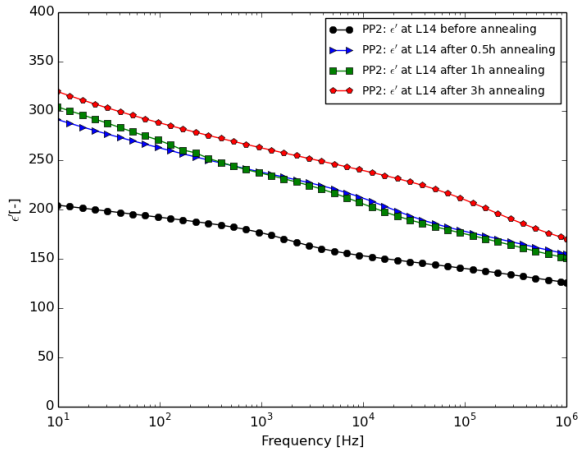

Figure 5.10: Measurements of ϵ' at L14 of the PP2 composite before and after annealing.

From the measurement results of ϵ' shown in figures 5.9 and 5.10, it can be seen that the annealing treatment leads to a small improvement in the ϵ' magnitude. Over the whole frequency range all the annealing treatments lead to an improvement of up to 35%. Moreover when comparing the behaviour of ϵ' with increasing frequency, the same quasi linear decrease with increasing frequency can be seen before and after annealing. Similarly to the findings on the high MFI composite, all three annealing times used lead to similar ϵ' magnitudes. Based on these observations it can be said that the annealing treatments are not useful to improve the real permittivity magnitude of the low MFI composite.
Next to that the measurements of the conductivity σ' at locations 2 and 14 of the low MFI composite can be seen in figures 5.11 and 5.12.

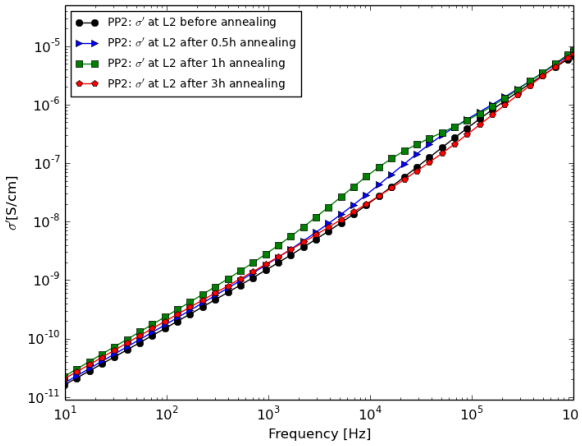

Figure 5.11: Measurements of σ' at L2 of the PP2 composite before and after annealing.

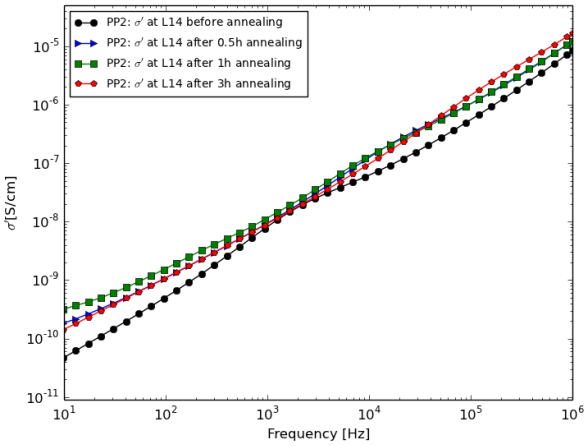

Figure 5.12: Measurements of σ' at L14 of the PP2 composite before and after annealing.

Comparing the resulting magnitude of σ' of the low MFI composite before and after the annealing treatment shown in figures 5.11 and 5.12, no consistent trends can be observed. For location 2 it even has been observed that the annealing treatment lead to a lower magnitude of σ'. For σ' at location 14 it can be observed that the annealing slightly increased the conductivity magnitude in the frequency range below 10^3 Hz. But both the conductivity before and after annealing linearly increase with increasing freqeuncy and no quasi-DC behaviour is observed. Thus it can be said that in terms of the conductivity σ' non of the annealing treatments used is effective to improve the conductivity of the low MFI composite.
When comparing the effect of the different annealing treatment on the high and low MFI composites, large differences can be observed. For the high MFI composite both ϵ' and σ' experienced a large improvement in magnitude over the whole frequency range. In contrast to that the electrical properties of the low MFI only show very small changes in magnitude due to annealing. These differences in annealing efficiency can be related to the flow abilities of the composite material. When annealing a composite sample there are two main factors that influence change in morphology and thus the improvement of the electrical properties. First of all due to the application of high temperatures, the polymer chains of the matrix material start to relax, which leads to mobility within the composite [49]. This mobility enables the CNT fillers to re-orientate and form conductive networks within the matrix. This reorientation mainly occurs due to Brownian diffusion of the CNTs [50]. So based on that it is expected that the applied annealing temperature applied for the low MFI composite does not lead to sufficient mobility for the CNTs to move and re-orient. Similarly it has been indicated by Pan et al. [29] that composites containing polymers with a high molecular weight, which corresponds to a higher melt viscosity, require longer annealing times due to reach their maximum electrical properties, due to their lower mobility. Next the mobility during annealing, the initial morphology, can be a factor for the lower annealing efficiency of the low MFI composite. In chapter 4.2 it has been indicated that the low MFI composite has an overall thicker insulating skin layer and has worse conductive networks in the core of the sample. So it is expected that the combination of lower mobility and worse initial morphology is the reason for the low annealing efficiency of the low MFI composites.

Next to the effect on the electrical property magnitude, the effect of the different annealing treatments on the resulting in-plane distribution of the electrical properties is studied. The investigation on the in-plane distribution only is discussed using the measurements of the high MFI composite, as it already has been indicated that annealing of the low MFI composite is not very effective. In chapter 3.2 it already has been established the injection molded samples have a non-uniform distribution along the injection melt flow and that harder IM settings result in larger non-uniformity. Thus the effect of annealing on sample produced with setting IM3 is studied, as it has the largest property non-uniformity. The in-plane distribution of both ϵ' and σ' are studied at a frequency of 127 Hz. Mappings of the in-plane distribution of ϵ' and σ' at 127 Hz before and after 0.5 h annealing can be seen in figures 5.13 - 5.16. In addition to that mappings of both these properties before and after annealing for 1 h and 3 h can be found in Appendix C.

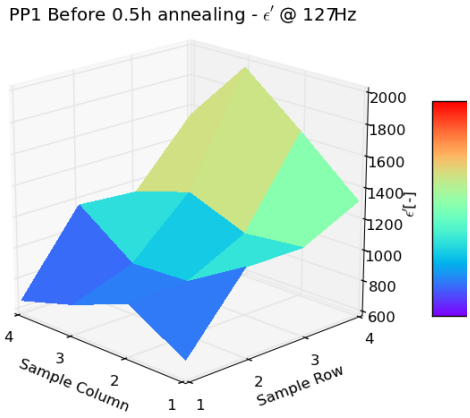

Figure 5.13: Mapping of ϵ' at 127 Hz before 0.5 h annealing

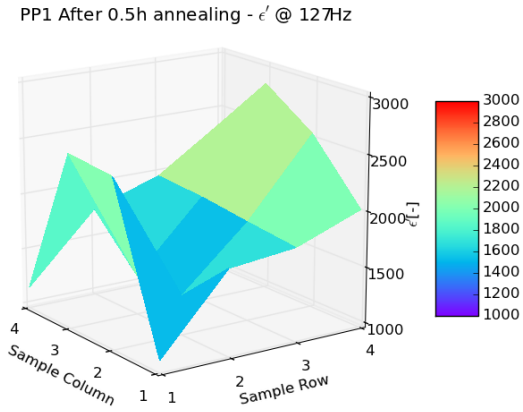

Figure 5.14: Mapping of ϵ' at 127 Hz after 0.5 h annealing at 150 °C.

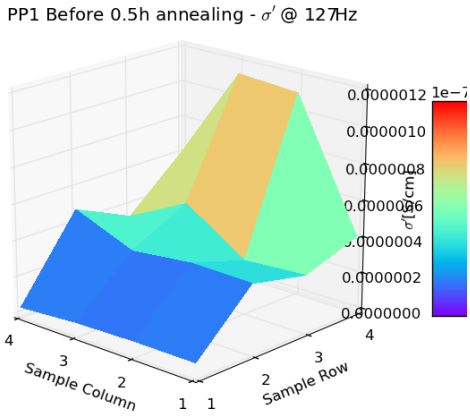

Figure 5.15: Mapping of σ' at 127 Hz before 0.5 h annealing.

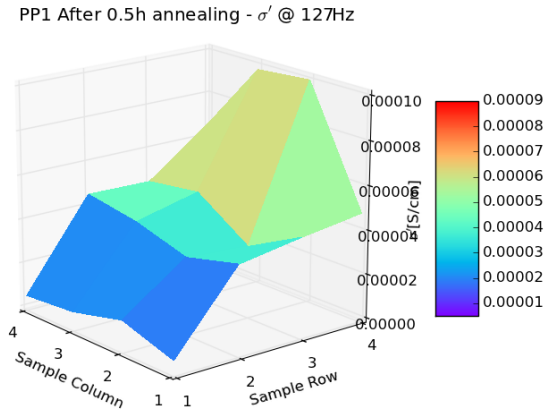

Figure 5.16: Mapping of σ' at 127 Hz after 0.5 h annealing at 150 °C.

Comparing the in-plane distribution of ϵ' and σ' before and after 0.5 h of annealing it can be seen that the trend of the in-plane distribution along the melt flow remain similar. For both these properties it is indicated that after annealing the electrical properties still remain smaller close to the injection gate and increase increase in magnitude with distance to the gate. It can be noticed that the magnitude of the electrical properties increased over the whole sample. But when comparing the shape of the mapping graph before and after the annealing treatment, it can be noticed that the shape of the mapping remains very similar. This indicates that annealing did not lead to a uniform in-plane property distribution, rather than shifting up the non-uniform in-plane distribution to higher property magnitudes. Moreover looking at the distribution of the electrical properties over the sample width, it can be seen that annealing does not lead to a more symmetric width distribution of the electrical properties. Similar observations on the in-plane property distribution can be made for longer annealing times of 1 h and 3 h when looking at the mappings shown in Appendix C. It thus can be said that longer annealing times are also not sufficient to achieve a uniform property in-plane distribution.
In order to study the impact of the annealing treatments on the property in-plane distribution in further detail, the row average differences of ϵ' and σ' for locations close and far away from the gate are compared before and after annealing. The differences in ϵ' and σ' between row 1/2 and row 4 are calculated using equation 3.4. Again it needs to be noted that the differences across the rows have been calculated using the row average of ϵ' and σ' at 127 Hz. The resulting differences before and after annealing can be found in table 5.1.

Table 5.1: Row Average differences between row 1/2 and row 4 of ϵ' and σ' before and after annealing.

	0.5 h Annealing		**1 h Annealing**		**3 h Annealing**	
	Before	**After**	**Before**	**After**	**Before**	**After**
ϵ' - Difference R1 - R4	-53.0%	-26.1%	-40.1%	-28.5%	-46.2%	-27.3%
ϵ' - Difference R2 - R4	-36.1%	-37.3%	-24.4%	-26.7%	-28.4%	-29.9%
	Before	**After**	**Before**	**After**	**Before**	**After**
σ' - Difference R1 - R4	-93.2%	-90.5%	-92.2%	-81.5%	-94.6%	-83.5%
σ' - Difference R2 - R4	-52.1%	-49.2%	-44.9%	-42.8%	54.9%	-34.6%

Looking at the row average differences shown in table 5.1 some further observations on the effect of the annealing treatments on the resulting property in-plane distribution can be made. For both the row averages of ϵ' and σ' a decrease in magnitude difference across the rows can be observed. Looking at the differences for the ϵ' row averages, it can be seen that annealing leads to an overall difference in the range of -26% to -36%, which is a slight improvement to before annealing, which had a difference range from -24% to -53%. It also can be noticed that all the annealing times used resulted in similar row differences. Comparing the differences before and after annealing of σ' it again can be observed that the differences slightly decrease. However the decrease in difference due to annealing is only up to 13%. And again it has been observed that longer annealing times do not lead to larger improvements in the property uniformity. Thus from the observations made it can be concluded that annealing the composite sample slightly decreases the non-uniformity of the electrical properties and that longer annealing times do not lead to larger improvements on the uniformity of the in-plane distribution.
All in all from the observations made on the effect of the annealing treatments on the electrical property in-plane distribution it can be said that annealing the high MFI samples at 150 $^\circ$ for 0.5 h, 1 h and 3 h is not sufficient to achieve a uniform in-plane distribution of the electrical properties. It has been shown that the in-plane distribution of both ϵ' and σ' remain similar before and after the annealing treatment. Thus the electrical properties tend to be smaller close to the gate and increase in magnitude with distance to the gate. However it has been shown that annealing slightly decreases the non-uniformity along the melt flow. In terms of the effect of the annealing time it can be said that all the annealing times used had the same effect on the resulting in-plane distribution of ϵ' and σ'.

Effect of Cooling Rate

In this subsection the effect of the cooling rate after the annealing treatment is discussed. The effect of the cooling rate only is studied with respect to the resulting property magnitude as it already has been indicated in the previous subsection that the annealing treatments only have a minor impact on in-plane distribution of the electrical properties. In addition to that the effect of the cooling rate only is studied using samples produced with setting IM3 containing the high MFI polymer PP1, since annealing of the low MFI composites did not yield significant improvements of the electrical properties.
In order to study the effect of the cooling rate, a slow cooling rate and a fast cooling rate have been defined. Slow cooling has been achieved by atmospherically cooling the sample to room temperature after annealing it for 0.5 h at 150 °C. And the fast cooling rate entails quenching the samples in tap cold water after the annealing treatment. The effect of the different cooling rates is studied by looking at the location wise magnitude of ϵ' and σ' at location 2 and 14. The measurement results for ϵ' at locations 2 and 14 can be seen in figures 5.17 and 5.18.

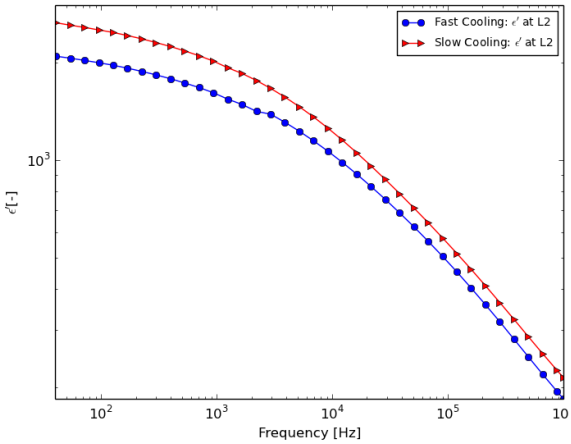

Figure 5.17: Measurement results of ϵ' at L2 for slow and fast cooling after 0.5 h annealing.

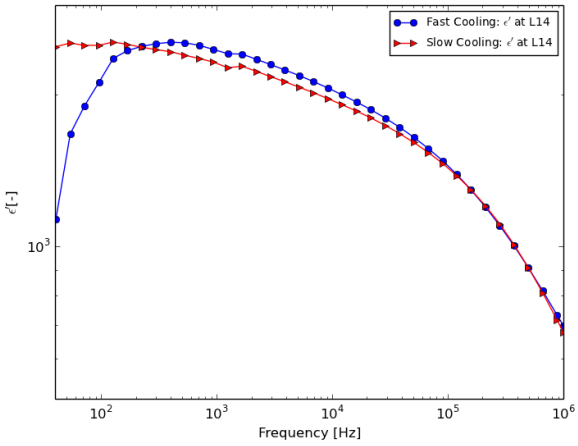

Figure 5.18: Measurement results of ϵ' at L14 for slow and fast cooling after 0.5 h annealing.

Comparing the measurement results of ϵ' after 0.5 h annealing at 150 °C using slow and fast cooling it can be noticed that the different cooling rates result in similar properties. At both locations 2 and 14 a similar improvement of ϵ' after the annealing can be seen. For both cooling rates it can be observed that the behaviour of ϵ' with increasing frequency is similar, indicating similar microstructres due to the different annealing treatment. Looking at the resulting magnitude of ϵ' it can be seen that at location 2 the slow cooling resulted in an overall higher property magnitude. However looking at location 14 the fast cooling resulted in a slightly higher magnitude of ϵ'. So it can be said that the measurement results of ϵ' do not clearly indicate the effect of the cooling rate on the change in property magnitude because of differences in magnitude across injection shots. From the measurement graphs it only can be concluded that irrespective of the cooling rate an overall improvement in ϵ' due to annealing is achieved and that the resulting microstructures are similar. In order to further study the change in magnitude of ϵ', the change in property magnitude has been calculated. The change has been calculated using equation 5.1. The percentual change is defined as the property magnitude after annealing divided by the property magnitude after annealing.

$$\Delta\% = \frac{x_{before}}{x_{after}} * 100 \tag{5.1}$$

The change in ϵ' after slow and fast cooling has been determined for each frequency and the resulting changes at locations 2 and 14 can be seen in figures 5.19 and 5.20.

The calculated change in figures 5.19 and 5.20 takes the property magnitude of ϵ' before the annealing treatment into account. Thus by looking at percentages the effect of different injection shots

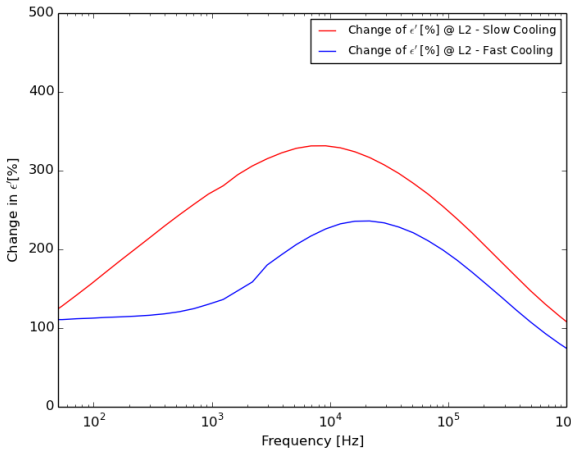

Figure 5.19: Change in ϵ' at L2 due to 0.5 h annealing and different cooling rates.

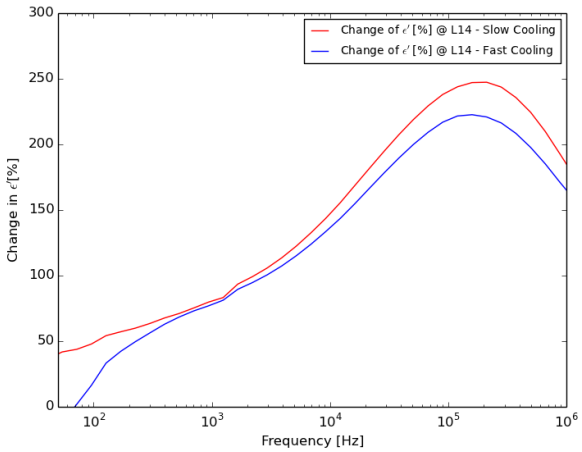

Figure 5.20: Change in ϵ' at L14 due to 0.5 h annealing and different cooling rates.

is accounted for. When comparing the change graphs for ϵ' it can be seen that the improvement of the property magnitude is overall lower for the fast cooling rate. At location 2 fast cooling resulted in a 57% lower improvement at 127 Hz compared to the slow cooling and in the range of 10^3 Hz to 10^4 Hz the improvement was up to 147% lower. For location 14 the differences due to the different cooling rates are smaller. However again at 127 Hz it can be seen that fast cooling results 21% smaller improvement and over the rest of the frequency range the improvement is 3% to 27% smaller. Based on these observations it can be said that for the overall property magnitude of ϵ' fast cooling after the annealing treatment reduces improvements in property magnitude.
In addition to that the effect of the different cooling rates after annealing on the conductivity σ' is looked at. In figures 5.21 and 5.22 the measurement results of σ' at locations 2 and 14 for the slow and fast cooling rate can be seen.

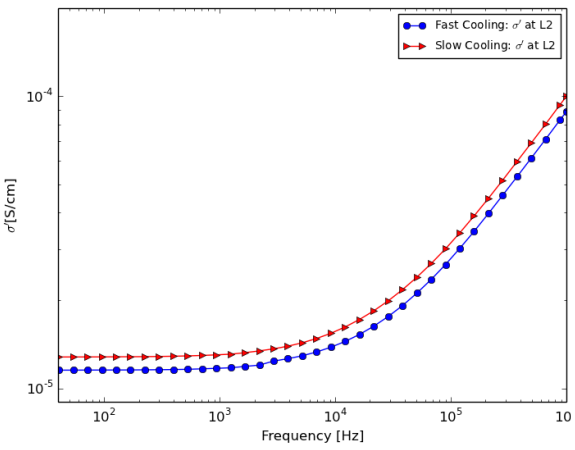

Figure 5.21: Measurement results of σ' at L2 for slow and fast cooling after 0.5 h annealing.

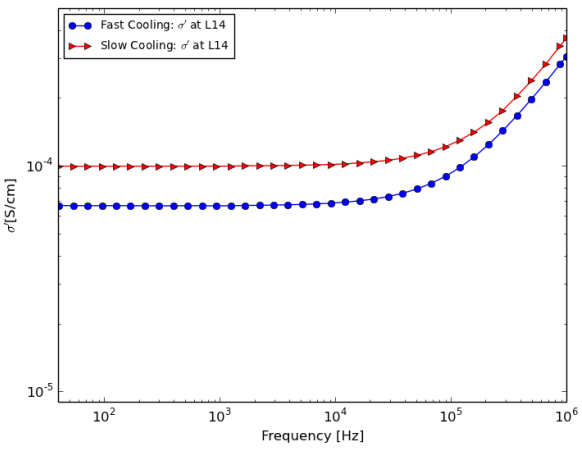

Figure 5.22: Measurement results of σ' at L14 for slow and fast cooling after 0.5 h annealing.

Comparing the resulting measurements of σ' after slow and fast cooling, it can be seen that irrespective of the cooling rate the property magnitude is within the same order of magnitude. In addition to that it also can be seen that for both cooling rates σ' behaves similar with increasing frequency. At location 2 the transition from quasi-DC behaviour to AC behaviour occurs at ~200 Hz for both the slow and fast cooled sample and at location the transition for both samples is seen at 3*10^4 Hz. This thus

again indicates that the two different cooling rates result in similar microstrucutres after the annealing treatment. From the graphs it also is indicated that the slow cooling results in an overall higher magnitude of σ'. However in order to account for the differences in property magnitude before annealing across different injection shots, the perecentual change in σ' has been calculated using equation 5.1. The resulting changes in σ' at locations 2 and 14 due to the fast and slow cooling rate can be seen in figures 5.23 and 5.24. Using these figures the effect of the cooling rate on the property magnitude of σ' can be studied in further detail.
Comparing the change in σ' magnitude at locations 2 and 14 in figures 5.23 and 5.24, it again can be observed that the fast cooling rate results in overall less improvement of the property magnitude. For location 2 it can be observed that in the low frequency range of 1 Hz to 10^3 Hz fast cooling resulted in up to 29900% less improvement in property magnitude. The difference in improvement steadily decreases with increasing frequency to 73% less improvement at 10^6 Hz for the fast cooling rate. Also at location 14 it can be seen that fast cooling resulted in smaller improvements. In the low frequency range of 1 Hz to 10^3 Hz fast cooling had around 2550% smaller improvements and towards high frequencies this decreases to 156% at 10^6 Hz. So based on these observations it again can be said that fast cooling after annealing leads to less improvement in the magnitude of the conductivity σ'.

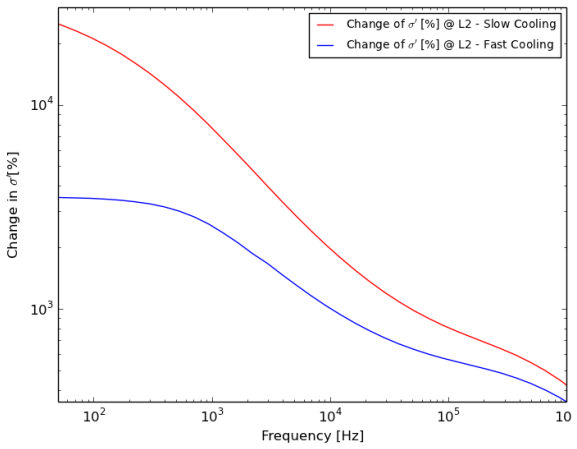

Figure 5.23: Change in σ' at L2 due to 0.5 h annealing and different cooling rates.

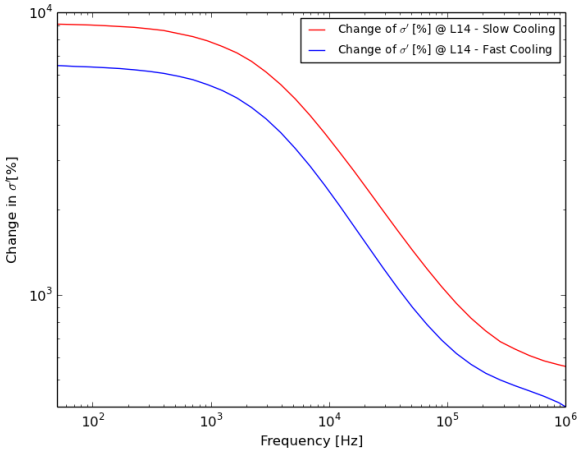

Figure 5.24: Change in σ' at L14 due to 0.5 h annealing and different cooling rates.

All in all it has been observed that fast cooling after annealing leads to less improvements on the electrical property magnitude. However when comparing the measurement graphs of ϵ' and σ' it is indicated that both cooling rates result in similar behaviour due increasing frequency and thus similar microstructres after the treatments are expected. The findings on the effect of the cooling rate presented in this section can be compared with findings presented in literature. Looking at literature on the topic of the cooling rate of the composite after annealing some opposing findings on the cooling rate effect can be found. Some researchers indicate that fast cooling of the composite enhances the electrical properties [31, 33] and other researchers have reported that slow cooling leads to higher electrical properties [32–34]. The main factor influencing the formation of conductive networks and thus high electrical properties is the crystallisation behaviour induced by the cooling rate. It has been indicated in literature that slower cooling of the composite leads to a higher degree of crystallinity [31, 34]. But next to the crystallisation behaviour there is a further factor influencing the effect of the cooling rate. It has been indicated by Fernandez et al. [33] that the filler volume used in the composite is decisive for the effect of the cooling rate on the resulting electrical property magnitude. Their research has shown for composites above the percolation threshold crystallisation leads to an increase in conductivity. Thus slower cooling of composites with a high filler loading is beneficial in terms of high electrical properties. Similar results have been observed in the experimental results presented in this section, since the composite used has a high CNT loading of 5 wt.% and thus higher electrical properties are found due to slow cooling. The increase in electrical properties can be directly related to the increased formation of crystal regions during slow cooling [32, 33]. It has been proposed that conductive network density

increases due to volume shrinkage associated with crystallisation of the microstructure [32, 33]. Similarly it has been described that the CNTs primarily cluster in the amorphous region of the composite matrix and the increase in crystallinity reduces the size of the amorphous regions, which induces the formation of more conductive networks [33]. Based on these observations from literature it is expected that the slow cooling rate after annealing leads to higher electrical properties due to increased crystallisation of the composite matrix. This crystallisation tends to decrease the distances between the CNT fillers and thus enhances the formation of conductive networks. Hence it is expected that the slow cooled samples have a higher degree of crystallinity, which leads to slightly more and better conductive networks through the thickness of the sample compared to the fast cooled samples. Thus it can be concluded that crystallinity of the polymer matrix is beneficial in terms of the electrical properties of the composite, as it promotes the formation of conductive networks. This finding however contrasts the reports in literature that increased crystallinity tends to be break down conductive networks [15, 16], as mentioned in the literature review 2.1. However the overall differences in microstuructre between the slow and fast cooled samples are expected to be small as the overall behaviour and magnitude of the electrical properties over the measured frequency range are similar.

Effect of Annealing on the composite morphology

In this subsection the effect of the annealing treatment on the morphology of the composite is further investigated. From the previous discussion it has been established that the annealing treatments used lead to an improvement of the conductivity σ' of up to 3 orders of magnitude and thus an improvement of the conductive networks is expected to be found.
Looking at literature some descriptions on the effect of annealing on the composite morphology can be found. In general it is described that the heating of the composite leads to more mobility of the CNT fillers in order to reaggregate and form further conductive networks within the polymer matrix [28, 29, 51]. The driving force for the formation of these conductive networks is the Brownian motion of the CNTs [51]. In terms of dispersion of the fibres it has been described that the reason for low electrical properties are tightly agglomerated CNTs combined with single CNTs, which do not form conductive networks [29]. An example for this dispersion type is illustrated in figure 2.3 a and b. In addition to that it has been established in chapter 3.2 that the electrical properties are lowered due to an insulating skin layer consisting of highly oriented CNTs and the non-uniform CNT concentration along the melt flow. After annealing the dispersion of the CNTs tends to change to loosely agglomerated CNTs, which form conductive networks [29]. This change in morphology has been reported to improve the conductivity of the composite up to 7 orders of magnitude [29]. A sketch of this dispersion type can be seen in figure 2.3 c. However it needs to be noted that most literature describing the effect of annealing on the composite morphology, deal with above melt temperature annealing. In terms of below melt temperature annealing, as performed in this study, it has been reported that the mechanisms on the electrical property enhancement are not fully understood yet [30].
As a first step in studying the annealing effect on the composite morphology, the effect on the skin layer and sample core is studied. In chapter 3.2 it has been established that the electrical properties of the composite are lowered due to an insulating skin layer. In this skin layer the CNTs tend to be oriented in the melt flow direction and thus no conductive networks through the sample thickness are formed. Upon removal of this layer it has been shown that towards the core of the sample more conductive networks are formed through the thickness, as an increase in σ' of 2 orders of magnitude has been found. Hence the measurement results of the as injection molded high MFI PP1 sample with removed skin layer and the annealed high MFI PP1 sample are compared. In figures 5.25 and 5.26 the resulting σ' at locations 7 and 10 after skin removal and after annealing can be seen. Looking at the remaining thickness of the grinded samples, it can be said that on each side of the sample up to 300 μm is removed and thus the skin layer is completely removed.

By comparing the measurement results of σ' shown in figures 5.25 and 5.26 some observations on the effect of 0.5 h annealing at 150 °C on the resulting composite morphology can be made. First of all it can be noticed that the conductivity of the annealed sample and the grinded sample without annealing are within the same order of magnitude. At location 7 annealing results in a slightly larger quasi-DC conductivity of $4.051*10^{-5}$ S/cm whereas the skin layer removal at location 10 results in a larger quasi-DC conductivity of 5.98^{-5} S/cm. In addition to that it can be seen that for both samples

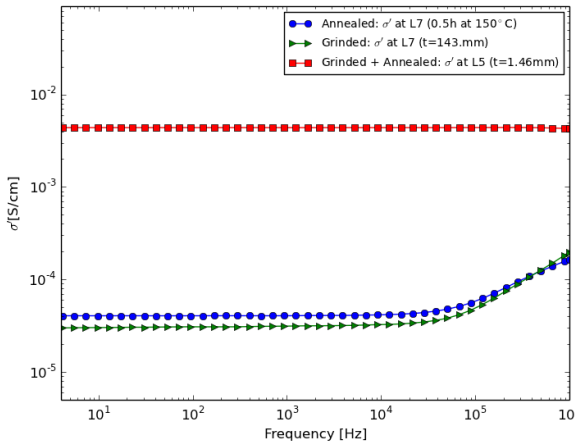

Figure 5.25: Comparison of σ' of the grinded and annealed sample at sample location 7.

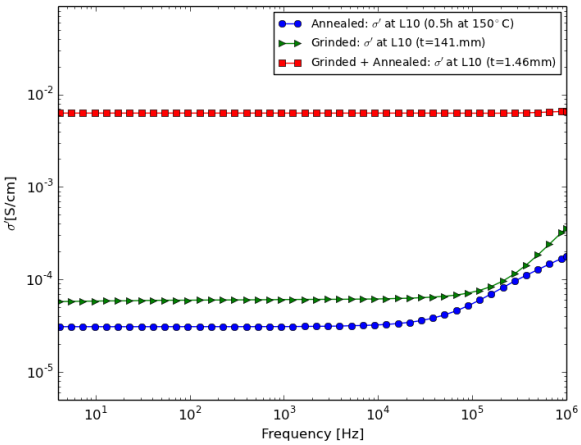

Figure 5.26: Comparison of σ' of the grinded and annealed sample at sample location 10.

the AC-conductivity transition frequency is similar. These observations indicate that the annealed sample and the core of the as injection molded sample have a similar average morphology.
In order to get a better understanding on the morphology changes due to the below melt temperature annealing treatment a further measurement is conducted. Again the skin layer of the high MFI composite sample has been removed by grinding the surface as described in section 3.1. After that the grinded sample has been annealed at 150 °C for 0.5 h. This additional measurement can also be seen in figures 5.25 and 5.26. It can be noted that annealing the sample after surface removal further enhances the magnitude of σ' by 2 orders of magnitude compared to the as IM grinded sample and the normal annealed sample. The σ' improvement of the sample core due to annealing is similar to the improvement observed due to annealing the sample without surface removal. So it can be said that the annealing treatment uniformly improves the morphology through the sample thickness. In addition to that it can be expected that the CNT networks found in the as injection molded sample core are not perfect either and some orientation of the fibres along the melt flow is expected to be present. Moreover the effect of the annealing treatment on the skin layer has been studied by grinding the sample to a thickness of ~300 μm and annealing the skin layer of the sample. The resulting σ' of the annealed skin layer after annealing can be seen in figure 5.27.

Comparing the magnitudes of σ' for the different composite samples shown in figure 5.27 some further observations can be made. First of all it again can be noted that the skin layer also experiences an improvement in conductivity by 2 orders of magnitude, when comparing it to the unannealed skin layer measurements shown in figures 3.21 and 3.22. This observation again confirms that the annealing treatment uniformly improves the sample morphology. From the figure it also can be noted that the conductivity of the annealed skin layer is within the same order of magnitude as the conductivity of the as injection molded annealed sample indicating that the BDS measurement of the as injection molded samples is dominated by the conductivity skin layer, as already mentioned in chapter 3. In addition to that by comparing the σ' magnitude of the annealed skin layer with the σ' of the unannealed sample core it can be noted that the core before annealing results in a similar σ' magnitude. However the frequency dependent conductivity behaviour of the core is different, indicating better conductive networks in the sample core even without annealing. Based on that observation it is expected that the morphology of the skin layer after annealing is similar to the morphology of the sample core of the as injection molded sample.
Looking at the results of the annealed sample core and the annealed skin layer it can be said that the below melt temperature annealing treatment does not eliminate the presence of the skin layer created due to the injection molding process. From the observations made it is expected that the annealing treatment enables the reorientation of the CNTs and thus reduces the effect of the insulating skin layer on the electrical properties by reorienting the CNTs and thus forming some new conductive networks through the thickness.

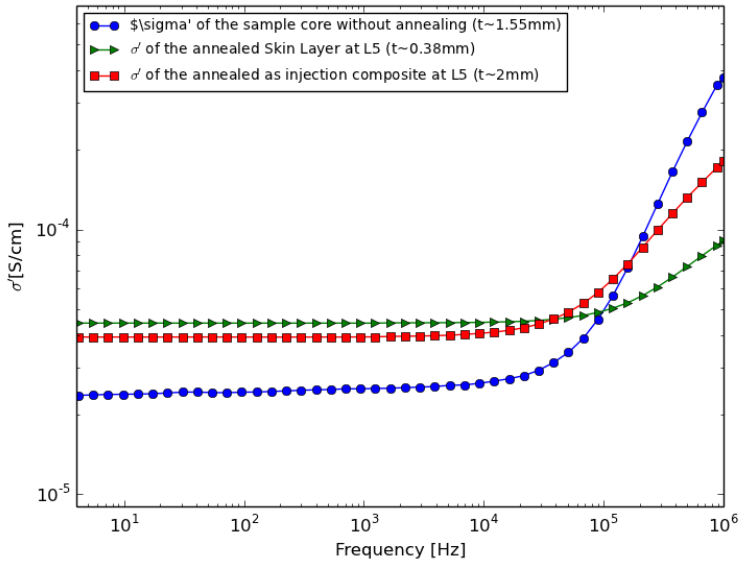

Figure 5.27: Comparison of σ' of the annealed skin layer with the normal annealed sample and the unannealed sample core at L7.

So all in all it is expected that the annealing treatment at 150 °C leads to a randomisation of the CNT fibre orientation in both the skin layer and the core of the composite due to the Brownian motion of the CNTs. Since it has been stated in literature, that if the polymer is well above the glass transition temperature the polymer chains are relatively free to move and thus allow the CNTs to reorient themselves [30]. This randomisation of the filler orientation reduces the orientation of the fibres in the melt flow direction and thus promotes the formation of conductive networks through the thickness of the sample. So it can be said that a below melt temperature heat treatment of an injection molded high MFI can be used to reduce the orientation of the CNTs within the insulating skin layer and the sample core and thus improve the electrical property magnitude of the composite. From the observations made it is also concluded that the below melt temperature annealing treatment is not sufficient to fully eliminate the effects of the injection molding process on the sample morphology and thus not create the maximal possible electrical properties.

In order to further study the impact of the below melt temperature annealing treatments on the morphology of the composites, the conductive behaviour of the annealed composites is studied using the universal power law as proposed by Jaschner [44]. Similarly to the study presented in chapter 3.2, the measurement data of σ' of the annealed samples is used to perform a power law fitting in order to determine the coefficients A and s. In chapter 3.2 it has been described that the coefficient s is an indicator for the presence of conductive networks in the composite, where a low value of s indicates an imperfect morphology and a high value of s indicates well interconnected networks through the sample morphology. Studying the exponent s against the distance travelled from the injection gate by the melt flow it has been seen that the exponent s linearly increases with increasing gate distance. Based on that observation it has been concluded that the with increasing distance to the gate more and better conductive networks are found. The improvement of the morphology is expected to occur due to a decreasing insulating skin layer thickness with increasing gate distance and an increasing CNT concentration with distance travelled from the gate. In addition to that is has been observed that due to harder IM settings the location wise exponents tend to be increasingly scattered. From that observation it has been concluded that the harder IM settings lead to a more anisotropic morphology. Lastly it has been shown from a column wise study of the exponent s against the gate distance that with increasingly harder IM settings decrease the similarity in morphology over the sample with and thus further increase the anisotropy of the morphology.
During the annealing treatments the high MFI samples produced by the hard setting IM3 have been

used in order to and in order to study the changes in the sample morphology due to annealing the power law study is repeated. In figures 5.28 - 5.30 the results of the linear regression analysis of the exponent s against the gate distance for the 0.5 h, 1 h and 3 h annealed samples can be seen.

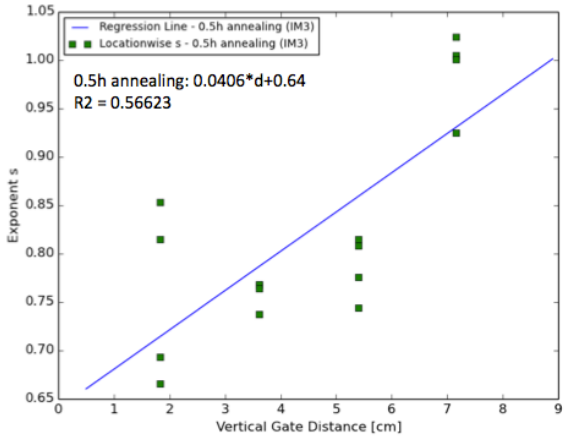

Figure 5.28: Linear Regression of the exponent s against the gate distance for sample PP1 IM3 after 0.5 h annealing at 150 °C.

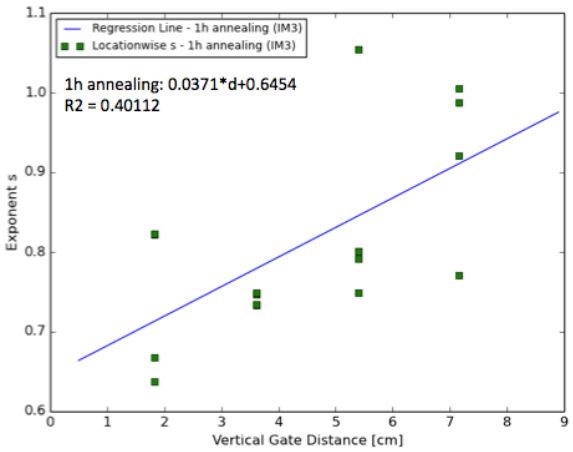

Figure 5.29: Linear Regression of the exponent s against the gate distance for sample PP1 IM3 after 1 h annealing at 150 °C.

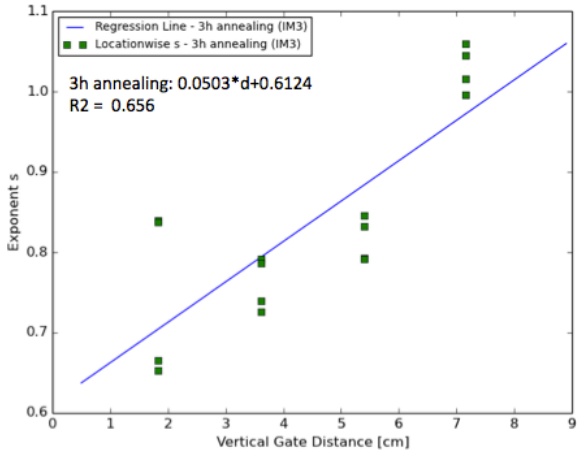

Figure 5.30: Linear Regression of the exponent s against the gate distance for sample PP1 IM3 after 3 h annealing at 150 °C.

Comparing the linear regression results of the exponent s against the gate distance of sample IM3 after annealing in figures 5.28 - 5.30 with the linear regression results of the as injection molded sample IM3 in figure 3.25 some further observations on the effect of the annealing treatment on the morphology can be made. For all three annealing treatments it can be observed that s tends to increase in magnitude with increasing distance to the gate, which is similar to the results of the as injection molded sample. This observation again indicates that there are morphology differences along the melt flow of the annealed samples. The increase in s with gate distance again indicates that for locations further away from the gate more conductive networks are expected to be found. Also comparing the regression coefficients of the three different annealed samples it can be observed that all the annealing times used lead to a similar morphology distribution along the melt flow. These observations on the evolution of the exponent s along the melt flow are in line with the finding presented earlier in this chapter that the investigated annealing treatments do not lead to a uniform in-plane distribution of the electrical properties and that longer annealing times are not sufficient to further improve the uniformity of the in-plane distribution. The non-uniform property distribution again can be explained due to the presence of the skin layer and the non-uniform CNT concentration along the melt flow. When comparing the scatter of the exponent s before and after annealing, some differences due to the annealing

treatment can be observed. The exponent s of the as injection molded sample IM3 shown in figure 3.25 shows a large degree of scattering with an R^2 value of 0.0084, which indicates large degree of anisotropy of the sample morphology. After annealing R^2 values in the range of 0.40112 to 0.656 are found, which indicates a decrease in scatter of the exponent s. This decrease in scatter can be seen as a reduction in anisotropy of the sample morphology. Similar to that it has been identified earlier in this chapter that the annealing treatment decreases the non-uniformity of the electrical property in-plane distribution, which can be explained with the decrease in anisotropy of the morphology. Comparing the location wise magnitude of the exponent s before and after annealing of sample IM3 it can be seen that annealing generally leads to higher values of s. This indicates that annealing results in a better morphology in terms of conductivity, due to the randomisation of the CNTs in the skin layer and the sample core promoting network formation.
In order to further study the effect of the annealing treatment on the sample morphology, a column wise study of the exponent s against the gate distance is performed. So the sample is divided into four columns, were column 1 for example corresponds to locations 1, 5, 9 and 13 as seen in in figure 3.1. A linear regression of the exponent s against the gate distance has been performed for each column of the annealed samples. The corresponding regression coefficients a and b, which represent the slope and the offset of the linear regression curve, and the R^2-values of each column for the three annealed samples can be found in table 5.2. When analysing the data presented in the table, it needs to be noticed that column 1 and 4 and column 2 and 3 are symmetric over the width of the width of the sample.

Table 5.2: Regression parameters of the column wise linear regression for the three injection molded samples.

		Coefficient - a	**Coefficient - b**	R^2
IM3: 0.5 h @ 150 °C	Column 1	0.028	0.733	0.4
	Column 2	0.0569	0.531	0.79
	Column 3	0.0394	0.613	0.87
	Column 4	0.0377	0.683	0.55
IM3: 1 h @ 150 °C	Column 1	0.0491	0.6828	0.55
	Column 2	0.0257	0.6236	0.68
	Column 3	0.0436	0.5722	0.85
	Column 4	0.03	0.7028	0.44
IM3: 3 h @ 150 °C	Column 1	0.0286	0.7359	0.53
	Column 2	0.0642	0.5117	0.90
	Column 3	0.0676	0.503	0.86
	Column 4	0.0407	0.6992	0.59

Before analysing the column wise regression data of the annealed samples, the regression data of as injection molded sample IM3 in table 3.7 is reviewed. From the results of the column wise study of the exponent s against the gate distance, it has been concluded from studying the regression coefficients a and b that for the hard injection molding setting IM3 no similarity of the morphology over the sample width is indicated. In addition to that relatively low R^2 values have been found indicating that s is scattered. From both these findings it has been concluded that the hard setting IM3 results in an anisotropic morphology along the melt flow and over the sample width, which is the reason for the non-uniform in-plane distribution of the electrical properties.
Now that the results of the as injection molded sample are reviewed, the results of the annealed samples can be studied. First of all the column wise regression coefficients a and b, shown in table 5.2, of the annealed samples are looked at. Comparing the regression coefficients for the symmetric columns, it can be seen that the annealing treatment reduces the differences between the coefficients of symmetric columns. For example after 3 h of annealing a of column 2 and 3 is very similar with values of 0.0642 and 0.0676. Looking at the effect of different annealing times, it can be seen that all the times used result in similar differences across the coefficients. Based on these observations it can be said that the below melt temperature annealing treatment reduces the anisotropy of the morphology across the sample width, which leads to an increase in electrical property magnitude similarity across the width of the composite sample. In addition to that it can be seen that all the annealing treatments

used lead to a decrease in scatter of s, which is represented by the higher R^2 values after annealing. This again is an indication for the decrease in anisotropy of the sample morphology due to annealing. So based on the findings on the exponent s along the melt flow and over the width of the sample, it can be said that annealing leads to an overall decrease in anisotropy of the sample morphology. This confirms the finding of a reduction of the non-uniform in-plane distribution of the electrical properties as described earlier in this chapter.

Up to this point in the discussion on the effect of the annealing treatment on the sample morphology, it has been established that below melt temperature annealing is capable to reduce the effect of the oriented CNTs in both the skin layer and the core of the sample on the electrical properties by randomising the CNT orientation. However it also has been observed that the morphology still remains anisotropic along the melt flow and over the width of the sample, which results in a non-uniform in-plane distribution of the electrical properties. So in addition to the skin layer, as described in chapter 3.2, it is expected that the initial overall dispersion of the CNTs in the polymer matrix also has an effect on the electrical properties and their distribution. In literature it has been described that the extend of agglomeration and overall dispersion of the CNTs within the polymer matrix leads to a lowering of the electrical properties and that annealing tends to decrease the degree of agglomeration and up to 7 orders of magnitude improvement of the conductivity have been reported [29]. However in this chapter only up to 3 orders of magnitude improvement in conductivity due to below melt temperature have been found. This indicates that the below melt temperature annealing treatment has no effect on the overall dispersion of the CNT fibres in the polymer matrix.
So in order to further study the dispersion of the CNTs within the polymer matrix, scanning electron microscopy (SEM) has been performed using the as injection molded IM3 sample and the 0.5 h at 150 °C annealed IM3 sample. For the SEM investigation locations 14 and 15, as described in figure 3.1, are used since for locations furthest away from the injection gate the best morphology in terms of conductive networks is expected. The study of the composite morphology has been conducted using a JEOL JSM-7500F scanning electron microscope and in addition to that it needs to be mentioned that the observed surface has not been additionally treated. In figures 5.31 and 5.32 two example pictures of the composite morphology of the as injection molded sample IM3 at location 14 can be seen.

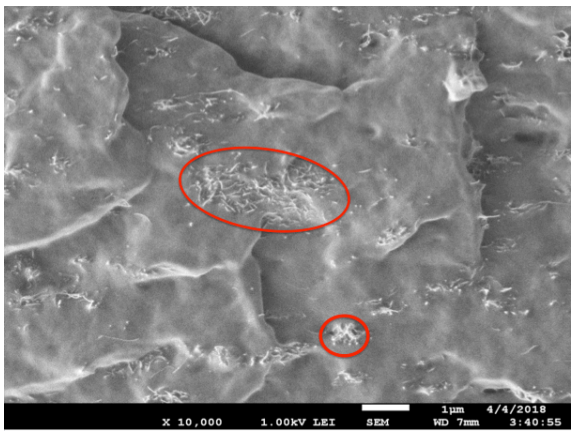

Figure 5.31: Picture of the morphology at a depth from the surface of ~10 μm - 20 μm of the as injection molded sample at location 14.

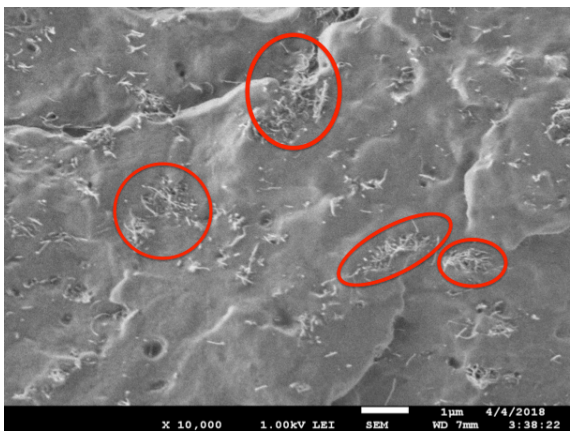

Figure 5.32: Picture of the morphology at a depth from the surface of ~500 μm of the as injection molded sample at location 14.

Looking at figures 5.31 and 5.32 a qualitative description of the as injection molded morphology can be given. In both pictures CNT agglomerates of with varying sizes can be seen, as indicated by the red circles. In both figures it can be seen that the CNTs primarily are found in small and larger clusters/agglomerates. In addition to that it can be noticed that there is no large scale interconnection between the CNT agglomerates by individual CNTs. Thus for the as injection molded sample it can be said that no optimal CNT dispersion in terms of high electrical properties is achieved since the CNTs are primarily found in agglomerates with minimal interconnection. In addition to that it can be said that this morphology is found through the whole sample depth as figure 5.31 corresponds to a depth

of 10 μm - 20 μm from the sample edge and figure 5.32 is in the core at a depth of 500 μm.
As a next step the morphology and the CNT dispersion of the 0.5 h high MFI sample at location 15 is looked at. Two example pictures of the resulting morphology can be found in figures 5.33 and 5.34.

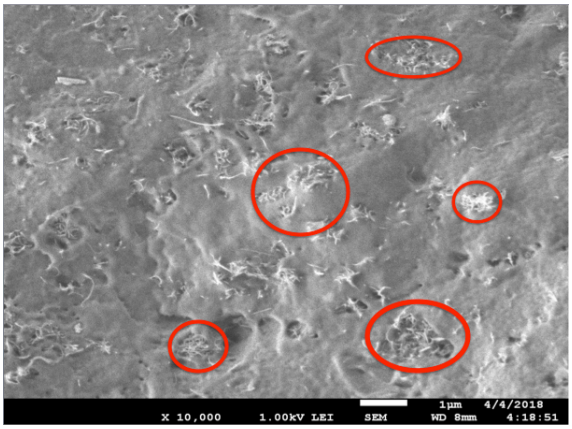

Figure 5.33: Picture of the morphology at a depth from the surface of ~120 μm of the 0.5 h annealed high MFI sample at location 15.

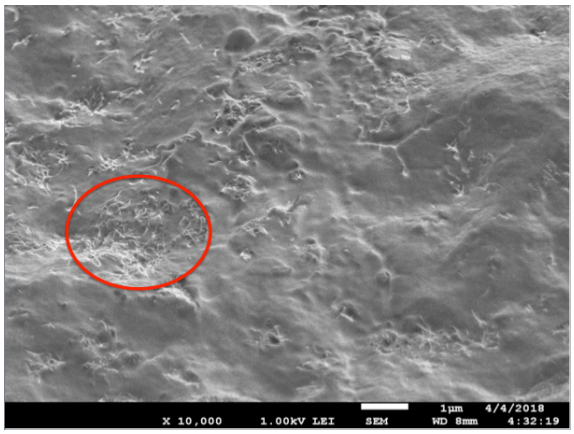

Figure 5.34: Picture of the morphology at a depth from the surface of ~350 μm of the 0.5 h annealed high MFI sample at location 15.

Again when looking at the sample morphology after annealing, agglomeration of the CNTs can be seen as indicated by the red circles in figures 5.33 and 5.34. Similarly to the morphology before annealing, after annealing the CNTs are primarily found in agglomerates and no large scale interconnection between the agglomerates can be seen. This observation confirms that the below melt temperature annealing process does not have an effect on the overall dispersion of the CNTs because before and after annealing a similar dispersion of the CNTs within the polymer matrix is found. It can be said that the below melt temperature annealing treatment does not lead to the formation of further conductive networks between the CNT clusters in the polymer matrix. Based on that observation it can be explained why the below melt temperature annealing treatment is less efficient in improving the electrical properties compared to the above melt temperature annealing as described in literature [29]. The improvement of the electrical properties is expected to occur due to the randomisation of the CNT orientation, which increases the tube-to-tube contacts within the agglomerates.
In order to better explain the non-uniform in-plane distribution of the electrical properties, the sample morphology of the 0.5 h annealed sample for a location close to the injection gate has been looked at. In figure 5.35 and 5.36 the morphology of the annealed sample at location 2 is shown.

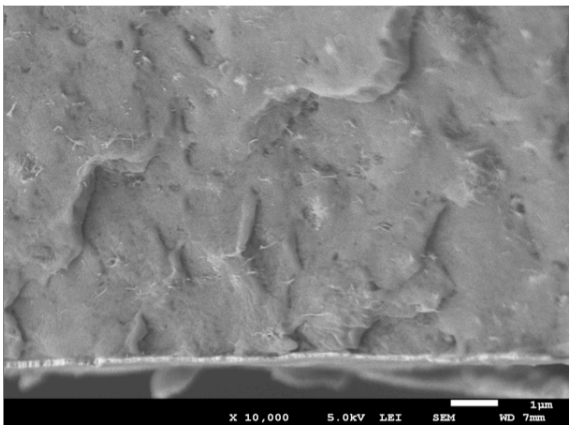

Figure 5.35: Picture of the morphology at a depth from the surface of ~10 μm of the 0.5 h annealed high MFI sample at location 2.

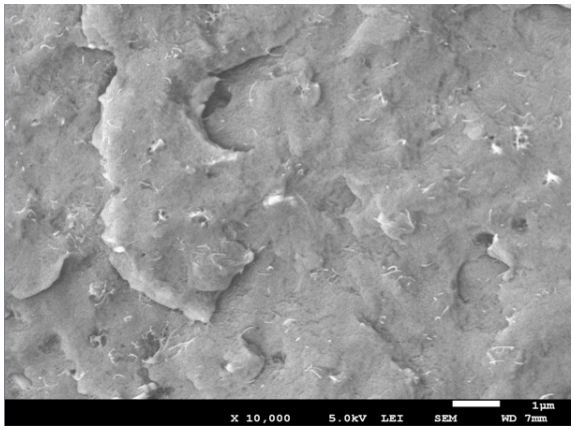

Figure 5.36: Picture of the morphology at a depth from the surface of ~500 μm of the 0.5 h annealed high MFI sample at location 2.

In order to better explain the non-uniform in-plane distribution of the electrical properties, the sample morphology of the 0.5 h annealed sample for a location close to the injection gate has been looked at. In figure 5.35 and 5.36 the morphology of the annealed sample at location 2 is shown. Comparing the morphology of the annealed sample close to the injection gate in figures 5.35 and 5.36 with the morphology far away from the injection gate as seen in figures 5.33 and 5.34, some differences can be identified. Close to the gate smaller agglomerates of the CNTs are found compared to far away from the gate. Close to the gate the gate the CNTs mainly are dispersed in small agglomerates or individual CNTs. Again close to the gate no large scale interconnection between the small agglomerates and the individual CNTs can be seen. The occurrence of smaller agglomerates and individual CNTs close to the gate can be explained by the shear forces experienced during the IM process. Close to the gate the shear forces are higher [3], which breaks down the CNT agglomerates. So for both locations close and far away from the gate bad CNT dispersion is observed in terms of high electrical properties, as there is no large scale interconnection between the agglomerates and individual CNTs. The increase in electrical property magnitude along the melt flow can be explained by looking at the CNT distribution along the melt flow as shown in figure 2.6. It has been reported that close to the gate lower CNT concentrations are found compared to far away from the gate [2]. This finding can be directly related to the morphology as seen in this study. A high concentration of CNTs far away from the gate can be related to the occurrence of larger agglomerates and thus higher electrical properties. In contrast to that a low concentration of CNTs is more likely to form small agglomerates and lead to smaller electrical property magnitudes as seen close to the gate.

Based on the observations made in this section, a description of the effect of the below melt temperature annealing treatment on the composite morphology can be given. The below melt temperature annealing treatments lead to an improvement of the conductivity σ' up to 3 orders of magnitude. This can be related to the fact that the orientation of the CNTs in the skin layer and sample core gets randomised during annealing, which reduces the impact of the insulating skin layer and the overall CNT orientation on the electrical properties of the composite. In terms of CNT dispersion it can be said that the below melt temperature annealing treatment has no impact on the overall dispersion of the CNTs within the polymer matrix. For the injection molded samples before and after annealing it has been identified that the CNTs are mainly found in clusters of varying sizes with minimal interconnection between the clusters. Along the melt flow differences in CNT dispersion and concentration are identified, which results in the non-uniform in-plane distribution of the electrical properties. It is expected that the use of higher annealing temperatures or a better initial dispersion of the CNTs in the polymer matrix will lead to higher overall electrical properties and to a more homogeneous distribution of the electrical properties.

5.3. Summary and Recommendations

In this section the findings on the effect of the below melt temperature annealing treatment on the properties of the composites are summarised and recommendations for further research are given. The findings presented in this chapter are summarised by reflecting them to the research questions given in chapter 2.

The first research question of this chapter deals with the impact of the below melt temperature annealing treatment on the electrical properties and their in-plane distribution. For the high MFI composite a melt temperature of 165 °C has been determined and thus annealing has been performed at 150 °C to prevent the sample from melting. Due to the annealing treatment at 150 °C both the real permittivity ϵ' and the conductivity σ' improved in magnitude over the whole frequency range from 1 Hz to 10^6 Hz. For the conductivity σ' an improvement of up to 3 orders of magnitude in the low frequency range has been found due to below melt temperature annealing. In terms of the in-plane property distribution it has been shown that the distribution of both ϵ' and σ' still remains non-uniform after annealing. So again it has been seen that the property magnitude increases with distance to the injection gate. However it has been shown that the property non-uniformity both along the melt flow and over the width of the sample decreases due to annealing. Annealing also has been perfomed using the low MFI composite, which has a melt temperature of 160 °C and annealing has been performed at 145 °C. For the low MFI composite no relevant improvements in both ϵ' and σ' have been observed over the

whole frequency range. Thus it can be said that for the low MFI composite, below melt temperature annealing is not sufficient to improve the electrical properties of the composite.
The second research question deals with the effect of varying annealing times on the resulting electrical property magnitude and their in-plane distribution. During the study presented in this chapter annealing times of 0.5 h, 1 h and 3 h have been used. For the high MFI composite it has been shown that 0.5 h is sufficient to achieve the maximum improvement of the electrical properties. Longer annealing times did not yield further improvements of the electrical properties. In terms of the in-plane distribution it also has been shown that all the annealing times used lead to similar in-plane distributions. Looking at the low MFI composite none of the annealing times used during the experiments presented in this chapter lead to improvements of the electrical properties of the composite.
The third research question deals with the effect of the cooling rate after annealing on the resulting electrical property magnitude. In order to study the effect of the cooling rate, the high MFI samples have been annealed for 0.5 h at 150 °C and after that a slow cooling rate, by means of atmospheric cooling, and a fast cooling rate, by means of quenching in water, have been used. For both cooling rates it has been seen that the magnitude of both ϵ' and σ' improved over the whole frequency range. The properties for both cooling rates are within the same order of magnitude. But it has been shown that fast cooling after annealing leads to leads to smaller improvements of the electrical properties. It has been concluded that slow cooling promotes the formation of crystal regions in the composite matrix, which tends to decrease the CNT-to-CNT distances and thus promotes the formation of conductive networks.
Lastly the question on the effect of the below melt temperature annealing treatment on the composite morphology is answered. In chapter 3 it has been concluded that injection molding leads to the formation of an insulating skin layer and a non-uniform CNT concentration along the melt flow, which leads to lower electrical properties and a non-uniform in-plane property distribution. It has been shown that the below melt temperature annealing treatment is able to reduce the effect of the insulating skin layer on the electrical properties. Due to annealing the orientation of the CNTs in the skin layer gets randomised and thus promotes the formation of conductive networks through the thickness of the composite. However it also has been noted that the CNTs in the sample core experience reorientation and thus the conductive networks are further improved. Thus after annealing differences in morphology between the skin layer and the sample core still are present, which lower the overall electrical properties of the composite. Moreover it has been shown that the morphology of the annealed sample still is anisotropic along the melt flow and over the width of the sample, which explains the non-uniform property distribution. Looking at the composite morphology it has been shown that below melt temperature annealing has no impact on the large scale dispersion of the CNTs in the polymer matrix. Before and after annealing agglomeration and no large scale interconnection of the CNTs has been found. In addition to that it has been indicated for both before and after annealing that close to the gate lower CNT concentrations are found compared to locations far away from the gate. This again shows that below melt temperature annealing has no effect on the CNT dispersion, which leads to the non-uniform electrical property distribution. The randomisation of the CNTs during below melt temperature annealing only effects the small scale morphology as it increases the tube-to-tube contacts in the CNT clusters.

Based on the observations and conclusions made on the below melt temperature annealing of carbon nanocomposites, some recommendations for further research are given in order to further explore the effects of annealing on the electrical properties and the sample morphology. Looking at the low MFI composite it has been shown that the below melt temperature annealing treatment did lead to improvements of the electrical properties. For further research it is recommended to use longer annealing times in order to check if it leads to improvements of the electrical properties. Moreover it has been seen that there are opposing views in literature on the effect of the cooling rate on the resulting electrical properties. It also has been indicated that the filler volume of the composite is decisive for the effect of the cooling rate. In this study it has been shown that for a high filler loading a slow cooling rate is beneficial for high electrical properties. For further research is recommended to repeat the cooling rate experiments using composites with a lower filler loading in order to check if the conclusion made in this chapter still holds true. In addition to that it has been concluded that slow cooling is beneficial for the electrical properties as it leads to the formation of crystal regions, which promote the formation of conductive networks. For further work it is recommended to further investigate the effect of crystallinity on the filler dispersion and the resulting electrical properties.

6

Part 4: Dielectrophoresis on injection molded carbon nanocomposites and study of the resulting electric properties

In this chapter the effect of dielectrophoresis (DEP) on the electrical properties of the injection molded carbon nanocomposites is studied. From the study presented in chapter 5 it has been indicated that below melt temperature annealing improves the morphology and electrical properties of the composite by randomising the orientation of the CNTs and thus promotes the formation of new conductive networks. However it has been shown that the overall dispersion of the CNTs is not effected by the below melt temperature annealing treatment. Hence an electric field is applied to the composite sample during the annealing treatment to provide an additional driving force to further improve the dispersion of the CNTs and thus further improve the electrical properties.
In section 6.1 the experimental setup used to perform the dielectrophoresis experiments is described. Followed by that in section 6.2 the experimental results of the dielectrophoresis experiments are shown and discussed. Lastly in section 6.3 the main findings of this chapter are summarised and recommendations for further research are given.

6.1. Experimental Procedure

In this section the experimental procedure used for studying the effect of dielectrophoresis on the electric properties of the injection molded composite samples is described. During the study presented in this chapter, composite samples containing the high MFI polypropylene matrix and a 5wt.% filler loading of CNTs have been used. These samples have been produced using the normal injection molding setting IM1. Further details on the composite materials and the production process used can be found in the experimental section 3.1.

Definition of the Dielectrophoresis Experiments

In order to study the effect of dielectrophoresis on the electric properties of the composite samples, an experimental setup has been defined to perform this process. A schematic of the DEP setup used can be found in figure 6.1.

The DEP treatment is conducted by placing the composite sample in between two aluminium electrodes, which act as capacitors to apply an electric field on the sample. The composite sample is loaded into the DEP setup with the core-side facing up and the cavity side facing down towards the heater plate. During the DEP treatment an AC electric field is applied to the composite sample, as this is

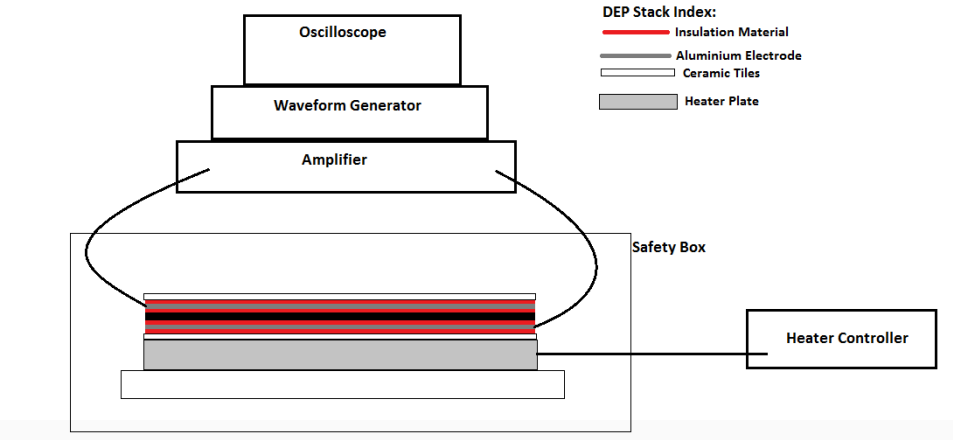

Figure 6.1: Schematic of the DEP setup used during the experiments.

expected to promote a uniform dispersion of the CNTs through the sample thickness. The electrodes have been wrapped with FEP foil in order to insulate the electrodes from the sample and thus avoid shorting the electrical circuit. The electric field is created by connecting the two electrodes to the control setup.
This setup consists of an Agilent 33210A waveform generator, which controls the shape, the amplitude and the frequency of the electrical signal. This signal is applied to the aluminium electrodes by connecting the electrodes to a TREK Model 10/10B-HS high voltage amplifier via electrical wires. As already mentioned an AC electric field is applied using a signal with a sinusoidal shape and a frequency of 200 Hz. During the DEP treatments different peak-to-peak voltages are used to study the effect of varying electric field strengths on the resulting electrical properties. The applied electric signal is monitored using the Keysight InfiniiVision DSO-X-2002A oscilloscope. In order to ensure a stable electric field during DEP, the phase angle between the electric signal applied and the AC circuit is monitored using the oscilloscope. The two aluminium electrodes serve as capacitors when a phase angle of $\phi \sim 90\,^{\circ}$ is shown by the oscilloscope and a short circuit is observed by a phase angle of $\phi \sim 0\,^{\circ}$.
In addition to that the sample is heated during DEP in order to create mobility for the CNTs to move within the polymer matrix. The heater setup consists of a heater plate, which is controlled using a thermocouple and a Jumo cTron16 PID Controller. The heater plate is placed on a ceramic tile on the bottom of the DEP setup. In order to ensure uniform heating of the composite sample during the DEP treatment, aluminium oxide plates (described as ceramic tiles in figure 6.1) are placed on top and below the electrodes. A further aspect that needs to be mentioned is that, the DEP setup is clamped together to ensure a uniform heating of the sample and a uniform distribution of the electric field. In figures D.1, D.2 and D.3 additional pictures of the DEP setup used during the experiments can be seen. Lastly it needs to be mentioned that the DEP setup is placed inside a box for safety reasons.
In table 6.1 an overview of the conducted DEP experiments can be found. DEP is performed using varying heater temperatures and varying electric field strengths in order to study the effect of these process parameters on the resulting electrical properties. It needs to be noted that the electric field strength can be derived from the applied voltage since the field strength is equal to the voltage divided by the distance between the electrodes. In addition to that the the voltage given represents the peak-to-peak voltage.

Looking at table 6.1 it can be noted that the heater temperatures used during DEP are higher compared to the annealing temperatures used in chapter 5. However due to prior investigations it can be said that these heater temperatures will not melt the composite sample and thus create comparable temperature conditions as during the annealing experiment. In addition to that the DEP experiment is performed without applying a voltage to the heated sample in order to create a reference measurement. So in total 18 DEP experiments are performed over a voltage range from 0 V to 2000 V and a heater temperature range from 160 °C to 210 °C.
The DEP procedure for each temperature and each applied voltage is conducted for 0.5 h. This DEP

Table 6.1: Overview Matrix of the DEP experiments performed during the presented study.

		Applied Voltages			
		0 V	**500** V	**1000** V	**2000** V
Heater Temperature	**160 °C**	X		X	
	170 °C	X	X	X	X
	180 °C	X	X	X	X
	190 °C	X	X	X	X
	200 °C	X		X	
	210 °C	X		X	

time has been chosen since it has been concluded from the results in chapter 5 that 0.5 h of annealing at 150 °C is sufficient to improve the electrical of the high MFI composite. In order to ensure uniform uniform heating, the sample is heated for 15 minutes prior to the 0.5 h of DEP. During this heating phase the electric field already is applied to the setup. It also needs to be noted that during the DEP experiments a circular cut-out with a diameter of 50 mm of the high MFI IM1 samples has been used. The cut-out has been taken from the centre of the sample and thus corresponds to locations L6, L7, L10 and L11 as depicted in the sample mask shown in figure 3.1.
After the DEP treatment, the samples are prepared for the BDS measurements as described in the experimental section 3.1. This entails the gold sputtering of the sample surfaces and cutting of the sample. After the sample preparation steps, the electrical properties of the sample are measured by means of BDS. The electric properties of L6, L7, L10 and L11 are measured over a frequency range from 1 Hz to 10^6 Hz. Further details on the BDS measurement procedure used can be found in section 3.1.

6.2. Experimental Results and Discussion

In this section the experimental results of the DEP treatments at varying heater temperatures and electric field strengths are shown an discussed. As a first step the changes in electrical property magnitude due to the DEP treatments is studied. This is followed by a comparison of the DEP results with the annealing results and the differences in results are further investigated.
From the experimental description in section 6.1 it has already been indicated that the DEP treatment has been performed with heater temperatures ranging from 160 °C to 210 °C and in order to study the effect of the electric field, voltages in the range between 0 V to 2000 V have been applied during the treatment. The effect of the DEP treatment is studied by looking at the conductivity σ' at 127 Hz (quasi-DC region) and 100 kHz (AC region). In figures 6.2 and 6.3 the resulting σ' magnitude at 127 Hz and 100 kHz for the varying electric field strengths and heater temperatures can be seen. When looking at these figures it needs to be noted that the sample with 0 V serves as a reference since no electric field has been applied during the annealing phase.

As a first step the improvement of the conductivity σ' at 127 Hz due to the DEP treatments, shown in figure 6.2, is looked at. It can be noted that a heater temperature of 160 °C does not yield any improvement of σ' compared to the as injection molded sample, which has a magnitude of σ' in the range of 10^{-7} S/cm. Increasing the temperature further yields an improvement of 1 order of magnitude. Looking at the graph it can be noted that the temperature range from 170 °C to 190 °C yields a similar order of magnitude of improvement of σ' and it also can be noticed that the application of an electric field does not lead to further improvements. For heater temperatures up to 210 °C an overall improvement of σ' of 6 orders of magnitude has been found. But again for a heater temperature of 210 °C the application of an electric field does not further enhance the magnitude of the conductivity σ' compared to the reference sample with 0 V.
Similarly when looking at the improvement of σ' at 100 kHZ, shown in figure 6.3, it can be noted that the application of an electric field during the annealing process does not lead to further improvements of the magnitude of σ'. Again at 160 °C no improvement of σ' compared to the as injection molded sample is found and for the temperature range from 170 °C to 190 °C only a slight improvement of up to 1 order of magnitude is seen. And again for higher temperatures up to 210 °C a large improvement

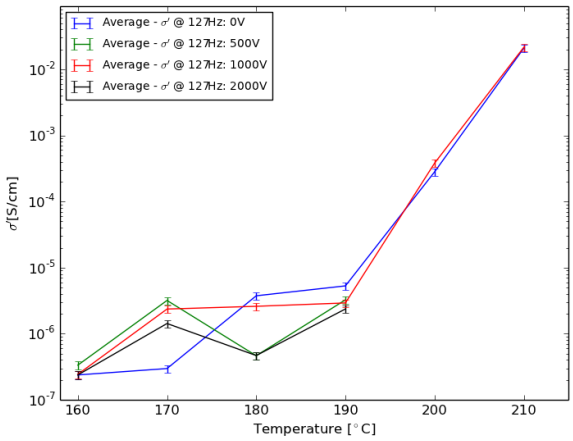

Figure 6.2: Improvement of the conductivity σ' at 127 Hz due to the DEP treatments at varying temperatures.

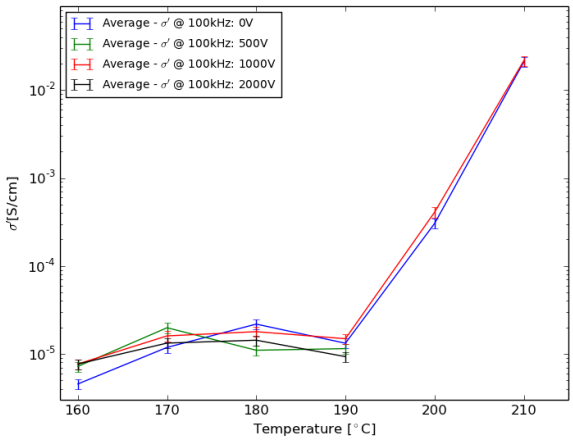

Figure 6.3: Improvement of the conductivity σ' at 100 kHz due to the DEP treatments at varying temperatures.

of the conductivity is found with an increase of 5 orders of magnitude.
All in all from analysing the change in σ' due to the DEP treatment it can be said that the application of an electric field during the annealing process does not further improve the electrical properties of the composite. It thus is expected that changes in conductivity are due to the heating of the sample. However when comparing the improvement of σ' during the DEP process with the annealing improvements described in chapter 5.2 some differences can be observed. First of all it can be noted that during the DEP experiments higher temperatures have been used compared to the 150 °C during annealing. However due to bad insulation etc. of the DEP setup it is expected that heater temperatures between 160 °C - 180 °C should yield similar annealing temperatures as for the annealing experiments of chapter 5. From the annealing experiments in chapter 5.2 it has been concluded that 0.5 h of annealing at 150 °C improves σ' at 127 Hz up to 3 orders of magnitude. In order to better compare the σ' measurements of the annealed sample with the DEP sample at 0 V and 1000 V with varying heater temperatures, additional comparative plots can be found in figures D.4 - D.13. Directly comparing the DEP treatments with heater temperatures 170 °C to 190 °C with the oven annealed samples it can be observed that DEP leads to half the improvement of σ' compared to the below melt temperature annealing treatment. However during the DEP experiments at 180 °C and 190 °C it has been noted that the sample surface pointing towards the heater partially melted, indicating temperatures above the melt temperature. Further increasing the heater temperature to 200 °C and 210 °C fully melted the composite samples and thus lead to higher improvements of the electrical properties as this gives rise to more mobility for the CNTs to improve their dispersion. Looking at the improvement of σ' due to heater temperatures of 210 °C, similar improvements of σ' during melt annealing at 200 °C as described in literature have been found [27]. From the observations made comparing the DEP measurements with the annealing measurements it can be said, that the experimental results of these two treatments are not directly comparable due thermal differences and inaccuracies of the DEP setup. But nevertheless the conclusion that the application of an additional electric field during annealing is not effective in further enhancing the electrical properties still holds true.

Moreover the observation that heater temperatures of 170 °C to 190 °C only yield half the improvement of below melt temperature annealing indicates that the experimental setup used during DEP non-uniformly heats the sample and leads to a thermal gradient through the sample thickness. This thermal gradient is expected to create a non-uniform morphology through the sample thickness. In order to better understand the thermal effects during the DEP experiments on the sample morphology further experiments to investigate these effects have been conducted.
As a first step in examining the thermal effects during the DEP experiments, the effect on the sample morphology is to be quantified. The study of the thermal effects on the sample morphology has been done using a heater temperature of 180 °C and no electric field (0 V) has been applied to the sample. The morphological differences are investigated by means of BDS measurements. An illustration of the

first experiment to study the thermal effects can be seen in figure 6.4.

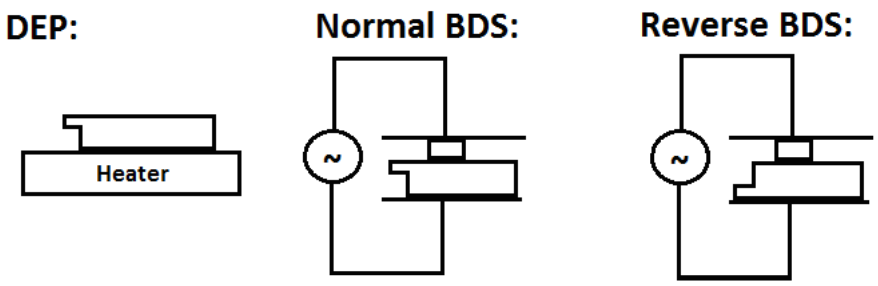

Figure 6.4: Descriptive sketch of the reverse BDS experiment to determine the thermal effects during DEP.

In figure 6.4 it is indicated that during the DEP experiments the cavity side of the composite sample faces towards the heater and for all the BDS measurements described up to this point the upper electrode during BDS has been applied to the sample side facing away from the heater (core side). So in order to study the effect of the heating process on the sample morphology, the gold sputtering of the sample annealed at 180 °C with 0 V has been removed and reapplied in reverse. Hence the reverse sputtering/BDS uses the side facing towards the heater (cavity side) as the upper electrode and the side facing away (core side) as the bottom electrode. The resulting BDS measurements of the normal BDS and reverse BDS can be seen in figure 6.5.

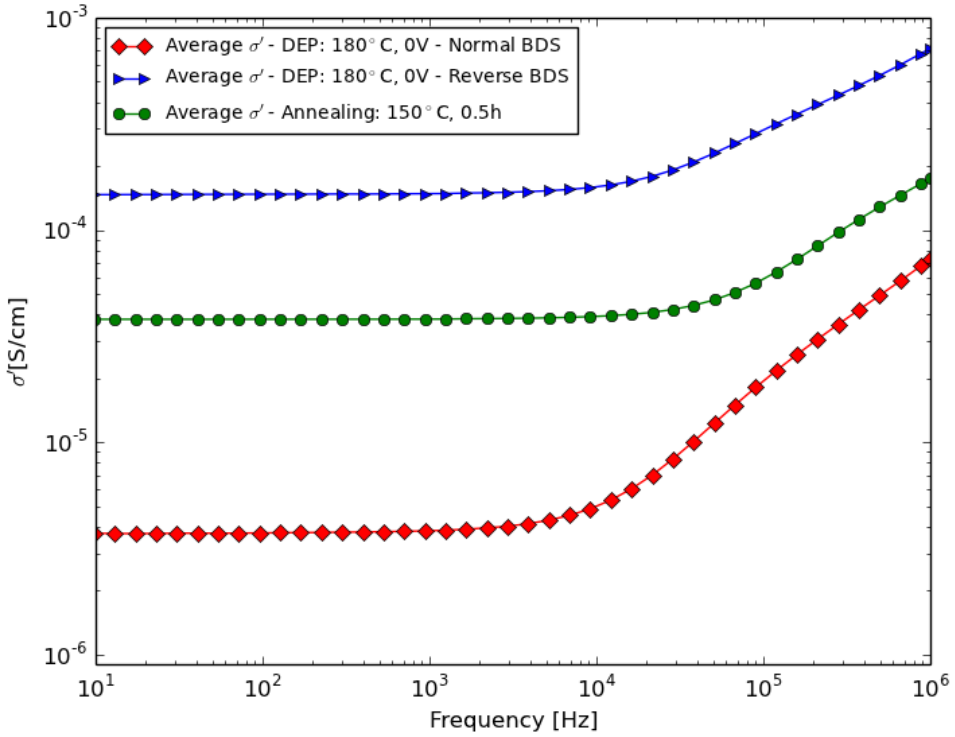

Figure 6.5: Comparison of the measurement results of σ' for the normal BDS process against the reverse BDS process.

Looking at the measurement of the normal BDS and reverse BDS shown in figure 6.5 some observations on the thermal effects during DEP can be made. The normal BDS measurement shows a quasi-DC conductivity magnitude in the range of 2*10^{-6} S/cm, which is one order of magnitude order of magnitude higher than the conductivity of the as injection molded sample. However the measure-

ment σ' of the reverse BDS has a quasi-DC magnitude of $10^{-4}\ S/cm$ and thus is 2 orders of magnitude larger than the normally measured σ' after DEP. In addition to that it can be noted that the reverse BDS measurement yields a magnitude of σ', which is about one order of magnitude larger than the conductivity of the annealed sample at 150 °C. Comparing the conductivity magnitude of the reverse BDS measurement with the result of the DEP experiments at 200 °C, shown in figure 6.2, it can be noted that they are within the same order of magnitude. This can be explained due to the fact that the sample side facing towards the heater during DEP at 180 °C showed partial melting of the surface. When performing the normal and reverse BDS measurement it would be expected that both these measurements yield similar magnitudes of σ' as this would suggest a relatively homogeneous morphology through the sample thickness. However it has been observed that the different measurement procedures yield large differences in the σ' magnitude. This observation suggest that there are differences in the morphology through the sample thickness, which have been induced by a thermal gradient through the sample thickness during DEP. It is expected that the sample side facing towards the heater experiences higher temperatures and thus creates more mobility for the CNTs to reorient and form new networks. In order to further study the thermal gradient during the DEP process, a further experiment has been defined. A descriptive sketch of the second experiment investigating the thermal gradient is shown in figure 6.6.

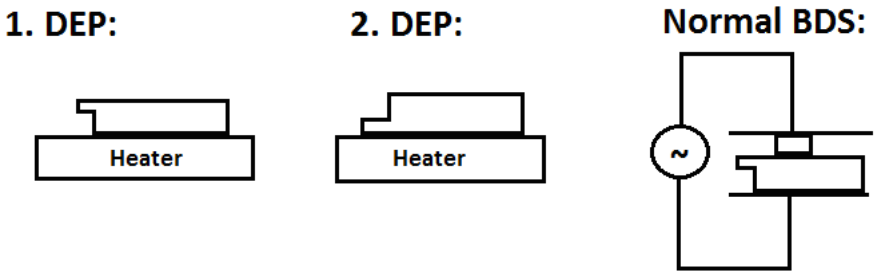

Figure 6.6: Descriptive sketch of the double DEP experiment to study the thermal effects during DEP.

In order to further study the thermal gradient through the sample thickness during DEP, the DEP process is performed twice on the same sample as depicted in figure 6.6. For this experiment again a heater temperature of 180 °C has been used while no electric field is applied (0 V). In the first DEP step the cavity side of the sample faces towards the heater and in the second DEP step the core side faces towards the heater. After that the normal BDS procedure is performed in order to measure the electric properties of the composite. The outcome of this experiment in comparison with the results of the other experiment on the thermal gradient described before can be seen in figure 6.7.

Looking at the measurement results, presented in figure 6.7, some further observations on the thermal gradient during the DEP experiments can be made. First of all it can be noted that the double DEP treatment leads to an increase of σ' into the $10^{-2}\ S/cm$ range and quasi-DC behaviour is measured over the whole frequency range. Similar measurement results can be observed for the DEP experiments at 210 °C during which the composite was fully molten, shown in figures D.12 and D.13. Also when comparing the double DEP conductivity measurements with the normal BDS measurement and reverse BDS measurement of the DEP process at 180 °C with 0 V some differences can be identified. The conductivity double DEP is 4 orders of magnitude larger compared to the quasi-DC conductivity of the normal BDS measurement and the double DEP is 2 orders of magnitude larger than the reverse BDS measurement.
In order to check the conductivity of the double DEP sample, reverse BDS has been performed on this sample as well. A comparative plot of the normal BDS measurement and the reverse BDS measurement of the double DEP sample can be found in figure D.14. From that comparison it can be seen that the reverse BDS results in a σ' measurement that is within the same order of magnitude as the normal BDS measurement. The differences between the two measurements are within the accuracy range of the BDS measurement repetition described in the repeatability study of section 3.2.1. Using this observation it can be said that the double DEP process creates a uniform sample morphology through the sample thickness and thus is not effected by the thermal gradient.

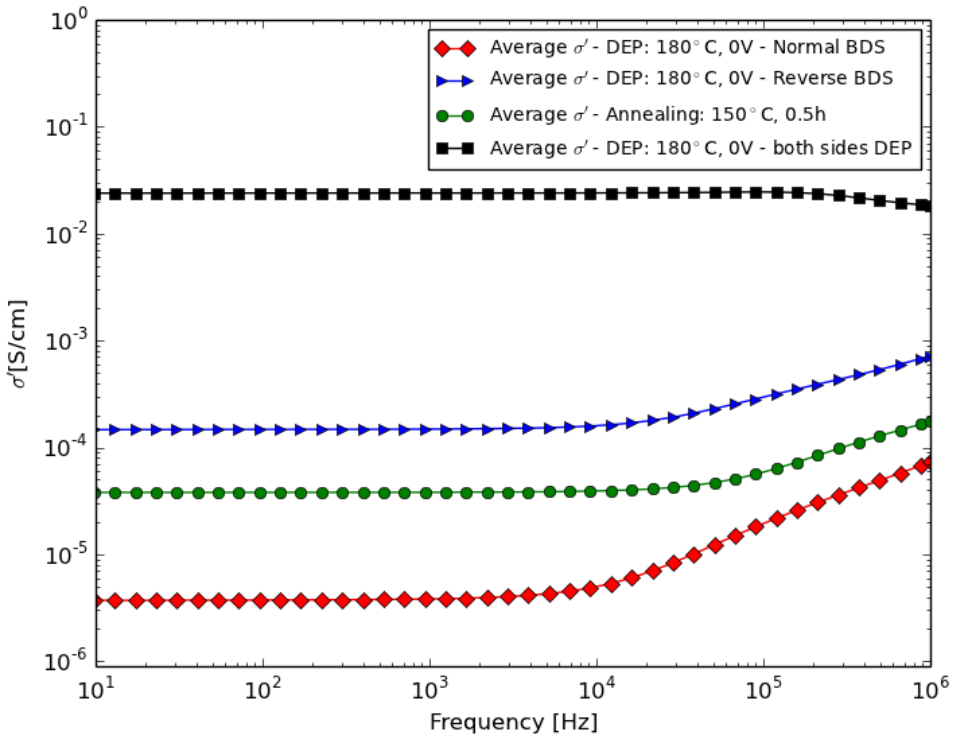

Figure 6.7: Comparison of σ' magnitude due to the single and double DEP treatment.

All in all from the observations made during the previously described experiments it can be concluded that the DEP setup leads to a thermal gradient through the sample thickness. This thermal gradient leads to a non-uniform temperature profile through the sample thickness and thus does not provide uniform annealing conditions for the CNTs to reorganise within the polymer matrix. Due to that reason it is expected that the DEP setup creates a non-uniform morphology through the sample thickness. Looking at the conductivity magnitudes after DEP, presented in figures 6.2 and 6.3, it is expected that the σ' magnitudes between 160 °C to 190 °C are most effected by the presence of the thermal gradient since these temperatures are very close to the melting temperature of the composite. Hence the sample side facing away from the heater does not reach a sufficiently high temperature to provide mobility for the CNTs to move. However it again needs to be noted that the finding of a thermal gradient during the DEP experiments does not change the conclusion that the additional application of an electric field during annealing does not further improve the electrical properties of the composite.

Looking at the DEP efficiency plots in figures 6.2 and 6.3, some further observations can be made. Looking at the σ' improvement at 127 Hz it can be seen that the DEP treatments 0 V at 170 °C, 500 V at 180 °C and 2000 V at 180 °C do not follow the overall improvement trend seen due to the DEP treatment. However when looking at the improvement of σ' at 100 kHz no such outlier measurements are found. In the high frequency range all the samples seem to have a similar σ' improvement due to the DEP treatments. In order to further investigate the differences in DEP efficiency in the low and high frequency range, the BDS measurements of σ' are to be looked at in more detail. In figures 6.8 and 6.9 the BDS measurements of σ' of the samples after DEP treatments at 170 °C and 180 °C are shown.

Looking at the measurement results shown in figures 6.8 and 6.9 some observations can be made. Looking at the measurement results of the previously defined outlier measurements (0 V at 170 °C, 500 V at 180 °C and 2000 V at 180 °C) it can be observed that in the low frequency range, the quasi-DC conductivity is within a similar order of magnitude compared to the as injection molded sample. In

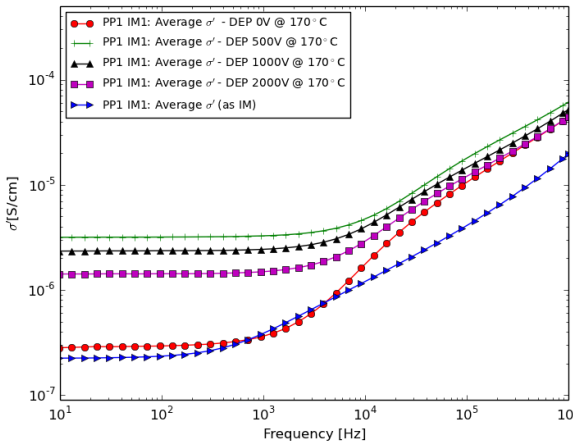

Figure 6.8: Average σ' due to DEP treatments at 170 °C.

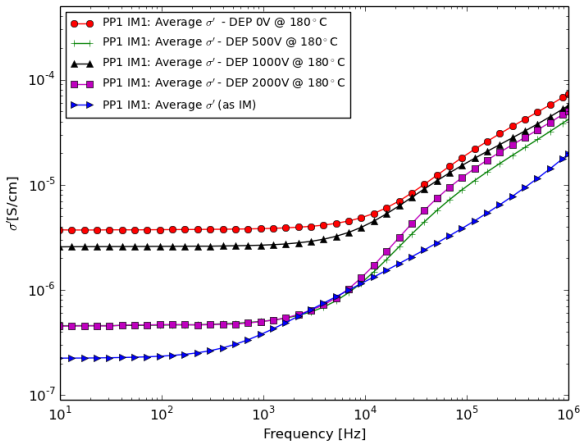

Figure 6.9: Average σ' due to DEP treatments at 180 °C.

contrast to that the other samples after DEP show an improvement of 1 order of magnitude after DEP. With increasing frequency a transition to frequency dependent AC conductivity behaviour is seen. Normally a quasi linear increase of the conductivity with frequency is found in the high frequency range. However the identified outlier samples after DEP show a non-linearity of the AC conductivity, where after the transition frequency the conductivity first follows a similar frequency dependent behaviour as the as injection molded sample. But at a frequency of $\sim 10^4\ Hz$ a jump in the frequency dependent behaviour can be seen after which the outlier samples follow a similar frequency dependent conductivity behaviour as the other samples after DEP. This observation indicates that the DEP treatment of these samples only was efficient in improving the morphology for the high frequency conductivity behaviour. When trying to relate this observation to the resulting composite morphology it is expected that the thermal gradient during DEP induces some non-uniformity of the morphology through the sample thickness, which results in this non-linear AC conductivity slope. However it needs to be noted that the physical process of the frequency dependent conductivity behaviour is not fully understood yet [45]. Thus when looking at literature no further explanations for such non-linear behaviour can be found.

All in all from the observations made during the DEP experiments it can be said that the application of an electric field during the annealing process of the carbon nanocomposite is not effective in further enhancing the electrical properties of the composite. In addition to that it has been shown that the experimental setup used during DEP results in a thermal gradient through the sample thickness and thus leads to a non-uniform change in morphology through the sample thickness. This thermal gradient is expected to be the reason for lower improvements of σ' at lower heater temperatures (160 °C to 190 °C) and it is also expected that the non-linear AC conductivity behaviour is induced by the thermal gradient during DEP.

6.3. Summary and Recommendations

In this section the results of the dielectrophoresis experiments are summarised and recommendations for further research on this topic are given. The results are summarised by reflecting the findings of this chapter to the research questions for this task defined in subsection 2.2.
The first research question to be answered looks at the effect of the dielectrophoresis treatment on the electrical properties of the carbon nanocomposite. From the experimental results it has been shown that the conductivity σ' both at a low and a high frequency tend to increase in magnitude due to the treatments used. However it has been observed that the application of an electric field during heating of the composite sample does not further enhance the electrical properties of the composite. Hence it has been concluded that the additional application of an electric field during annealing (dielectrophoresis) is not effective in further enhancing the electrical properties of the composite.

The next research question to be answered deals with the effect of the temperature during the dielectrophoresis treatment. More specifically dielectrophoresis close to the melt temperature of the composite is to be investigated. When looking at the effect of the DEP temperature it first of all needs to be noted that the experimental setup resulted in a thermal gradient through the sample thickness, which lead to a non-uniform temperature profile through the sample thickness. Due to this thermal gradient the general trend of the temperature used during DEP can not be clearly defined (especially for temperature very close to the melt temperature!). However it has been observed that higher heating temperatures lead to larger improvements of the conductivity of the composite. Looking at the effect of the applied electric field at different heating temperatures, it again can be said that irrespective of the treatment temperature no further improvement of σ' due to the application of an electric field has been observed.
Lastly the question with respect to the effect of the electric strength during DEP on the resulting electrical properties is answered. From the experimental results presented in this chapter it has been observed that irrespective of the electric field strength applied during DEP the same order of magnitude of improvement in conductivity has been achieved. Hence it again can be concluded that the application of an electric field during annealing the composite is not effective in further improving the electrical properties.

Based on the observations and conclusions made in this chapter some recommendations for further research on the topic of dielectrophoresis of carbon nanocomposites can be given. First of all it is recommended to perform in-line resistivity measurements during the DEP treatment in order to get a better understanding on the effect of the electric field on the morphology of the composite during the treatment. Moreover when looking at related literature it has been observed that the application of an electric field during annealing tends to decrease the percolation time. Based on that it is recommended to repeat the DEP experiments using shorter treatment times in order to better observe the effect of varying electric field strengths on the resulting electrical properties. One further recommendation is to repeat the DEP experiments using a different experimental setup in order to ensure uniform heating of the composite and thus create clear trends on the effect of the treatment temperature on the resulting electrical properties. It is recommended to perform DEP in a similar oven as used in the annealing experiments described in chapter 5. Lastly it is recommended to perform DEP using higher annealing temperatures and/or higher electric field strengths as this might lead to an observable effect of the DEP treatment on the electrical properties.

7

Summary & Conclusion

The objective of this master thesis research is to study the electrical properties of injection molded carbon nanocomposites. It has been described that the addition of carbon materials such as carbon nanotubes to a polymer matrix gives rise to good electrical properties, which enables the potential application of these composites in electrical devices or for electromagnetic interference shielding applications. A further interesting aspect of these composites is the possibility of producing them via injection molding, which is the most used production process for plastic components, since it is enables the cost effective and fast production of large quantities. In literature some research efforts with respect to injection molding of carbon nanocomposites and potential heat treatments to enhance the electrical properties have been described. However some shortcomings in the current state-of-the-art knowledge have been identified and are to be addressed in this master thesis research. By addressing these shortcomings a deeper understanding on injection molding of carbon nanocomposites is to be created in order to enable the use and production of carbon nanocomposites on an industrial scale.
In order to get a better understanding on the electrical properties of injection molded carbon nanocomposites, the research conducted in this report has been divided into four parts. In the first part the effect of the injection molding process on the electrical properties and the morphology of the composite has been investigated. Followed by that in the second part the effect of the polymer matrix material on the resulting electrical property magnitude and morphology of the composite is studied. In the third part of this research the possibility of a below melt temperature annealing treatment is presented in order to change the electrical properties of the injection molded composite. Lastly in the fourth part of this thesis the process of dielectrophoresis on injection molded carbon nanocomposites is looked at with respect to the effect on the electrical properties.

Looking at the first research part the effect of the injection molding process on the composite has been determined. The composites studied consist of polypropylene with 5 wt.% of carbon nanotubes and the composites posses a conductivity in the range of $10^{-7}\ S/cm$. It has been shown that the electrical properties of the composite are non-uniformly distributed along the injection melt flow, where the electrical properties tend to increase in magnitude with increasing distance to the injection gate. Over the sample width it has been indicated that the electrical properties tend to be similar in magnitude. Moreover it has been shown that harder injection molding settings tend to increase the non-uniformity of the electrical properties along the melt flow direction and over the sample width. Looking at the resulting morphology due to injection molding it has been shown that injection molding leads to the formation of a skin layer with oriented CNTs in the melt flow direction, which lowers the electrical properties. In addition to that it has been indicated that the skin layer thickness tends to decrease in thickness with distance to the injection gate. Next to that it has been indicated that the CNT concentration tends to increase along the melt flow. Based on these two observations on the composite morphology the non-uniform electrical property distribution along the melt flow can be explained.

In the second part of this master thesis the effect of the polymer matrix material on the electrical properties is studied. It has been shown that using polymers with better flow ability properties (low viscosity or high melt flow index) are favourable for high electrical properties. This has been explained

due to the fact that better flow ability properties decrease the shear forces experienced by the melt during processing and thus creates a more favourable morphology. Looking at the morphology it has been found that composites with better flow ability properties lead to the formation of a thinner skin layer and a better networked sample core during injection molding. However the effect of the injection molding settings on the electrical properties and their in-plane distribution remains the same irrespective of the flow ability properties of the composite.

In the third research part different below melt temperature annealing treatments have been used to enhance the electrical properties and their in-plane distribution. First of all it has been observed that 0.5 h of annealing at 150 °C is sufficient to improve the conductivity of a composite with a high melt flow index by up to 3 orders of magnitude to conductivity magnitudes in the range of 10^{-5} S/cm - 10^{-4} S/cm. In contrast to that below melt temperature annealing does not improve the electrical properties of a low melt flow index composite. Looking at the effect of the annealing treatment on the electrical property in-plane distribution it has been shown that it still remains non-uniform as before. However a decrease in non-uniformity along the melt flow and over the sample width has been observed. Looking at the effect on the sample morphology it has been shown that below melt temperature annealing tends to randomise the orientation of the CNTs, which promotes the formation of new tube-to-tube contacts increasing the electrical properties. But the overall dispersion of the CNTs in the polymer matrix is unaffected by the annealing treatment. It has been shown that before and after annealing the CNTs are mainly found in agglomerates with no large scale interconnection. Moreover it has been shown that the annealing treatment does not eliminate the presence of the skin layer as the improvement of the morphology is uniform through the sample thickness.

Lastly in the fourth part dielectrophoresis as an additional treatment to improve the electrical properties has been investigated. During dielectrophoresis the composite sample is heated up and an electric field between 500 V and 2000 V is applied, which serves as an additional driving force to improve the dispersion of the CNTs. From the experiments it has been shown that the additional application of an electric field during annealing below and above the melt temperature of the composite does not further enhance electrical properties.

Looking at the findings presented in master thesis research it can be said that a great effort has been performed to broaden the knowledge on the electrical properties of injection molded carbon nanocomposites. Using the findings presented in this work the optimal processing settings and composite materials for the highest electrical properties can be defined. Moreover additional treatments to further enhance the injection molded composites electrical properties and their distribution have been described while keeping the geometry of the sample stable. However no full solution for the composites non-uniform in-plane distribution of the electrical properties after injection molding has been found. So for further research it is recommended to further investigate industrially feasible treatments to further improve the uniformity of the electrical property in-plane distribution of injection molded composites.

Bibliography

[1] S. Torres-Giner, A. Chiva-Flor, J.L. Feijoo, *Injection-molded parts of polypropylene/multi-wall carbon nanotubes composites with an electrically conductive tridimensional network,* Polymer Composites **(37)**, pp. 488 (2016).

[2] M. Wegrzyn, S. Juan, A. Benedito, E. Gimenez, *The influence of injection molding parameters on electrical properties of pc/abs-mwcnt nanocomposites,* Journal of Applied Polymer Science **(130)**, pp. 2152 (2013).

[3] Jyri Tiusanen, Daniel Vlasveld, Jyrki Vuorinen, *Review on the effects of injection moulding parameters on the electrical resistivity of carbon nanotube filled polymer parts,* Composites Science and Technology **(72)**, pp. 1741 (2012).

[4] A. Chandra, A.J. Kramschuster, X. Hu, L.S. Turng, *Effect of injection molding parameters on the electrical conductivity of polycarbonate/carbon nanotube nanocomposites,* ANTEC **(4)**, pp. 2171 (2007).

[5] Gulrez et al., *A review on electrically conductive polypropylene and polyethylene,* Polymer Composites **(35)**, pp. 900 (2014).

[6] C.A. Martin et al., *Formation of percolating networks in multi-wall carbon-nanotube–epoxy composites,* Composite Science and Technology **(64)**, pp. 2309 (2004).

[7] Shi-Hong Wu, Iwamoto Mashaharu, Toshiaki Natsuki, Qing-Qing Ni, *Electrical conduction and percolation behaviour of carbon nanotubes/upr nanocomposites,* Journal of Reinforced Plastics and Composites, **(25)**, pp. 1957 (2006).

[8] Y. Ngabonziza, J. Li, C.F. Barry, *Electrical conductivity and mechanical properties of multiwalled carbon nanotube-reinforced polypropylene nanocomposites,* Acata Mechanica **(220)**, pp. 289 (2011).

[9] B.F. Jogi, M. Sawant, M. Kulkarni, P.K. Brahmankar, *Dispersion and performance properties of carbon nanotubes (cnts) based polymer composites: A review,* Journal of Encapsulation and Adsorption Sciences, **(2)**, pp. 69 (2012).

[10] Jyri Tiusanen, Daniel Vlasveld, Jyrki Vuorinen, *Review on the effects of injection moulding parameters on the electrical resistivity of carbon nanotube filled polymer parts,* Composites Science and Technology **(72)**, pp. 1741 (2012).

[11] Young Seok Song, Jae Ryoun Youn, *Influence of dispersion states of carbon nanotubes on physical properties of epoxy nanocomposites,* Carbon **(43)**, pp. 1378 (2005).

[12] Ha-Da Bao, Yao Sun, Zhuo-Yue Xiong, Zhao-Xia Guo, Jian Yu, *Effects of the dispersion state and aspect ratio of carbon nanotubes on their electrical percolation threshold in a polymer,* Journal of Applied Polymer Science **(12)**, pp. 735 (2013).

[13] J.O. Aguilar, J.R. Bautista-Quijano, F. Avilés, *Influence of carbon nanotube clustering on the electrical conductivity of polymer composite films,* Express Polymer Letters **(4)**, pp. 292 (2010).

[14] B.J. Yang, K.J. Cho, G.M. Kim, H.K. Lee, *Effect of cnt agglomeration on the electricalconductivity and percolation threshold of nanocomposites: A micromechanics-based approach,* CMES **(103)**, pp. 343 (2014).

[15] S.C. Tjong, G.D. Liang, S.P. Bao, *Effects of crystallization on dispersion of carbon nanofibers and electrical properties of polymer nanocomposites,* Polymer Engineering and Science **(48)**, pp. 177 (2008).

[16] Shu-Hang Liao et al, *Preparation and properties of carbon nanotube/polypropylene nanocomposite bipolar plates for polymer electrolyte membrane fuel cells,* Journal of Power Sources **(185)**, pp. 1225 – 1232 (2008).

[17] Dimitrios Bikiaris, *Microstructure and properties of polypropylene/carbon nanotube nanocomposites,* Materials **(3)**, pp. 2884 (2010).

[18] Hua Deng et al, *Effect of melting and crystallization on the conductive network in conductive polymer composites,* Polymer **(50)**, pp. 3747 – 3754 (2009).

[19] Jin-Ping Peng, Hui Zhang, Long-Cheng Tang, Yu Jia, Zhong Zhang, *Dielectric properties of carbon nanotubes/epoxy composites,* Journal of Nanoscience and Nanotechnology **(12)**, pp. 1 (2012).

[20] Mohammad Arjmand , Amir Ameli , Uttandaraman Sundararaj, *Employing nitrogen doping as innovative technique to improve broadband dielectric properties of carbon nanotube/polymer nanocomposites,* Macromolecular Materials and Engineering **(301)**, pp. 555 – 565 (2016).

[21] Tony McNally, Petra Pötschke, *Polymer–carbon nanotube composites* (Woodhead Publishing, 2011) cH.11: Electromagnetic properties of polymer–carbon nanotube composites.

[22] D. Nuzhnyy et al., *Broad-band conductivity and dielectric spectroscopy of composites of multi-walled carbon nanotubes and poly(ethylene terephthalate) around their low percolation threshold,* Nanotechnology **(24)**, pp. 9 (2013).

[23] T. Villmow, S. Pegel, P. Pötschke , U. Wagenknecht, *Influence of injection molding parameters on the electrical resistivity of polycarbonate filled with multi-walled carbon nanotubes,* Composite Science and Technology **(68)**, pp. 777 (2008).

[24] J. Qiu, L. Wang, K. Uchiya, E. Sakai, *Effects of injection molding conditions on the electrical properties of polycarbonate/carbon nanotube nanocomposites,* Polymer Composites **(37)**, pp. 3245 (2016).

[25] A. Ameli et al., *Process-microstructure-electrical conductivity relationships in injection-molded polypropylene/carbon nanotube nanocomposite foams,* Composites: Part A **(96)**, pp. 28 (2017).

[26] A. Ameli, P.U. Jung, C.B. Park, *Electrical properties and electromagnetic interference shielding effectiveness of polypropylene/carbon fiber composite foams,* Carbon **(60)**, pp. 379 (2013).

[27] D.H. Park et al., *Electrical resistivity of polycarbonate/multiwalled carbon nanotube composites under varying injection molding conditions,* Journal of Applied Polymer Science **(113)**, pp. 450 (2009).

[28] H. Deng et al., *Effect of melting and crystallization on the conductive network in conductive polymer composites,* Polymer **(50)**, pp. 3747 (2009).

[29] Yongzheng Pan et al., *Annealing induced electrical conductivity jump of multi-walled carbon nanotube/polypropylene composites and influence of molecular weight of polypropylene,* Journal of Polymer Science: Part B: Polymer Physics **(48)**, pp. 2238 (2010).

[30] G. Fei et al., *Relationship between electrical conductivity and spatial arrangements of carbon nanotubes in polystyrene nanocomposites: The effect of thermal annealing and plasticization on electrical conductivity,* Composite Science and Technology **(146)**, pp. 99 (2017).

[31] Dong Xiang, Eileen Harkin-Jones, David Linton, *Effect of cooling rate on the properties of high density polyethylene/multi-walled carbon nanotube composites,* AIP Conference Proceedings **(1664)**, 070005 (2015).

[32] Geon-Oh Lim, Kyoung-Tae Min, Gue-Hyun Kim, *Effect of cooling rate on the surface resistivity of polymer/multi-walled carbon nanotube nanocomposites,* Polymer Engineering and Science **(50)**, pp. 290 (2010).

[33] Mercedes Fernández, Maite Landa, María Eugenia Muñoz, Anton Santamaría, *Electrical conductivity of pur/mwcnt nanocomposites in the molten state, during crystallization and in the solid state,* European Polymer Journal **(47)**, pp. 2078 (2011).

[34] A.B. Espinoza-Martınez et al., *Effect of mwnts concentration and cooling rate on the morphological, structural, and electrical properties of non-isothermally crystallized pen/mwnt nanocomposites,* Journal of Applied Polymer Science **(132)**, 41765 (2015).

[35] Gaurav Kasaliwal, Andreas Go¨ ldel, Petra Po¨tschke, *Influence of processing conditions in small-scale melt mixing and compression molding on the resistivity and morphology of polycarbonate–mwnt composites,* Journal of Applied Polymer Science **(112)**, pp. 3494 (2009).

[36] I. Alig et al., *Establishment, morphology and properties of carbon nanotube networks in polymer melts,* Polymer **(53)**, pp. 4 (2012).

[37] H. Pang et al., *The effect of electric field, annealing temperature and filler loading on the percolation threshold of polystyrene containing carbon nanotubes and graphene nanosheets,* Carbon **(49)**, pp. 1980 (2011).

[38] C.A. Martin et al., *Electric field-induced aligned multi-wall carbon nanotube networks in epoxy composites,* Polymer **(46)**, pp. 877 (2005).

[39] O. Osazuwa et al., *Electrically conducting polyolefin composites containing electric field-aligned multiwall carbon nanotube structures: The effects of process parameters and filler loading,* Carbon **(72)**, pp. 89 (2014).

[40] C. Zhang, J. Zhu, M. Ouyang, C. Ma, *Electric field controlled formation and dissociation of multiwalled carbon nanotube conductive pathways in a polymer melt,* Applied Physics Letters **(94)**, 11915 (2009).

[41] C. Ma et al., *Alignment and dispersion of functionalized carbon nanotubes in polymer composites induced by an electric field,* Carbon **(46)**, pp. 766 (2008).

[42] Mei-Juan Jiang et al., *Broad-frequency dielectric behaviors in multiwalled carbon nanotube/rubber nanocomposites,* Journal of Applied Physics **(6)**, 084902 (2009).

[43] P. Yadav et al., *Synthesis and dielectric characterization of polycarbonate/multi-wall carbon nanotubes nanocomposite,* Arabian Journal of Chemistry (2015).

[44] Jonscher, A. K. , *The 'universal'dielectric response,* Nature **(267)**, pp. 673 (1977).

[45] B.M. Greenhoe et al., *Universal power law behavior of the ac conductivity versus frequency of agglomerate morphologies in conductive carbon nanotube-reinforced epoxy networks,* Journal of Polymer Science, Part B: Polymer Physics **(54)**, pp. 1918 (2016).

[46] S. Boukheir et al., *Structural characterization and electrical properties of carbon nanotubes/epoxy polymer composites,* Journal of Applied Polymer Science **(134)**, 44514 (2017).

[47] K.A. Mauritz, *Dielectric relaxation studies of ion motions in electrolyte-containing perfluorosulfonate ionomers. 4. long-range ion transport,* Macromolecules **(22)**, pp. 4483 (1989).

[48] Y. Kazemi et al., *Conductive network formation and destruction in polypropylene/ carbon nanotube composites via crystal control using supercritical carbon dioxide,* Polymer **(129)**, pp. 179 (2017).

[49] Yamin Pan et al., *Viscoelastic and electrical behavior of poly(methyl methacrylate)/ carbon black composites prior to and after annealing,* Polymer **(113)**, pp. 34 (2017).

[50] Shuangmei Zhang et al., *Dynamic percolation in highly oriented conductive networks formed with different carbon nanofillers,* Colloid Polymer Science **(290)**, pp. 1393 (2012).

[51] A. Combessis et al., *Understanding dynamic percolation mechanisms in carbonaceous polymer nanocomposites through impedance spectroscopy: Experiments and modeling,* Journal of Applied Polymer Science **(116)**, 034103 (2014).

A

Task 1: Additional Figures

Mappings of σ' at 1MHz for the three IM settings:

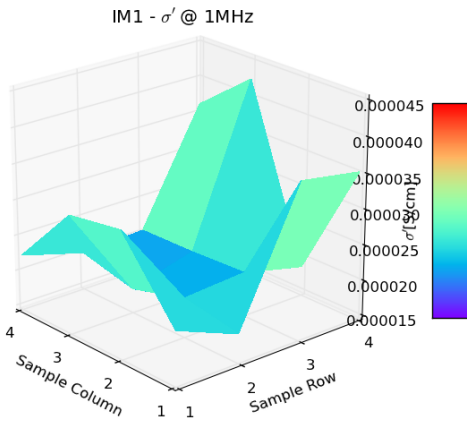

Figure A.1: In-plane mapping of σ' at 1MHz for sample IM1.

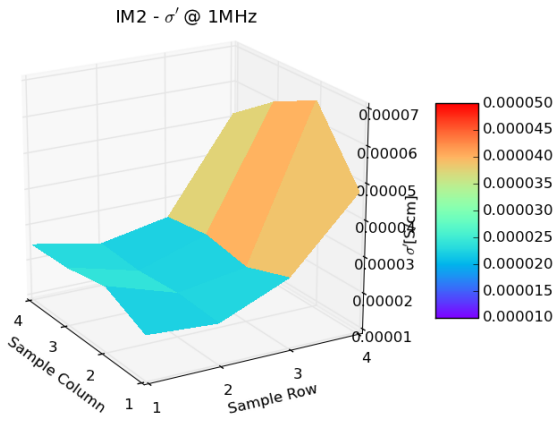

Figure A.2: In-plane mapping of σ' at 1MHz for sample IM2.

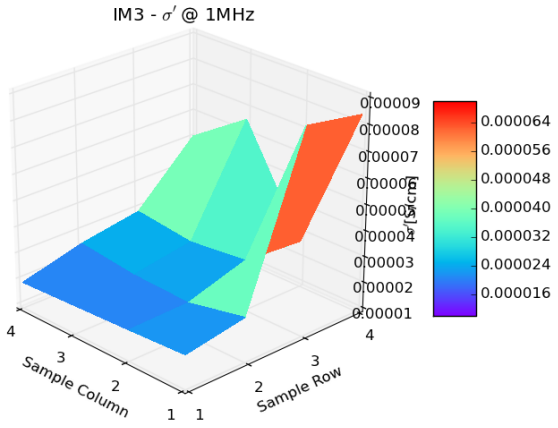

Figure A.3: In-plane mapping of σ' at 1MHz for sample IM3.

Comparison of locations with equal thickness after surface removal:

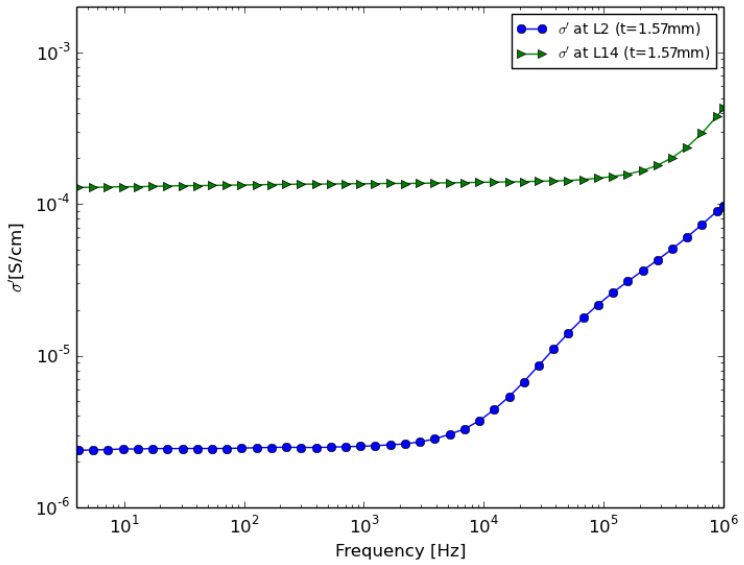

Figure A.4: Comparison of σ' after grinding at L2 and L14.

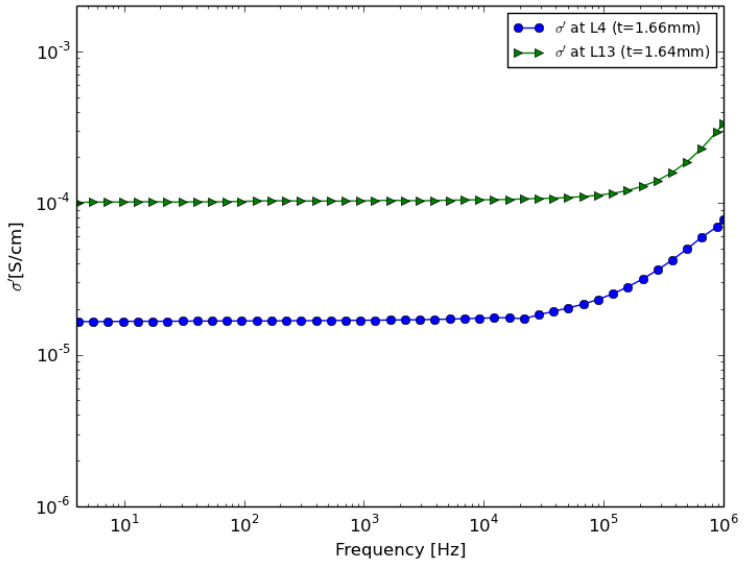

Figure A.5: Comparison of σ' after grinding at L4 and L13.

Example of the Samples used during BDS:

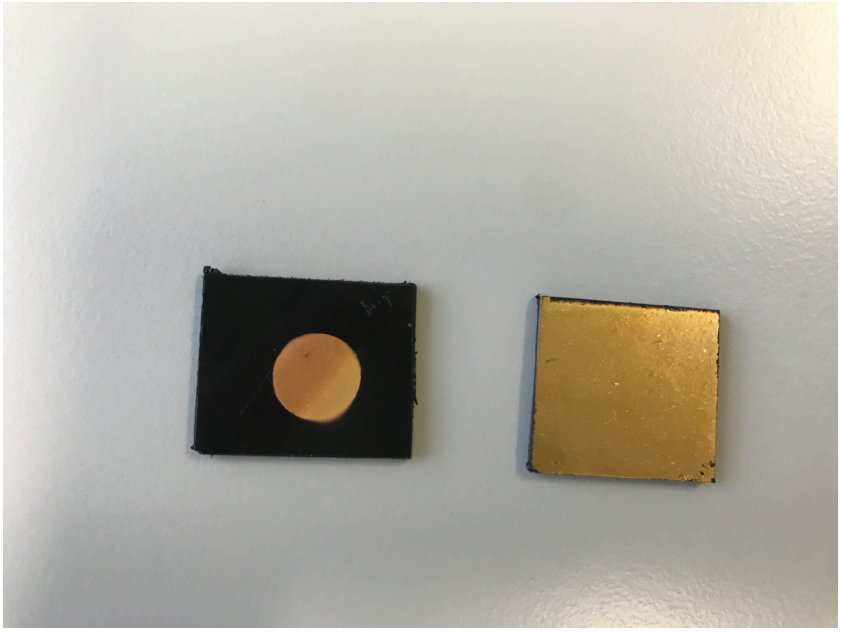

Figure A.6: Sputtered and cut samples used during BDS. On the left side the sputtered 9mm top electrode (core-side) can be seen and on the right side (cavity-side) has been sputtered without a mask.

Figure A.7: Example of a cut and sputtered sample loaded into the BDS sample cell. It can be noted that on top of the sample an additional small electrode has been placed.

B

Task 2: Additional Figures

Mapping of σ' at 1MHz for PP2 composites produced with all three IM settings:

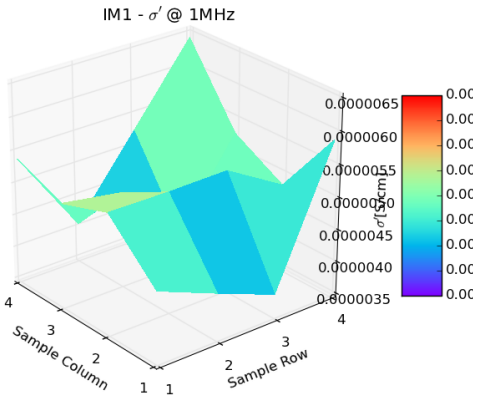

Figure B.1: In-plane mapping of σ' at 1MHz of sample IM1 containing PP2.

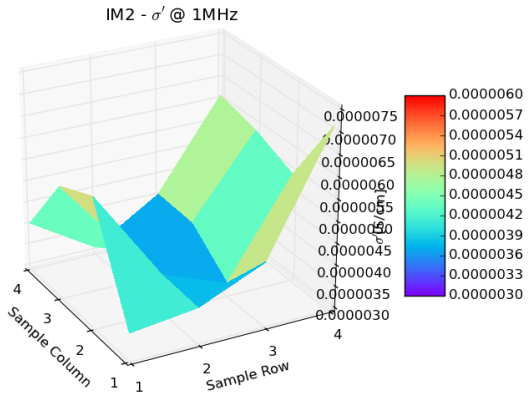

Figure B.2: In-plane mapping of σ' at 1MHz of sample IM2 containing PP2.

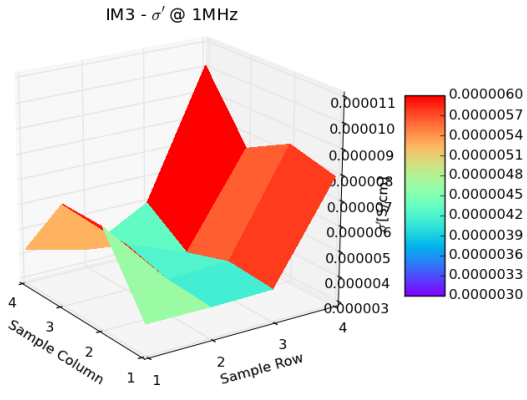

Figure B.3: In-plane mapping of σ' at 1MHz of sample IM3 containing PP2.

Comparison of PP1 and PP2 composite after surface removal:

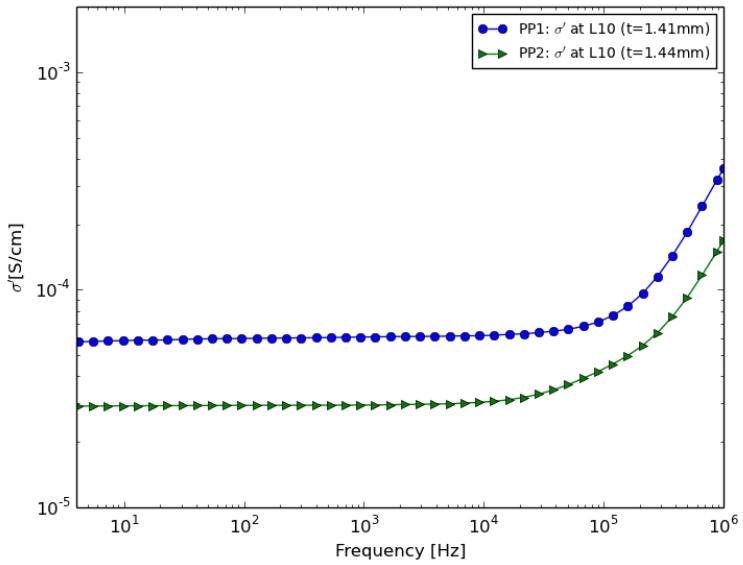

Figure B.4: Comparison of σ' of the PP1 and PP2 samples after surface removal at location 10.

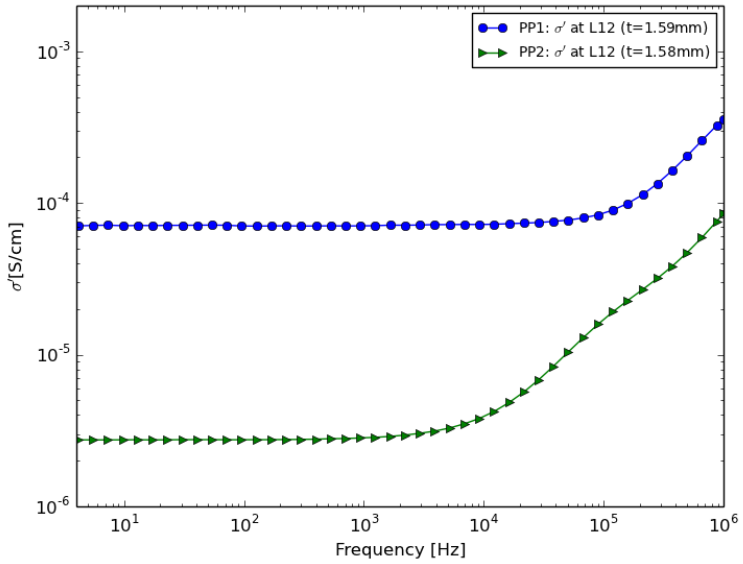

Figure B.5: Comparison of σ' of the PP1 and PP2 samples after surface removal at location 12.

C

Task 3: Additional Figures

Mappings of ϵ' and σ' at 127Hz of the PP1 composite before and after 1h annealing:

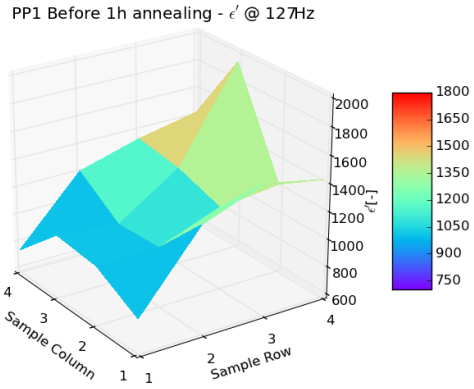

Figure C.1: Mapping of ϵ' at 127Hz before 1h annealing.

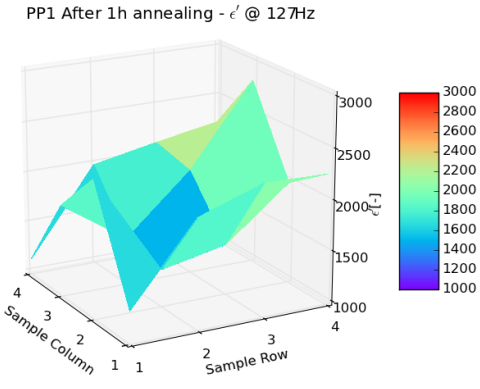

Figure C.2: Mapping of ϵ' at 127Hz after 1h annealing at 150°C.

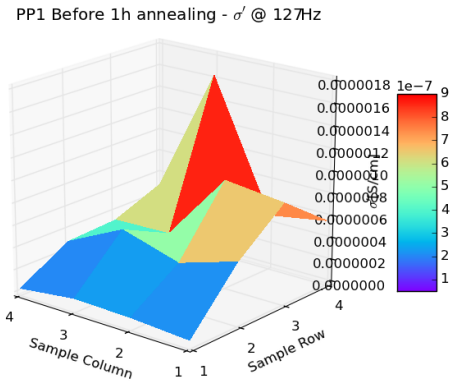

Figure C.3: Mapping of σ' at 127Hz before 1h annealing.

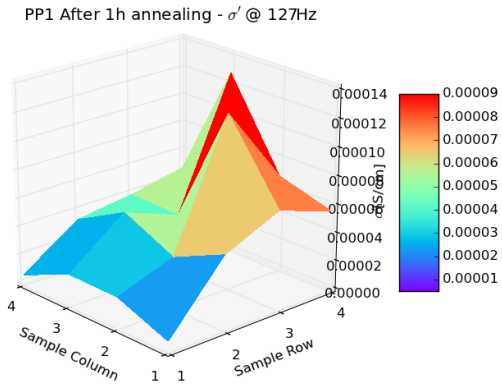

Figure C.4: Mapping of σ' at 127Hz after 1h annealing at 150°C.

Mappings of ϵ' and σ' at 127Hz of the PP1 composite before and after 3h annealing:

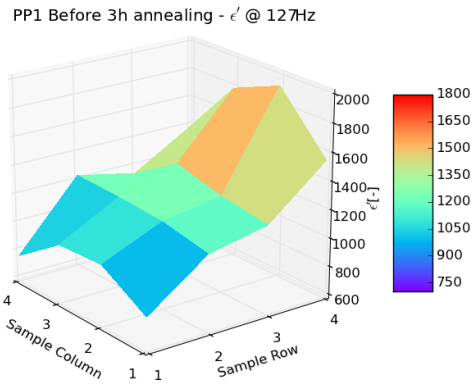

Figure C.5: Mapping of ϵ' at 127Hz before 3h annealing.

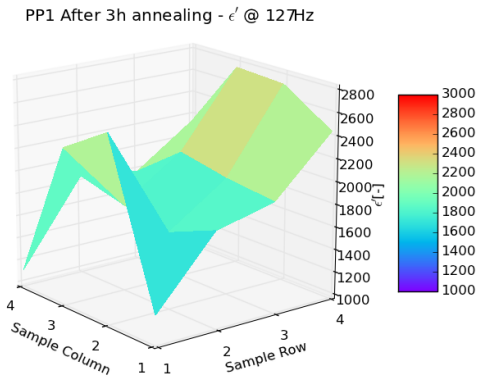

Figure C.6: Mapping of ϵ' at 127Hz after 3h annealing at 150°C.

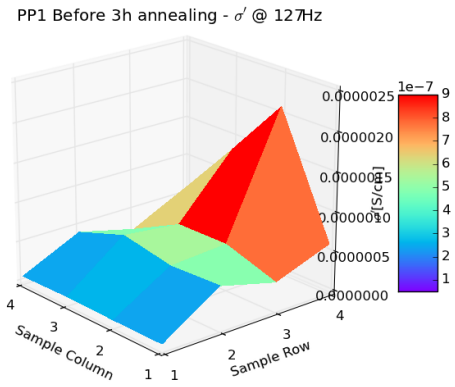

Figure C.7: Mapping of σ' at 127Hz before 3h annealing.

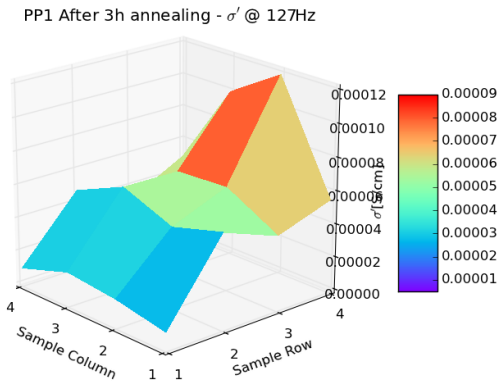

Figure C.8: Mapping of σ' at 127Hz after 3h annealing at 150°C.

D

Task 4: Additional Figures

Additional pictures of the DEP setup used:

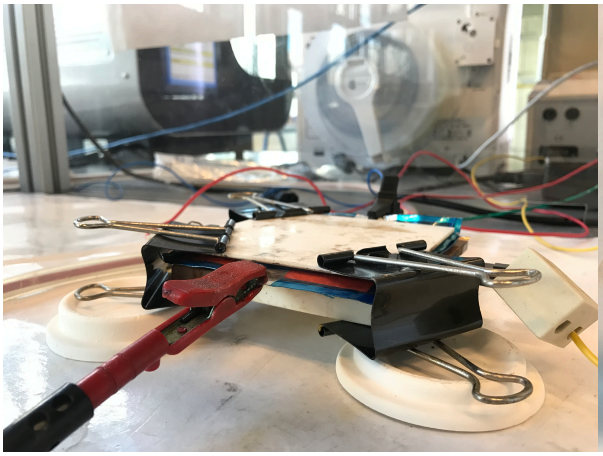

Figure D.1: Side view of the DEP setup used during the experiments.

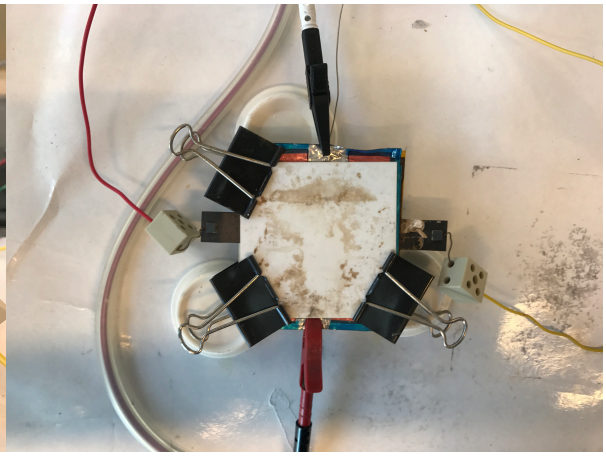

Figure D.2: Top view of the DEP setup used during the experiments.

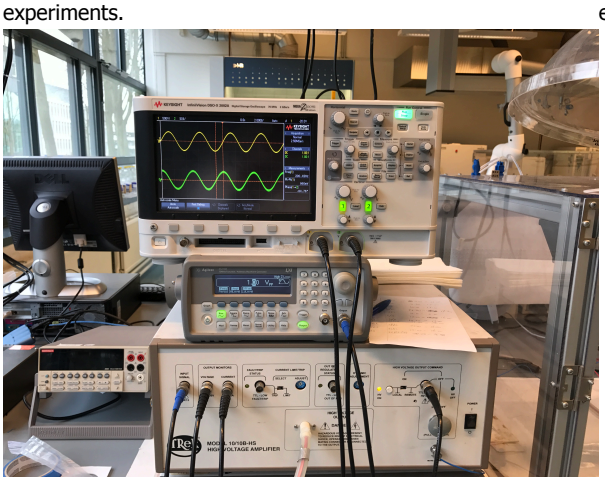

Figure D.3: Picture of the oscilloscope (top), waveform generator (middle) and the voltage amplifier (bottom).

Direct comparison of the DEP measurements with the Annealing measurements:

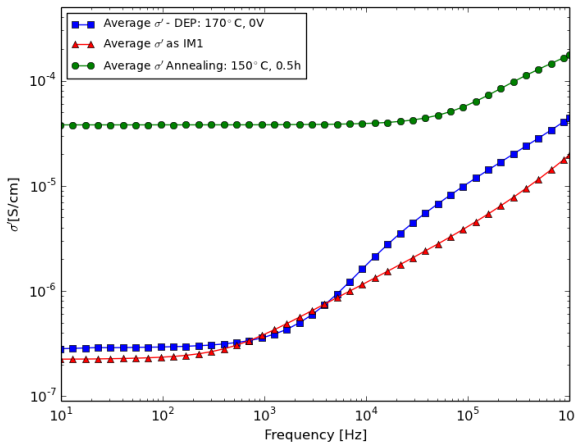

Figure D.4: Comparison of the average DEP measurements at 170°C with $0V$ with the measurement averages of the 0.5h annealed sample.

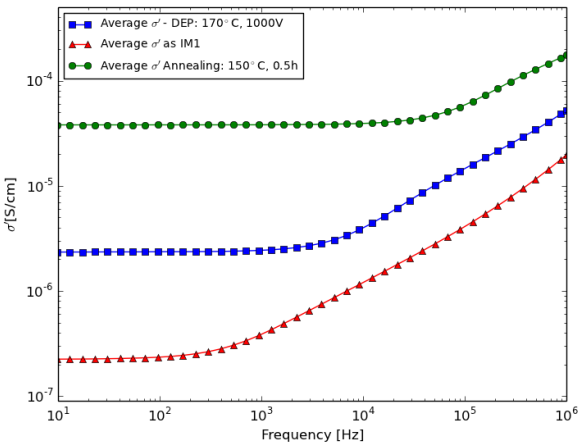

Figure D.5: Comparison of the average DEP measurements at 170°C with $1000V$ with the measurement averages of the 0.5h annealed sample.

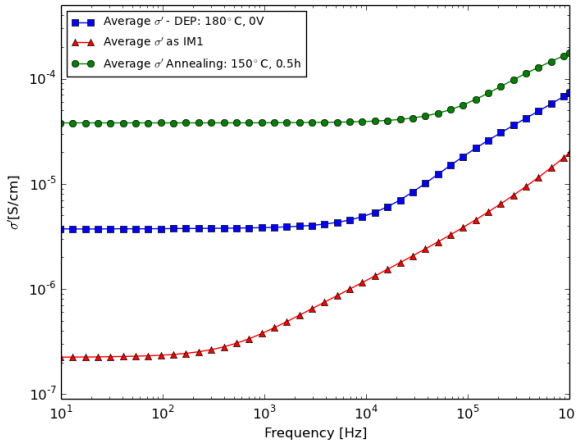

Figure D.6: Comparison of the average DEP measurements at 180°C with $0V$ with the measurement averages of the 0.5h annealed sample.

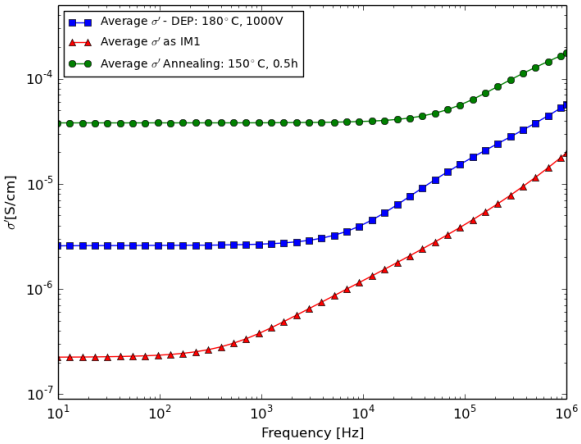

Figure D.7: Comparison of the average DEP measurements at 180°C with $1000V$ with the measurement averages of the 0.5h annealed sample.

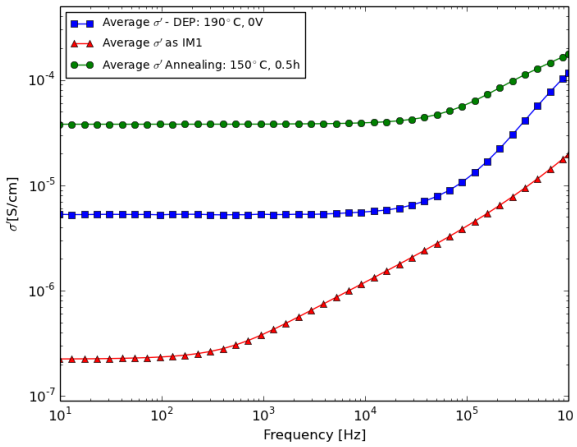

Figure D.8: Comparison of the average DEP measurements at 190°C with 0V with the measurement averages of the 0.5h annealed sample.

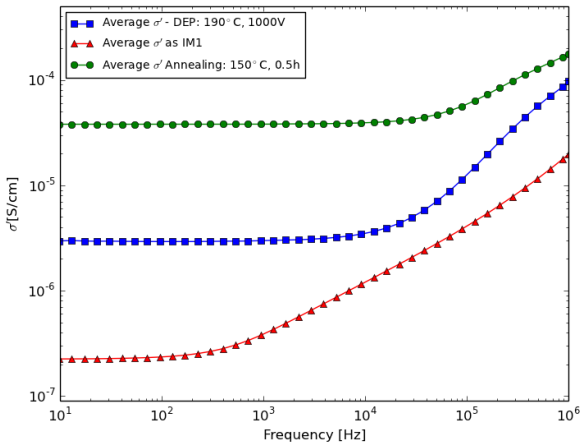

Figure D.9: Comparison of the average DEP measurements at 190°C with 1000V with the measurement averages of the 0.5h annealed sample.

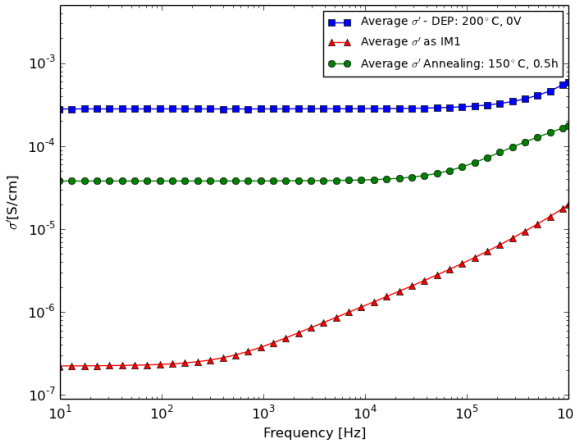

Figure D.10: Comparison of the average DEP measurements at 200°C with 0V with the measurement averages of the 0.5h annealed sample.

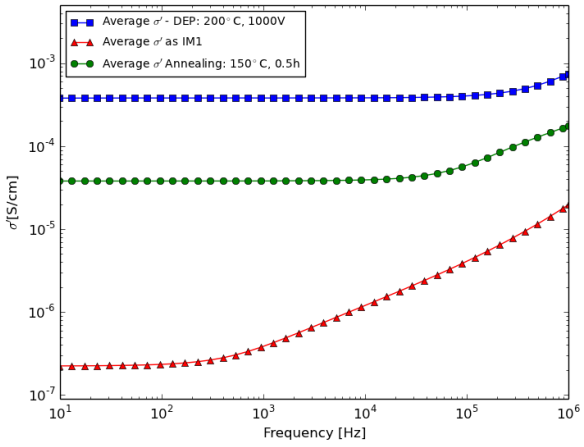

Figure D.11: Comparison of the average DEP measurements at 200°C with 1000V with the measurement averages of the 0.5h annealed sample.

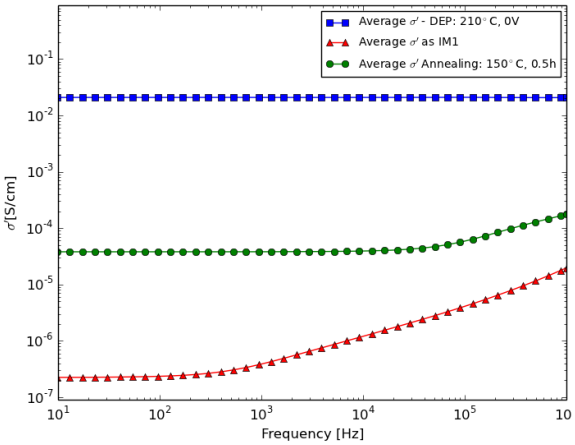

Figure D.12: Comparison of the average DEP measurements at 210°C with $0V$ with the measurement averages of the 0.5h annealed sample.

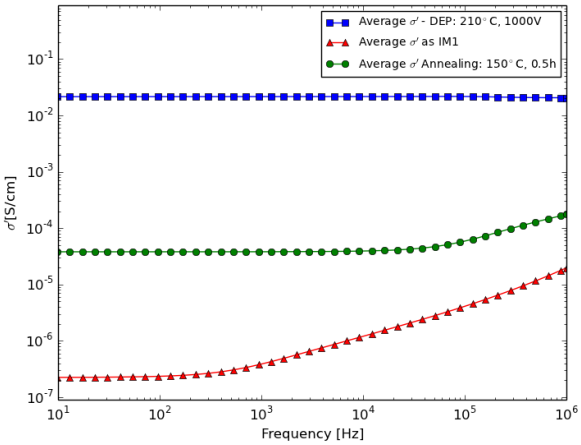

Figure D.13: Comparison of the average DEP measurements at 210°C with $1000V$ with the measurement averages of the 0.5h annealed sample.

Additional figures studying the thermal gradient during DEP:

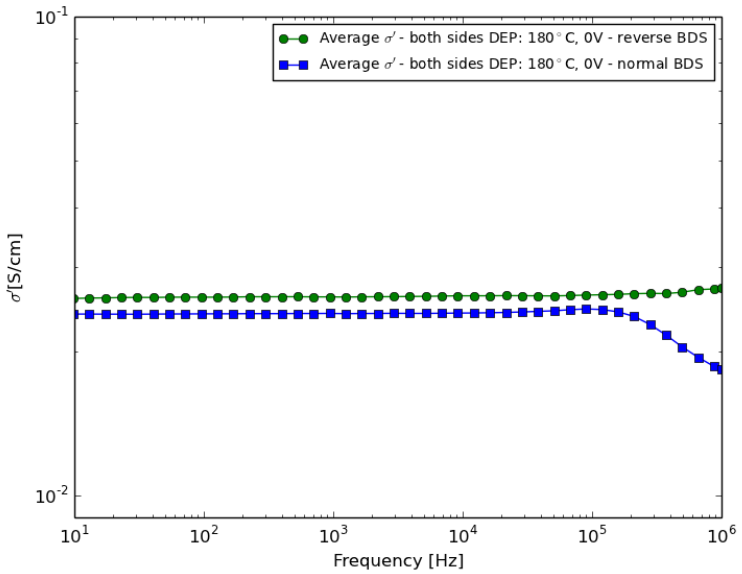

Figure D.14: Comparison of σ' magnitude of the double DEP sample using the normal BDS procedure and the reverse BDS procedure.